

# A flexible sideways-looking probe for detecting cortical bone proximity:

design, manufacturing, and evaluation of a prototype

F. Kardux





MASTER THESIS

---

**A flexible sideways-looking probe for  
detecting cortical bone proximity: design,  
manufacturing, and evaluation of a  
prototype**

---

*by*

FAMKE KARDUX

*to obtain the degree of Master of Science  
at the Delft University of Technology,  
to be defended publicly on Friday May 6, 2022 at 14:00 AM*

Student number: 4475739  
Project duration: June 1, 2021 – May 6, 2022  
Thesis committee: M.S. Losch, TU Delft  
Prof. dr. B.H.W. Hendriks, TU Delft & Philips  
Prof. dr. J. Dankelman, TU Delft  
Dr. N. Bhattacharya, TU Delft

*This thesis is confidential and cannot be made public until May 2024.*

An electronic version of this thesis is available from May 2024 at  
<http://repository.tudelft.nl/>.



## *Preface*

Before I introduce the topic of my graduation project, I want to say a few words about my experiences in the last year and express my gratitude to those who have helped me accomplish it. Last year, I had the opportunity to perform research on optical probe design, a completely new topic for me. This has made the past year a challenge, but more importantly, I enjoyed it from the beginning to the end. I have learned a lot about a topic with much potential to improve healthcare in the coming years. I hope that in a different role, I will be able to contribute more to this in the future. For now, I am happy and proud to show you my work for the last year.

This work would not have been the same without the support I received, and therefore, I would like to thank a few people. First of all, I want to thank Merle Losch, thank you for guiding me through the project, answering all my questions, and especially taking the time to extensively discuss any interesting or remarkable research findings. Besides, I would like to thank Benno Hendriks, thank you for sharing your knowledge, challenging me to think creatively, and introducing me to the facilities at Philips to do my experiments. To my master's student colleagues at the MISIT lab and BITE department, thank you for the fun times in the lab and for the feedback and inspiration during the bi-weekly meetings. Furthermore, I would like to thank the members of my graduation committee, Jenny Dankelman and Nandini Bhattacharya, for their time to evaluate my work. Also, I want to thank Joost Rutges from Erasmus MC for allowing me to attend a spinal fusion surgery.

Last but not least, aside from academic and content-related support, I had a lot of support from my family and friends, which I value more than they realize. Thank you to my parents, brother, Stijn, roommates, and friends for always listening to me, cheering me up, and celebrating my small and big successes.

*Famke Kardux*  
*Rotterdam, April 2022*



## *Abstract*

Spinal fusion is a surgical treatment involving stiffening parts of the spinal column to eliminate any relative motion and improve spine stability. A critical part of spinal fusion surgery is the placement of pedicle screws because it is highly complex and can damage the vascular structures and nerves near the vertebrae. To prevent complications, a new anchoring method is developed that strengthens screw contact by following the curved trajectory of the dense cortical shell while avoiding a cortical breach. Diffuse reflectance spectroscopy (DRS) is a technique that could be used in a bone drill to obtain real-time information about the location of the drill within the vertebra. In order to drill the correct trajectory, an optical probe using DRS should determine the parallel closeness of cortical bone to the drill tip. To show the potential of this novel technology for improving spinal fusion surgery, this master thesis introduces and validates a flexible sideways-looking probe using DRS to identify the proximity of cortical bone when measuring along the cortical shell of a vertebra.

In this study, the ideal optical design to detect the proximity of cortical bone is investigated by looking into the effect of fiber angulation on the photon propagation using Monte Carlo simulations and phantom experiments. A conceptual design was created based on the ideal optical design combined with the mechanical requirements to make the probe insertable into a vertebra. As a proof of concept, a prototype was developed and tested on a bone-mimicking phantom and porcine vertebrae.

The conceptual design comprises a flexible needle with two optical fibers attached to a rigid tip with a diameter of 2.9 mm. Two mirrors are positioned in the rigid tip, emitting light 45° off-axis and collecting light 90° off-axis with a source-detector separation of 2.1 mm. These light directions were chosen because they optimize the reflectance spectrum difference between cancellous and cortical bone due to a longer path length, making detecting cortical bone closeness easier. A prototype was made that demonstrates that the probe can detect the parallel proximity of cortical bone at a depth up to 1.5 mm in an ideal phantom setting. The prototype can distinguish between pure cancellous and cortical bone in porcine vertebrae. Additionally, the prototype can also be inserted into the pedicles and bent along the cortical wall of a vertebra. These positive findings show that the flexible sideways-looking probe created in this study can potentially improve spinal fusion surgery by enabling an increase in cortical bone contact without perforating it. Although proof of concept has been provided, it is essential to improve the design for safety and usability and improve tissue type identification accuracy before continuing to clinical trials.



# Contents

<b>Preface</b>	<b>iii</b>
<b>Abstract</b>	<b>v</b>
<b>1 Introduction</b>	<b>1</b>
1.1 Background	1
1.1.1 Spine anatomy	1
1.1.2 Spinal fusion surgery	2
1.1.3 Challenges	3
1.2 Research project	4
1.2.1 Diffuse reflectance spectroscopy-enhanced steerable bone drill	4
1.2.2 Goal and thesis outline	6
<b>2 Investigation of the ideal fiber orientation for detecting cortical bone closeness</b>	<b>9</b>
2.1 Introduction	9
2.1.1 Desired optical signal	9
2.1.2 Optical probe design	10
2.1.3 Goal and structure	11
2.2 Method	12
2.2.1 Monte Carlo simulations	12
2.2.2 Experimental design	14
2.3 Results	19
2.3.1 Monte Carlo simulations	19
2.3.2 Experimental design	19
2.4 Discussion	23
2.4.1 Interpretation of the results	23
2.4.2 Limitations	24
2.4.3 Conclusion	25
<b>3 Flexible sideways-looking probe to detect proximity of cortical bone within vertebra: a conceptual design study</b>	<b>27</b>
3.1 Design scope	27
3.1.1 Functional requirements	27
3.1.2 Specifications	29
3.2 Design strategies	29
3.2.1 Measure diffuse reflectance spectrum of target tissue	29
3.2.2 Be insertable in curved hole	30
3.2.3 Be manufacturable	33
3.3 Concept design	33
3.3.1 Final design	33
3.3.2 Theoretical performance	36

<b>4</b>	<b>Performance analysis of flexible sideways-looking probe: a phantom and ex-vivo study</b>	<b>39</b>
4.1	Introduction	39
4.1.1	Background	39
4.1.2	Goal and structure	39
4.2	Method	40
4.2.1	Prototyping	40
4.2.2	Phantom experiments	42
4.2.3	Ex-vivo experiments	42
4.2.4	Flexibility test	45
4.3	Results	45
4.3.1	Phantom experiments	45
4.3.2	Ex-vivo experiments	45
4.3.3	Flexibility tests	47
4.4	Discussion	47
4.4.1	Interpretation of the results	47
4.4.2	Limitations	49
4.4.3	Conclusion	50
<b>5</b>	<b>Overall conclusion</b>	<b>51</b>
5.1	Conclusion	51
5.2	Future recommendations	51
<b>A</b>	<b>2D Drawings</b>	<b>59</b>
<b>B</b>	<b>Design concepts</b>	<b>69</b>
<b>C</b>	<b>Geometry formula</b>	<b>73</b>

# List of Abbreviations

<b>DR</b>	<b>D</b> iffuse <b>R</b> eflectance
<b>DRS</b>	<b>D</b> iffuse <b>R</b> eflectance <b>S</b> pectroscopy
<b>LAD</b>	<b>L</b> ook <b>A</b> head <b>D</b> istance
<b>MC</b>	<b>M</b> onte <b>C</b> arlo
<b>NA</b>	<b>N</b> umerical <b>A</b> perture
<b>NIR</b>	<b>N</b> ear <b>I</b> nfra <b>R</b> ed
<b>SD</b>	<b>S</b> tandard <b>D</b> eviation
<b>SDS</b>	<b>S</b> ource <b>D</b> etector <b>S</b> eparation
<b>SNR</b>	<b>S</b> ignal <b>N</b> oise <b>R</b> atio



## Chapter 1

# Introduction

Spinal fusion surgery has become one of the most prevalent surgical procedures worldwide in the last 20 years [1]. Because of the aging population's ongoing growth, the number of operations will only continue to rise. Spinal fusion is a surgical procedure of stiffening parts of the spinal column that eliminates any relative motion in the spinal column to minimize pain and increase spine stability. An essential part of spinal fusion surgery is the placement of screws in the pedicles of vertebra, which operate as an anchoring mechanism to fuse two or more vertebrae. This aspect of the surgery is highly complex and can damage the vascular structures and nerves near the vertebrae if not done correctly. Due to its frequency and risks, incorrect placement of pedicle screws is a clinically and commercially relevant problem.

Delft University of Technology researchers are developing a new anchoring system and a steerable bone drill to improve the strength and accuracy of pedicle screws. Research is currently ongoing in collaboration with Philips Research's Image-guided-technology department to examine the deployment of a sensor system that can provide real-time information regarding the location of the bone drill inside the vertebra. This thesis will investigate a possible optical probe design to implement in a steerable bone drill. The following sections will serve as a primer for the reader to understand the essence of the problem and the research objective and strategy.

## 1.1 Background

### 1.1.1 Spine anatomy

The spinal column runs from the base of the skull to the tailbone and is made up of many bony building blocks called vertebrae that are linked by muscles, tendons, and ligaments. The spinal column consists of 33 vertebrae divided into five regions, namely cervical, thoracic, lumbar, sacral, and coccygeal, as shown in Figure 1.1A. Only the 24 vertebrae which are in the cervical, thoracic, and lumbar region are relevant for spinal fusion surgery.

The anatomy of the vertebra is slightly different depending on the region. However, each vertebrae is made up of an anterior body and a posterior vertebral arch, see Figure 1.1B. The vertebral body serves as weight-bearing. The vertebral arch is made up of eleven different parts: two pedicles, two laminae, and seven processes. The pedicles extend from the sides of the body to join the body to the arch. The lamina projects backward and medial-wards from each pedicle to join and complete the vertebral arch and form the vertebral foramen. Enclosed by the vertebral foramen is the spinal cord, which is a tube structure made up of nerve tissue that stretches from the brainstem to the lumbar area of the spinal column. The processes serve as

attachment points for muscles and ligaments. The vertebral body is formed of cancellous bone with a thin cortical bone coating, while the vertebral arch has thicker cortical bone coverings [2].

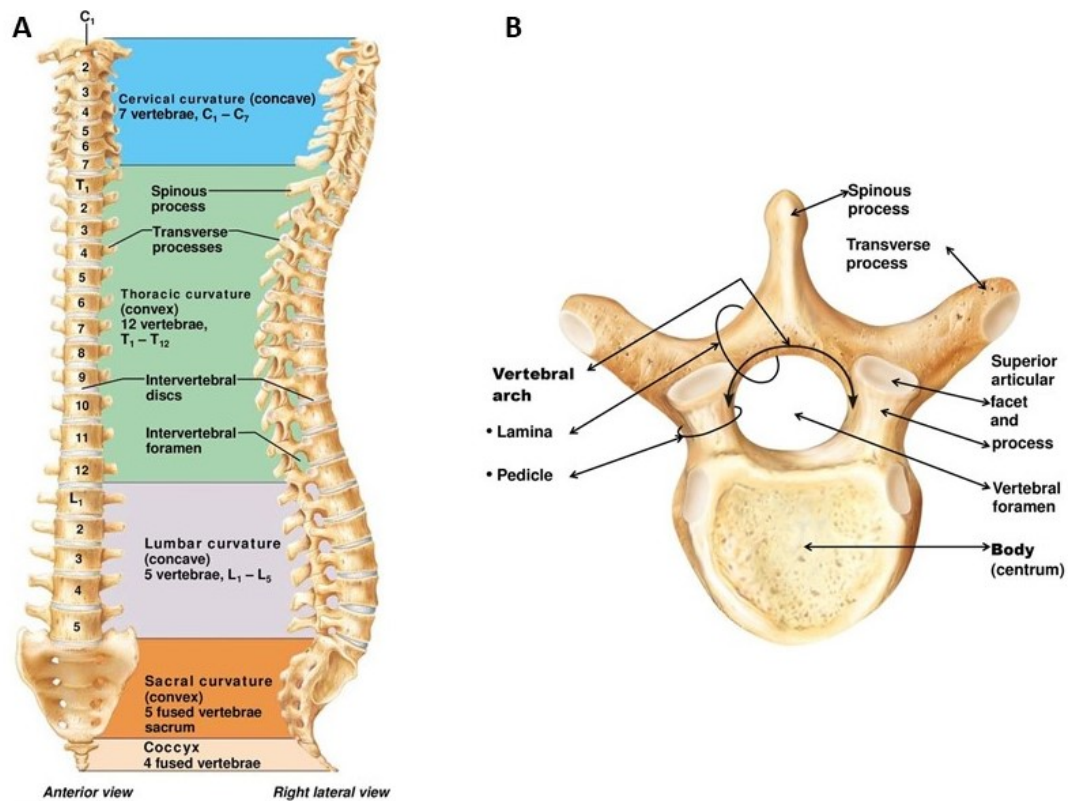


FIGURE 1.1: A) Spinal column including all regions [2], B) Cross section of vertebra [2].

Adjacent vertebrae in the spinal column are separated by an intervertebral disc, see Figure 1.1A. Each disc forms a symphysis, which is a type of cartilaginous joint. The function of this disc is to provide mobility by allowing slight movement between the vertebrae, to function as a shock absorber, and to act as spacing to help maintain a constant gap between the vertebrae to protect the nerves that run down the spine between the vertebrae.

### 1.1.2 Spinal fusion surgery

Spinal fusion is used to treat a variety of back disorders in which the stability or curvature of the spinal column is the source of pain. Spondylosis, spondylolisthesis, a ruptured disk, an accident, or trauma can all cause pain due to spinal instability. Spinal fusion is a surgical technique that joins two or more vertebrae intending to eliminate any relative motion between the affected vertebrae to improve the spine's stability and reduce back pain. The idea behind spinal fusion surgery is that if the bones are aligned appropriately and do not shift, the pain will disappear. The procedure can be performed at any level in the spine. However, the exact fusion technique depends on the level of the spine and the source of pain.

To treat spinal instability, spinal fusion surgery consists of two main steps [3]. The first step consists of inserting bone graft material between the afflicted vertebrae. The intervertebral disc is usually removed entirely or partially and replaced with bone graft material. This bone graft provides the foundation and environment to

allow the body to grow new bone and fuse a section of the spine. The next step is the hardware placement to stabilize the vertebrae and help the fusion process. In this step, anchoring screws, called pedicle screws, are inserted into the pedicles of two or more vertebrae. A rod is added to connect the individual screws and prevent relative motion between the vertebrae [4]. A construct including pedicle screws, connecting rod, and bone graft material is shown in Figure 1.2.

To treat pain caused by spinal deformities such as Scoliosis or Kyphosis, spinal fusion surgery also consist of two main steps [5]. However, the surgery starts with corrective maneuvers to correct the deformity. Following the correction, the corrected vertebrae are joined together using a hardware and bone graft material construct to keep the deformity corrected.

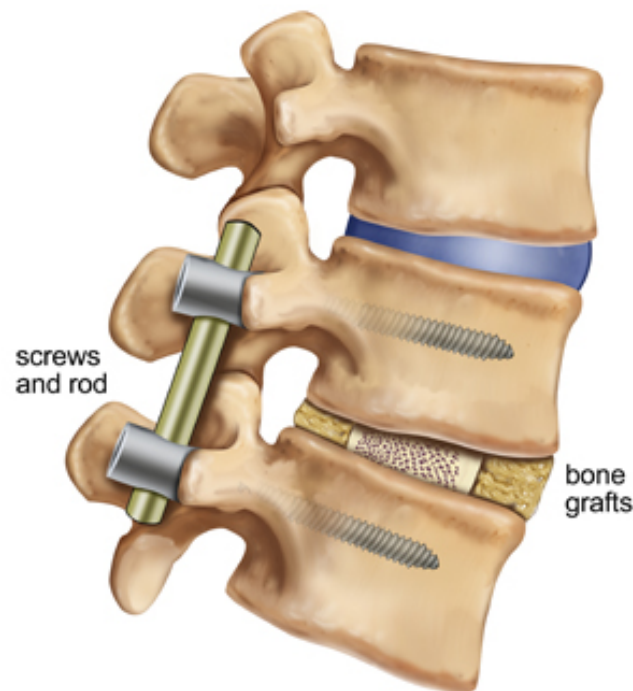


FIGURE 1.2: Schematic drawing of pedicle screws, rod and bonegraft material inserted in human spine [6].

### 1.1.3 Challenges

A complex procedure during spinal fusion surgery is the placement of the pedicle screws due to the small size of the pedicles and the proximity of critical nerves and vascular structures. If pedicle screws are positioned incorrectly, cortical breach, or perforation of the cortical wall of the vertebra, might occur, see Figure 1.3. This perforation can cause insufficient fixation and damage to the nerves and vessels. In order to avoid these complications, it is crucial to avoid a cortical breach. However, the strength of the connection between a vertebra and pedicle screw also relies on the contact area of the screw with the stronger cortical bone, which is located in the outer layer of the vertebra [7]. As a result, drilling close to the outer wall of the vertebra without perforating it is ideal for pedicle screw placement.

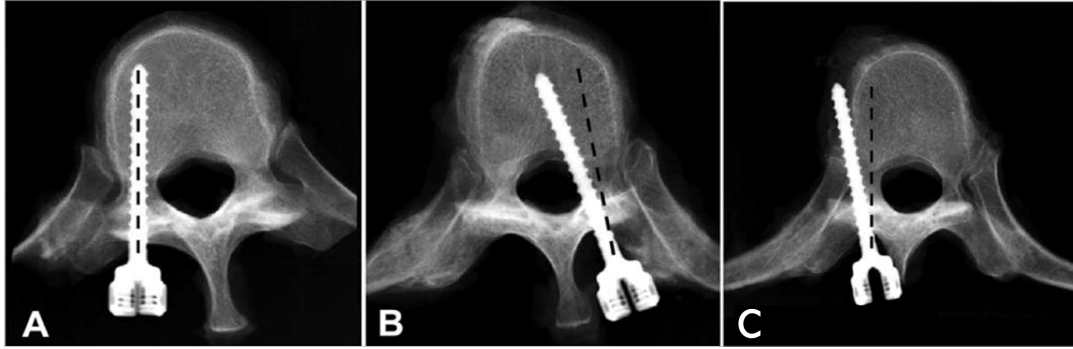


FIGURE 1.3: Three different pedicle screw placements [8]. A) Correct pedicle screw placement. B) Cortical breach in spinal canal. C) Cortical breach of outer cortex.

## 1.2 Research project

### 1.2.1 Diffuse reflectance spectroscopy-enhanced steerable bone drill

Researchers at Delft University of Technology are working on a new vertebral anchoring system that will increase the cortical bone contact [9]. In this new surgical procedure, the steerable bone drill should first drill through the pedicles, which are part of the vertebral arch, and then through the vertebral body. The drill should follow a curved path within the vertebral body near the cortical boundary without perforating it. A schematic view of the drill's desired path is indicated in Figure 1.4. This trajectory will provide enhanced cortical bone contact, resulting in higher fixation strength.

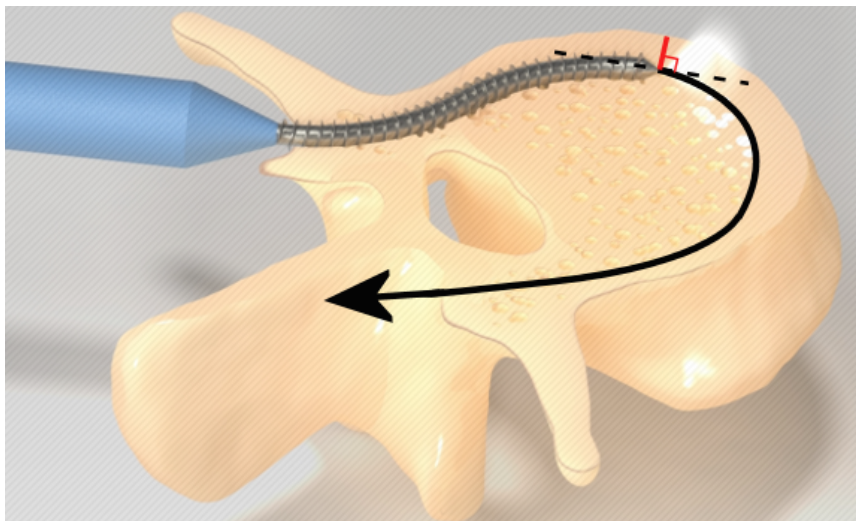


FIGURE 1.4: Concept of the steerable bone drill, the black arrow represents the desired path within the vertebra, and the red line indicates the shortest distance from the drill tip to the cortical boundary. Figure adapted from [9].

To ensure proper drilling along the cortical bone layer and to prevent a cortical breach, the surgeon needs to get real-time information about the location of the steerable bone drill in the vertebra. Diffuse reflectance spectroscopy (DRS) is a potential, cost-effective sensing technique that can be used to obtain this information. DRS is an optical spectroscopy technique in which the diffuse reflectance of light

within a tissue sample is studied. DRS measurements are mostly done with a fiber-optic probe. Such a probe contains one or more optical fibers facing a tissue sample. One optical fiber illuminates a tissue sample using a broad-band light source, while another optical fiber collects the light after interacting with the tissue. The major phenomena which occur during light-tissue interaction are absorption and scattering of light. The amount of scattering and absorption within a tissue, dependent on the concentration and type of biological chromophores within the tissue, determines the wavelength-dependent intensity of light collected by the collection fiber [10]. The intensity of the collected light of a specific wavelength is called reflectance. The dependence of the reflectance on the wavelength is called a reflectance spectrum. Because all tissues have unique chromophore concentrations, they have a unique reflectance spectrum. As a result, a reflectance spectrum can be used to determine the concentration of biological chromophores in a tissue sample and differentiate between different tissue types [10]. A schematic overview of the DRS technique, including information from the tissue sample visualized by a reflectance spectrum, is shown in Figure 1.5.

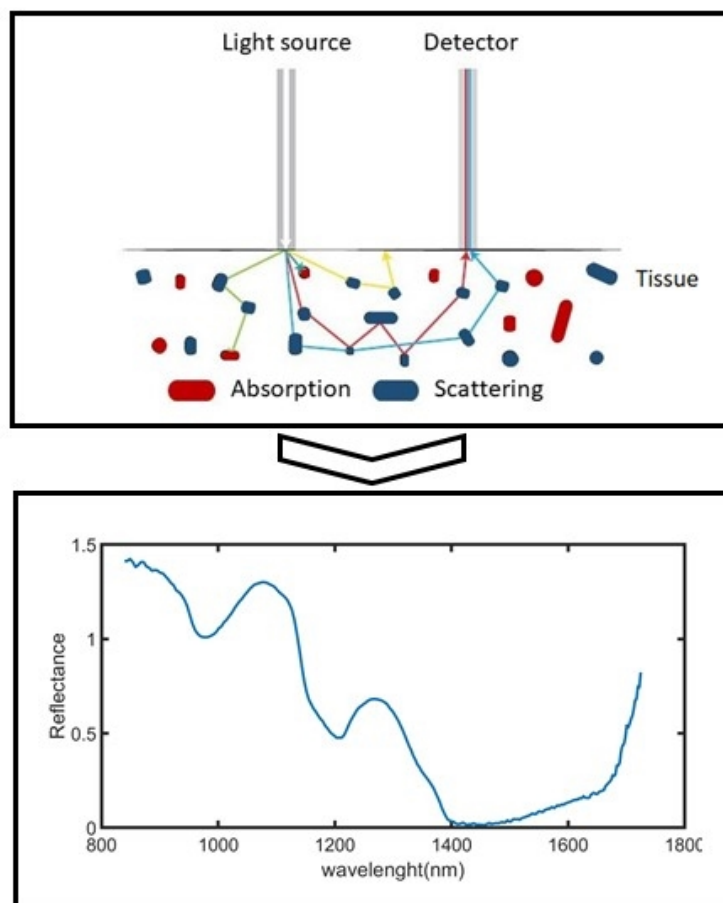


FIGURE 1.5: Schematic overview of DRS technique. Figure adapted from [11].

To avoid cortical breach while using a steerable bone drill, DRS should be utilized to detect the proximity of cortical bone to the drill tip. In order to accomplish this, with DRS, it should be possible to distinguish between cortical bone and cancellous bone. According to prior studies, DRS is already a promising technique for identifying the transition zone between the cancellous bone and cortical bone [12, 13].

However, one major drawback of using DRS in a steerable bone drill is that it is only possible to detect the cortical bone with a conventional probe if it is located in front of the optical probe. However, measuring the shortest distance towards the cortical boundary is essential to drill along the cortical bone layer without perforating it. The shortest distance when steering along the cortical wall is in the direction lateral on the drilling direction, see Figure 1.4. As a result, the DRS probe should be able to measure the optical properties of tissue located parallel to the probe's longitudinal axis. In other words, a design for a sideways-looking DRS probe that can be used in a steerable bone drill is required.

## 1.2.2 Goal and thesis outline

The aim of this thesis is to design, prototype, and test a flexible sideways-looking DRS probe that can detect the proximity of cortical bone when measuring along the cortical wall of a vertebra. The research process was divided into four research phases. A schematic overview of the different research phases is shown in Figure 1.6.

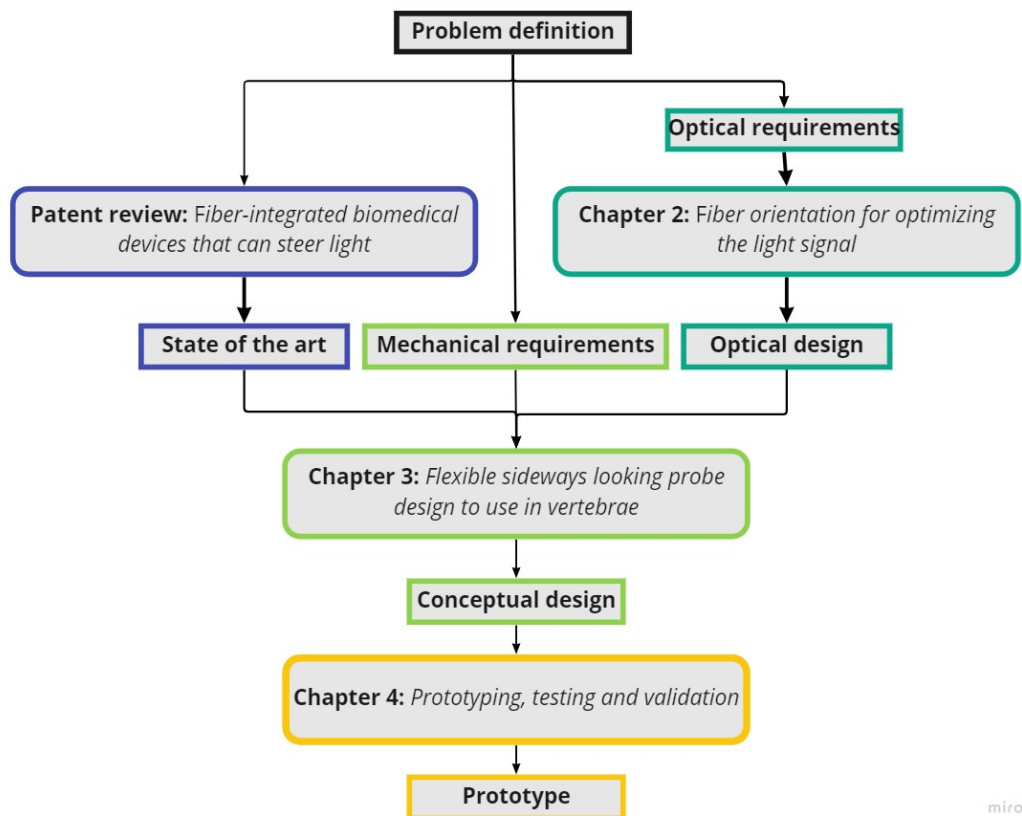


FIGURE 1.6: Project strategy including different researches phases.

The first part involved patent research into already-existing fiber-integrated biomedical devices that can steer light in the desired direction. This overview is intended to gather ideas for a sideways-looking probe design and gain insight into what has already been done and what still needs to be researched. The most important finding of this study is that there are still various opportunities to design unique biomedical devices that can collect light at an angle, including sideways looking probes. The development of innovative sideways-looking probe designs will benefit healthcare

by expanding the use of optical sensors in a wide range of medical devices. This patient review is published and open access available in Expert Review of Medical Devices [14].

The optical design of the probe is the subject of Chapter 2. The central question to be answered in this section of the study is: *What is the best fiber orientation to detect the proximity to cortical bone?* The purpose of this chapter is to look into the best optical design for detecting cortical bone located parallel to the probe's longitudinal axis.

Chapter 3 focuses on combining the optical design and mechanical requirements into a probe design that can be employed in a steerable bone drill. The major question to be answered in the section of the study is: *What is the best design for a sideways-looking probe that can detect the proximity of cortical bone along the cortical wall in a vertebra?* The goal of this section is to create a conceptual design.

Chapter 4 focuses on developing a prototype that can be tested and validated. The major question to be answered in the section of the study is: *How is the prototype of the flexible sideways-looking probe design performing?* The goal of this section is to create, test, and validate a prototype.



## Chapter 2

# Investigation of the ideal fiber orientation for detecting cortical bone closeness

## 2.1 Introduction

### 2.1.1 Desired optical signal

The goal of DRS in a steerable bone drill to use within a vertebra is to prevent cortical breach while drilling close to the cortical boundary. To do this, the surgeon needs to know how close the cortical boundary is to the drill tip. To make this possible, the DRS probe should measure the DR spectrum of the target tissue. This functional requirement of the probe can be separated in two sub-functions, the probe should illuminate the target tissue, and the probe should collect light scattered from the target tissue. To fulfill these requirements the DRS probe should include several specifications. One important specification is that the probe should measure the target tissue that lies parallel to the drilling direction.

Furthermore, in order to assess the proximity to cortical bone, the measured reflectance spectrum should include information to discriminate between cancellous and cortical bone. Therefore, a distinguishing criterion should be available. Previous studies have indicated that the lipid content is much higher in cancellous bone than in cortical bone. This suggests that lipid content is a useful criterion for distinguishing between these two types of bone [12]. The lipid content of a tissue has influence on the absorption and scattering characteristics. A significant feature is that fat chromophores cause a prominent absorption peak of light with a wavelength of 1211 nm [12]. As a result, a deep dip in intensity around 1211 nm should be visible in the reflectance spectrum of tissue with a high lipid content. Because cancellous bone contains more lipid than cortical bone, the reflectance spectrum of cancellous bone has a deeper drop around 1211 nm, as seen in Figure 2.1. To use this difference as distinguishing criterion, the optical probe should emit and collect light within the near infrared (NIR) light region.

Lastly, to assess the proximity of cortical bone, the optical probe should be able to measure the reflectance spectrum of tissue which is not in direct contact with the probe but is deeper in the tissue. The deepest layer of which an optical probe can measure optical tissue properties is called the look-ahead distance (LAD) of the probe. The probe should have a large LAD because the earlier cortical bone closeness is recognized, the easier a surgeon can anticipate it. However, a bigger LAD comes at the cost of a reduced signal-to-noise ratio (SNR) in the measured signal [15]. This has as an effect that the signal will be less clear and it will be harder to discriminate between cancellous bone and cortical bone. Therefore, a trade-off between

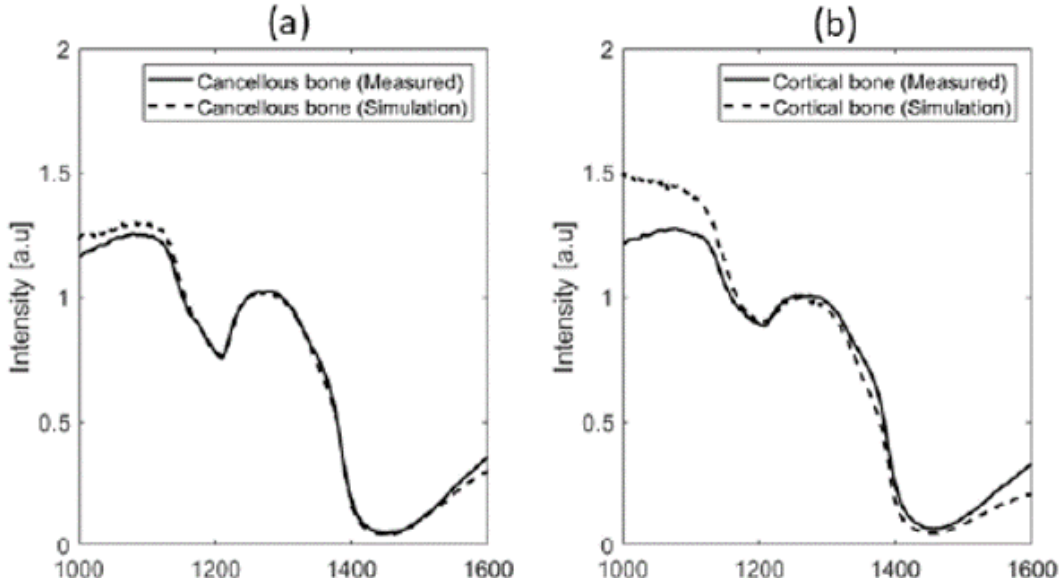


FIGURE 2.1: Reflectance spectrum of (a) pure cancellous bone and (b) pure cortical bone [12].

depth of detection and SNR must be determined to use DRS in a steerable bone drill. However, the LAD must be above a certain threshold to make the optical feedback within the steerable bone drill useful. The time a physician has to respond to the presence of cortical bone depends on the drill speed, LAD, and DRS measurement frequency. The drill speed is still unknown and the frequency is dependent on the spectroscope instead of the optical probe. Because this is not the subject of this research, it is assumed that the drilling speed and frequency could be adjusted so that a LAD of 1 mm is sufficient to detect cortical bone proximity. This is based on the LAD of a front-looking probe which has proven its potential to detect the proximity of cortical bone with two parallel fibers [16].

The optical requirements and specifications that the DRS probe should fulfill are summarized in Table 2.1. The specifications are formulated based on the desired optical signal that the optical should measure. The geometry of the optical probe, in particular the orientation of the fibers that determines which direction the light is sent and received, affects the measured signal of the optical probe. As a result, fiber orientation is a critical design consideration for the probe to accurately measure the desired optical signal.

Functional requirements	Specifications
<b>Measure DR spectrum of target tissue</b>	
- Illuminate target tissue	Target tissue: Parallel to drilling direction 1 mm depth
- Collect light scattered by target tissue	Light type: NIR light (1000-1400) nm SNR: Able to detect difference cancellous and cortical bone

TABLE 2.1: Optical requirements and specifications DRS probe.

### 2.1.2 Optical probe design

The orientation of the optical fibers within an optical probe affect the target tissue, the LAD, and the SNR. The optical probe to use within a steerable bone drill should

include two optical fibers. One optical fiber, the source, is used to illuminate the tissue with NIR light and the other optical fiber, the detector, will collect the light after it has interacted with the tissue. If a group of photons enter the tissue all photons will propagate through the tissue in a random walk, because of multiple scattering and absorption events. The most probable path of the photons that are collected by the collector has the shape of a banana, called the photon banana, see Figure 2.2 [15]. The optical probe has the highest optical sensitivity for the tissue within the photon banana, meaning that the optical properties of this tissue have an impact on the measured reflectance spectrum. The shape of the photon banana depends on the distance between the source and the detector, the source-detector separation (SDS). Therefore, the SDS plays a role in determining which layers of the tissue have a high optical sensitivity. Increasing the SDS will increase the LAD of the probe, as shown in Figure 2.2. Previous research into the use of DRS to prevent cortical breach in a conventional pedicle screw indicates that using an SDS of roughly 1.2 mm provides a good trade-off between SNR and LAD [13]. This SDS is limited by the maximum diameter of the optical probe related to the diameter of the pedicle screws. Since the design of the steerable bone drill is still unknown, it is assumed that this will be approximately the same as the conventional pedicle screws.

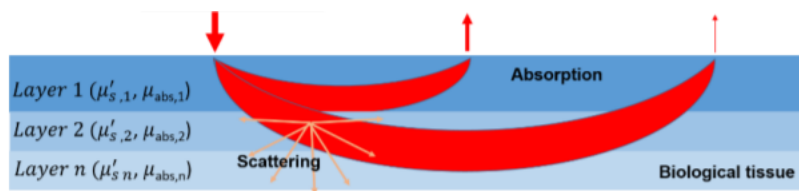


FIGURE 2.2: Examples of different photon bananas for different SDS [15].

The photon banana is a well researched phenomenon for an optical probe that measures the tissue which is in front of the probe with two parallel fibers [17, 18, 19, 20, 21]. However, for the application in a steerable bone drill the optical probe should measure the tissue in the direction that is 90° off-axis. To make this possible light should be emitted and collected off-axis as well. However, the optimal angle for emitting and collecting is still unknown. When the source emits light and the collector collects light from 90° off-axis, the optical probe will measure tissue parallel to the probe with a similar photon banana as shown in Figure 2.2. However, previous research showed that a relative angle between the source and detector can influence the optical sensitivity and the LAD of the optical probe [22, 23, 24]. These studies revealed that by orienting the source and detector towards each other, the signal from superficial layers in a narrow area can be better detected. This raises the question of whether angling the source and detector away from each other enables deeper layer detection across a larger area. This is useful when using a steerable bone drill because it can increase the area of measured cortical bone and may allow for earlier detection of cortical bone proximity without increasing the diameter of the bone drill. This study analyzes how much it is truly possible to change the photon path by angling the source and detector away from each other.

### 2.1.3 Goal and structure

In short, the goal of this study is to look into the effect of fiber angulation on the photon-banana and, as a result, on the detection of the proximity of cortical bone.

A Monte Carlo (MC) simulation and two experimental tests were done to evaluate this effect. First, MC simulations were run to provide insight into the various shapes of the photon-banana at various angulations. Additionally, two experiments were done to verify the simulations and to see what the effect of the change of the photon-banana is on the detection of the proximity of cortical bone. In Experiment 1, DRS measurements were performed on a bone phantom including a layer that simulates cancellous bone and a highly light absorbing layer. The goal of this experiment was to investigate the LAD and the areas with high optical sensitivity for different fiber angulations. In Experiment 2, DRS measurements were performed on a two layer bone-mimicking phantom consisting of one cancellous and one cortical bone layer. The goal of this experiment was to measure the effect of fiber angulation on the measured reflectance spectrum and how this influences the detection of cortical bone closeness. Based on these simulation and experiments, it should be possible to infer on the degree of control over the photon path within the tissue by angulating the source away from the detector and the target tissue.

## 2.2 Method

### 2.2.1 Monte Carlo simulations

#### Monte Carlo method

MC refers to a technique to simulate physical processes using a stochastic model [25]. In tissue optics, the MC method is often used to approximate the distribution of light within biological tissue. In this method, light is simulated as photon packets that make random walks as they travel through tissue. The random walk is chosen by statistically sampling the probability distributions for step size and angular deflection per scattering event. Many MC programs exist that allow for a computational approach to determine the light distribution in tissue using this statistical method [26]. In this study, the program MCMatlab is used [26]. This software is chosen because it is an open-source, user-friendly, and relatively efficient MC program that combines C's speed with MATLAB's familiarity and versatility. The MC program is based on a general method for implementation of the MC method in computer code described by Prahl et al. [25]. This chapter simply explains the MC method, which is used in the MCMatlab application. More thorough information may be obtained in the literature [25, 27].

A MC simulation starts with launching a packet of photons into the tissue. The packet of photons follows a particular photon path. This path is approached by variable step sizes that are determined by a probability density function. After each propagation step, the possibility of total internal reflection is checked. This is only possible when the photon packet propagates across a boundary into a region with a different refraction index. The probability that the photon packet which passes a boundary is internally reflected is determined by the Fresnel Reflection coefficient ( $R(\theta_i)$ ). This coefficient is described by the following formula:

$$R(\theta_i) = \frac{1}{2} \left( \frac{\sin^2(\theta_i - \theta_t)}{\sin^2(\theta_i + \theta_t)} + \frac{\tan^2(\theta_i - \theta_t)}{\tan^2(\theta_i + \theta_t)} \right) \quad (2.1)$$

where  $\theta_i$  is the incident angle on the boundary and  $\theta_t$  is the transmission angle. The relation between  $\theta_i$  and  $\theta_t$  is given by Snell's law. If a photon packet goes across a boundary without being internally reflected, it either exits the tissue or continues in a tissue layer with a different refractive index. Internally reflected photon packets

remain in the same tissue layer. For all photon packets which continue propagating in a tissue layer, a part of the photon packet is absorbed and the rest is scattered. The fraction that is absorbed and scattered is determined by the absorption ( $\mu_a$ ) and scattering coefficient ( $\mu_s$ ) of tissue, with the following formula:

$$fraction_{absorbed} = \frac{\mu_a}{\mu_a + \mu_s} \quad (2.2)$$

The Henyey-Greenstein phase function determines the direction of scattering. This function uses the scattering anisotropy ( $g$ ) of tissue, which is defined as the average cosine of the scattering angles ( $\cos(\theta)$ ), to approximate the angular dependence of light scattering. A random variable uniformly distributed over the interval zero to one ( $\epsilon$ ) is added to the function. The Henyey-Greenstein phase function combined with this random variable determines the scattering angle ( $\theta$ ) of a photon packet with the following formula:

$$\cos\theta = \begin{cases} \frac{1}{2g}(1 + g^2 - (\frac{1-g^2}{1-g+2g\epsilon})^2), & \text{if } g \neq 0 \\ 1 - 2\epsilon, & \text{if } g = 0 \end{cases} \quad (2.3)$$

After this scattering event, the procedure is repeated from calculating the stepsize to establishing the new scattering angle. However, at each step, the weight of the photon packet is reduced because of the fraction which is absorbed. If the weight of a photon packet falls below a certain threshold, then roulette is used to either extinguish or continue propagating the photon packet. A new photon packet is started at the emitter if the photon does not survive the roulette. For every photon packets, all reflection, transmission, scattering, and absorption events are recorded throughout the process. After propagating several photon packets, the net distribution of all photon paths provides a realistic approximation to reality. A flowchart describing this MC technique is shown in Figure 2.3.

### Design set-up

In this study, MC simulations were done to visualize the photon banana and the relationship between fiber angulation and shape. A one-layer tissue model consisting only of cancellous bone was developed to visualize the path within the cancellous bone. As input for the cancellous layer, the absorption and scattering coefficients of cancellous bone at a wavelength of 1211 nm were used, measured from human vertebra [13]. The anisotropy was assumed as 0.9, and the refractive index was set to 1. The optical probe was simulated as a light source and collector, separated by a distance of 1.2 mm. The light source emitted light with a Gaussian distribution with a near-field width of 0.1 mm and a far-field radial width of 0.11 rad. The light collector was defined as an optical fiber with a diameter of 0.2 mm and a numerical aperture (NA) of 0.22. These values were chosen to simulate the light beams of the optical fibers that will be used in the experiments as closely as possible. During the MC simulation  $2 * 10^8$  photons were emitted in the tissue. The simulations were performed with a tissue thickness of 3 mm. The angle between the source and detector varied between  $0^\circ$ ,  $10^\circ$ ,  $20^\circ$ ,  $30^\circ$ , and  $45^\circ$  in the different simulations.

The percentage of the collected photons that passes through a particular tissue area were calculated to investigate the photon banana in the tissue for the different fiber angulations. This percentage of collected photons represents the proportion of photon packets scattered through a tissue area as a fraction of the total number of photon packets collected by the collector. The percentage of collected photons

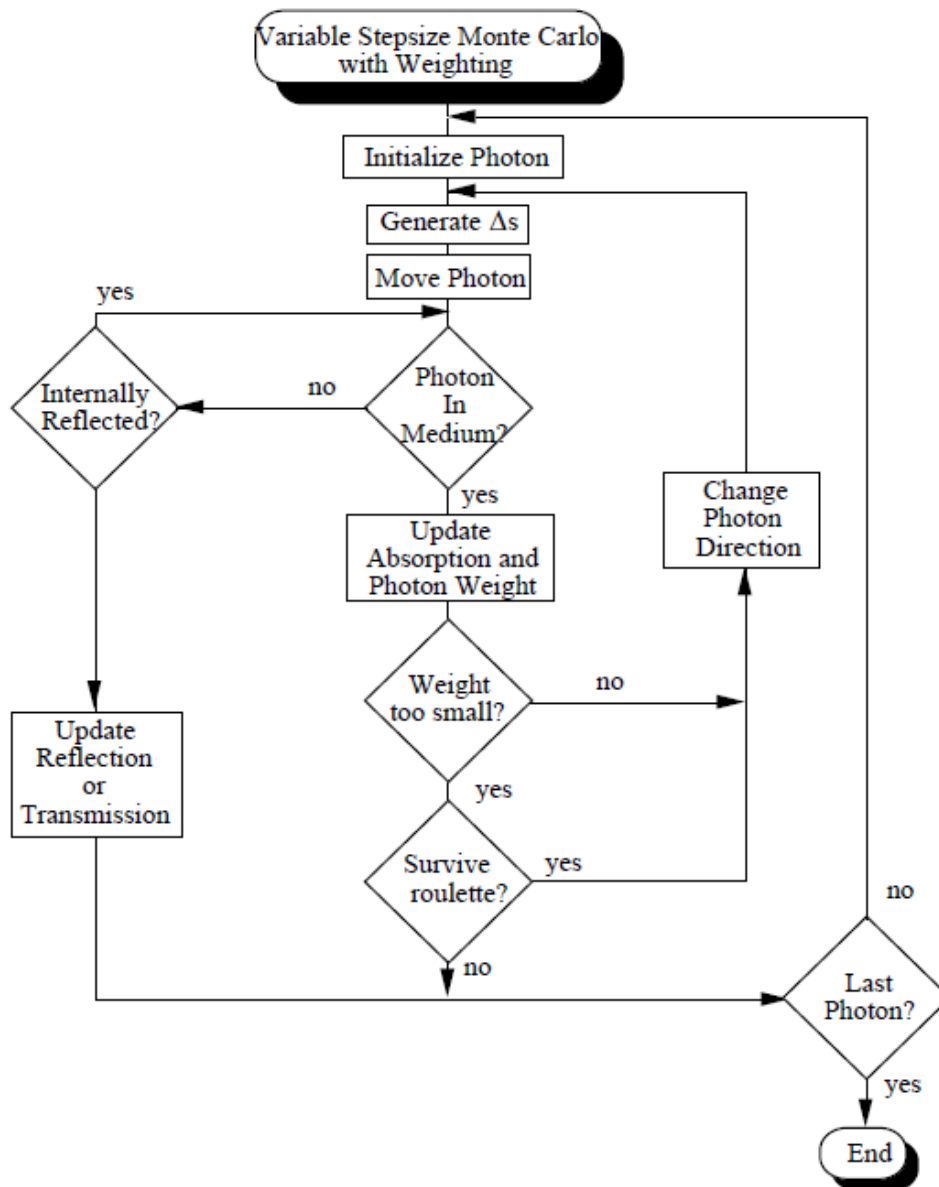


FIGURE 2.3: Flowchart of variable step-size MC technique [25].

that passes through a particular tissue area were plotted in  $xz$ -plane of the tissue, with the photons in the  $y$ -direction projected on it. This was done for all different angulations to properly compare the different photon bananas. In addition, for all angulations, the intensity of the total number of collected photons was determined in order to gain insight into the change in SNR caused by angulating the fibers.

## 2.2.2 Experimental design

### Phantom preparation

In the first experiment, a two-layer phantom was used to test the effect of angulated fibers on the LAD and the areas with high optical sensitivity. The phantom's bottom layer was made of a highly absorbing black tape from HPX [28]. The top layer was constructed of pure coconut milk, which is a low-cost, easy-to-use material that can

be utilized to replace intralipid, which is typically employed to simulate fat in optical phantoms [29]. The used coconut milk was from the brand Go-Tan and had a fat fraction of 18% [30]. For the phantom production, the highly absorbing tape was fixed at the inside of a small cup such that it covered the whole bottom. Thereafter, the coconut milk was poured on top with a thickness of at least 5 mm.

In the second experiment, a two-layer bone mimicking phantom was used to test the effect of angulated fibers on the detection of cortical bone proximity. To mimic the situation in the vertebra, the bottom layer of the phantom had optical properties comparable to cortical bone and the upper layer to cancellous bone. Most significantly, the fat fraction difference between the two layers was comparable. The cortical bone layer of the phantom was made of gelatin mixed with scattering particles (barium sulfate), ions (sodium chloride), and a preserving agent (sodium benzoate). The exact quantities are listed in Table 2.2. This layer did not contain any fat, so it had a fat fraction of zero. The top layer was made of pure coconut milk from the brand Go-Tan with a fat fraction of 18% [30]. Therefore, the difference in fat fraction between the two layers was 18%. This is close to the fat fraction difference between cancellous and cortical bone which varies between 20%-30% [31].

For the bone phantom production, the cortical bone layer was made by heating water, sodium chloride, barium sulfate, and sodium benzoate to 50° while stirring at 350 rpm. When the temperature reached 50°, gelatin was added and the temperature was raised to 70°. Thereafter, the mixture was cooled to 40° and poured into small cups. Finally, the cups with the mixture were stored in the freezer for one hour to allow the gelatin to harden. After the cortical layer was produced, the coconut milk was poured on top of the solid gelatin layer to complete the phantom. The thickness of the coconut layer was at least 5 mm.

Water	Sodium chloride	sodium benzoate	barium sulfate	gelatin
100 ml	1 g	0.1 g	3 g	15 g

TABLE 2.2: Quantities of substances in cortical bone phantom layer.

### Probe design

In both experiments, the focus was on investigating the effect of fiber angulation. Therefore, a fiber optic probe was designed where it was possible to change the relative angulation between the fibers. The fiber optic probe was built such that two optical fibers could be fixed within the probe and the relative angulation between the optical fibers at the distal end could change between 0° and 45°. The maximum angulation of 45° is chosen based on a minimum SNR value; if the angle is greater than 45 degrees, the SNR will be severely reduced. The SDS between the distal end of the optical fibers was 1.2 mm and independent of the angulation. The SDS was determined based on an earlier study that found 1.2 mm to be a good compromise between SNR and LAD [13]. The 3D model of the probe for different fiber angles and the exploded view including all parts of the probe are shown in Figure 2.4. Furthermore, 2D drawings including dimensions of all different parts are added to Appendix A.

The probe was designed in Solidworks [32] and pre-processed in PreForm [33]. The probe was printed with a Formlab 3B printer [34], out of the material Tough 1500 V1 [35], and with a layer thickness of 0.050 mm. After the probe was printed, two step-index multimode fiber optic cables from Thorlabs [36] were inserted in the probe. These specific optical cables have a core and cladding diameter of 0.24 mm,

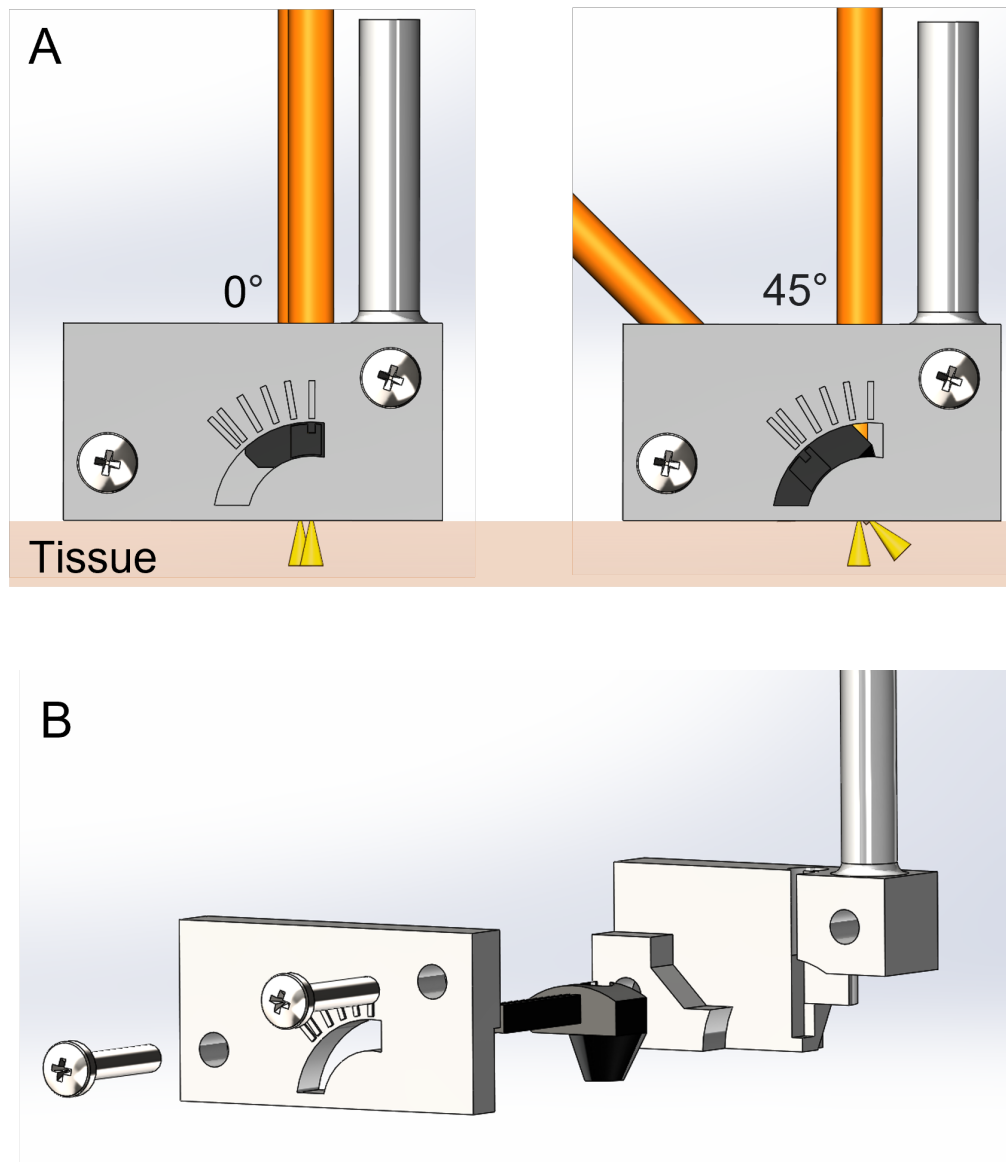


FIGURE 2.4: A) Probe design with adjustable relative angulation between the fibers (orange) and a constant SDS of 1.2 mm. The black part is the moving part to alter the fiber angulation. The yellow cones show the NA of the fibers. B) Exploded view of probe including all parts.

a coating diameter of 3.0 mm, a NA of 0.22, and a low OH concentration. The fibers were stripped at the distal end such that only the optical fiber core, cladding, and a thin protective layer were left. To ensure that the stripped optical fibers could be properly secured, two holes of 0.4 mm were drilled within the probe at the location where the light should leave or enter the probe. After the fibers were placed into the probe, the screws were tightened to hold all parts together. It was possible to change the angulation of the probe by loosening the screws and rotating the illumination fiber to a desired angle between 0° and 45°.

### Experimental measurements

The experimental setup consisted of the optical probe, a 3D printed holder, a micro stage, a spectrometer, and a bone phantom. The optical probe was fixed within the holder that was fixed to a micro stage. The spectrometer was connected to the optical probe, and a bone phantom was placed below the optical probe. The entire test set-up is shown in Figure 2.5. Before the measurements were started, the spectrometer and optical probe were calibrated. First, the spectrometer was internally calibrated for the wavelength, and afterward, the optical probe was calibrated for the intensity with a white reference (Spectralon white [37]). During the measurements the spectroscope emitted and collected light wavelengths from 900 to 1700 nm. The integration time of the spectrometer was 1000 ms.

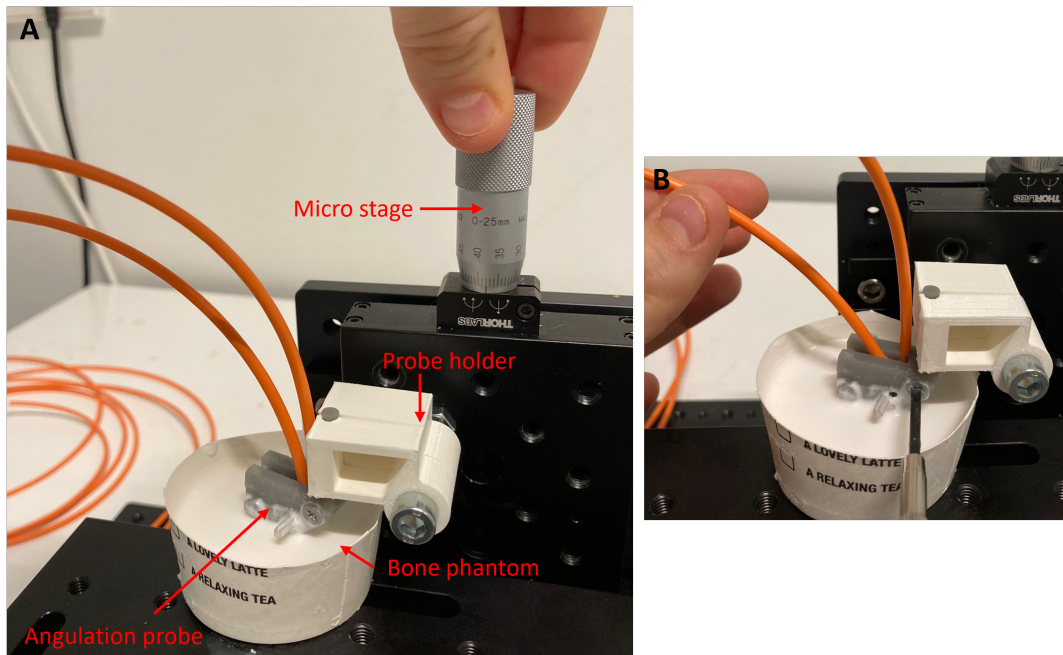


FIGURE 2.5: A) Test set-up including micro stage, 3d printed holder, probe for different fiber angulations, and a bone phantom. B) Test set-up showing manoeuvre to change angulation of probe between measurements.

The bone phantom including cancellous bone and a fully absorbing layer was used during Experiment 1. Before starting the measurements, the illumination fiber within the optical probe was fixed at an angle of  $0^\circ$  relative to the collecting fiber facing the absorbing layer. A bone phantom without the coconut milk on top was placed below the optical probe. The height of the optical probe was lowered until it was in direct contact with the fully absorbing layer. This was the starting point of the measurements, indicating 0 mm distance between the probe and the highly absorbing layer. At this point, coconut milk was poured on top of the absorbing layer. Reflection measurements were taken while varying the distance between the probe and the absorbing layer from 0 to 3 mm in 0.2 mm increments. At each distance, 10 reflectance measurements were taken. In addition, 10 measurements were taken in the pure cancellous bone layer without the absorbent layer underneath. The angulation of the probe was changed after the reflection measurements of all distances were measured for one angulation. This was done by unscrewing the screws securing the probe and rotating the illumination fiber towards the desired angle while

the collecting fiber always faced the absorbing layer. The same measurements were done for the other angulations,  $10^\circ$ ,  $20^\circ$ ,  $30^\circ$ , and  $45^\circ$ . Finally, for all angulations, all steps were repeated to triple the amount of measurements.

The bone phantom including cortical and cancellous bone was used during Experiment 2. The starting point of the measurements was defined as the point where the optical probe was in direct contact with the cortical bone layer. Reflection measurements were taken while varying the distance between the probe and the absorbing layer from 0 to 3 mm in 0.4 mm increments. Furthermore, 10 reflectance measurements were taken in the pure cortical and cancellous layer. Respectively, the experiment steps were the same as the first experiment.

### Data analysis

The raw data from the collected measurements by the spectrometer in both experiments contained the collected light intensity for all wavelengths. To get the reflectance spectrum out of the raw intensity, the following post-processing step was applied for all measurements for the wavelength range 900 nm - 1700 nm:

$$Reflectance(\lambda) = \frac{MeasuredIntensity(\lambda) - BackgroundIntensity(\lambda)}{CalibrationIntensity(\lambda)} \quad (2.4)$$

Furthermore, all reflectance spectra were filtered with a Savitzky-Golay smoothing filter of the third order with a frame length of 21. This is done to remove the noise from the reflectance spectrum.

The LAD and areas of highest optical sensitivity were investigated using the measurements of Experiment 1. The LAD and optical sensitivity were determined only for the light with a wavelength of 1211 nm. This wavelength was chosen since it is at this wavelength that the fat content impact is most noticeable. As a result, the LAD for which the probe can discriminate between cancellous and cortical bone was determined by the probing depth of this wavelength. The collected measurements contained the reflectance data for different fiber angles ( $\theta$ ) and distances between the absorbing layer and the optical probe ( $D$ ). Furthermore, the reflectance intensity of pure cancellous bone for all fiber angles was set as a reference ( $I_0(\theta)$ ), meaning no photons were absorbed by the absorbing layer. The ratio between the measured intensity at  $D$  ( $I(D, \theta)$ ) and  $I_0(\theta)$  determines the percentage of photons that does reach a certain tissue depth, calculated with the following formula:

$$P(D, \theta) = 100 - \frac{I(D, \theta)}{I_0(\theta)} * 100 \quad (2.5)$$

The relation of  $P$  versus  $D$  was determined for all different fiber angles, which made it possible to conclude the effect of fiber angulation on probing depth and optical sensitivity. The steepest slope of this relation showed the depth that is reached by the biggest amount of photons and, therefore, the depth with the highest optical sensitivity. The LAD was defined as the maximum depth which the photons can reach. The LAD follows from the point where the number of photons that reach a certain depth is bigger than 2 times the standard deviation (SD) of the measured intensity in pure cancellous bone [38].

Experiment 2 was designed to look into the effect of fiber angulation on the detection of the proximity of cortical bone. As explained in Section 2.1.1, the changes in reflectance spectra of light within the NIR region range 1000-1400 nm can be used

to distinguish between cancellous and cortical bone. To properly compare the variations in the reflectance spectra, all spectra were normalized to the intensity measured at the wavelength of 1211 nm. This normalizing wavelength was chosen because it best demonstrates the difference in fat absorption peak between the two phantom layers reflectance spectra. The reflectance spectrum of the pure cortical layer with a certain fiber angle was subtracted from all other spectra with the same fiber angle. This was done because the resulting spectra clearly highlight fat content's influence on the spectra for the different angulations. All the data with the same fiber angle and different distances from the cortical bone were combined into a single graph. The relation between change in reflectance spectrum and distance between probe and cortical bone was used to indicate the influence of cortical bone closeness on the spectra. By comparing this influence for different fiber angles, the effect of fiber angulation on the detection of cortical bone closeness was determined.

## 2.3 Results

### 2.3.1 Monte Carlo simulations

Figure 2.6A-E show an approximation of the photon paths of the collected photons through the tissue for different fiber angulations. The photon banana is depicted on the  $xz$  plane, with all photons projected on it in the  $y$ -direction. The colors in the diagrams represent the percentage of collected light that passes through a particular tissue area. The horizontal green line indicates that nearly the same percentage of collected photons reach the maximum depth for all fiber angulations. The vertical green line demonstrates that increasing the relative angulation between the fibers will increase the width of the photon banana. This has as an effect that the area of the photon banana and the average path length of the photons increases as well. The average path length of the photon banana with an angulation of  $0^\circ$  is approximately 1.8 mm, calculated by the circumference of a half-circle through the tissue area with the highest percentage of collected photons, see blue path in Figure 2.6A. It is assumed that the change in average path length is similar to the change in tissue area of the photon banana with the highest percentage of collected photons. The MC simulations show that when the angulation changes from  $0^\circ$  to  $45^\circ$ , the tissue area increases roughly 20%. Furthermore, Figure 2.6F shows that increasing the angle of the source reduces the intensity of the collected light. When the source has an angle of  $45^\circ$ , half of the amount of photons are collected compared to a source with an angle of  $0^\circ$ .

### 2.3.2 Experimental design

Figure 2.7A shows the measured intensity of light at 1211 nm of measurements in pure cancellous bone ( $I_0$ ) for different angulations. This graph shows that the intensity of collected light decreases when the angle of the emitting fiber increases. Furthermore, Figure 2.7B shows the relation between probing depth and percentage of collected photons that reach that depth for each fiber configuration. All SDs of the mean amount of photons that reach a certain depth for the different angulations overlap each other. Furthermore, the graph shows that for all angulations, 100% of photons reach a probing depth of 0 mm and nearly no photons reach the probing depth from 1.5 mm and beyond. When the probing depth is increased between 0 and 1.5 mm, the percentage of photons that reach a higher depth decreases. The graph's steepest slope occurs between 0.4 and 0.6 mm probing depth, as indicated

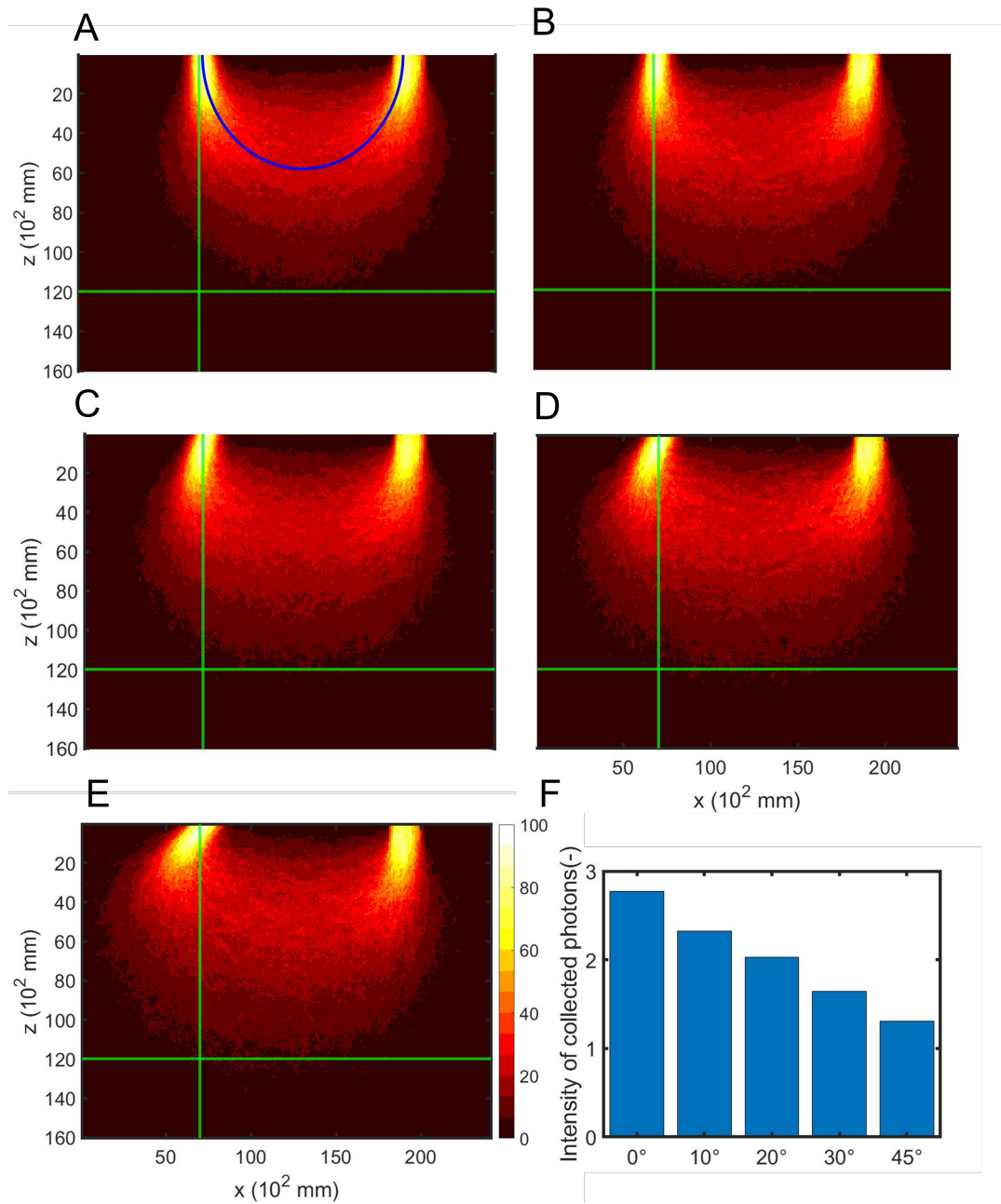


FIGURE 2.6: A-E) MC simulations of the photon banana in cancellous bone for different fiber angles (A-0°, B-10°, C-20°, D-30°, E-45°). The average path length with an angulation of 0° is represented by the blue line in (A). The color scale in the diagrams represent the percentage of collected light that passes through a particular tissue area. F) Intensity of total collected light for different fiber angles.

by the black stripped lines. The maximum standard deviation (SD) in the measured intensity at a depth that no photons reach is 3.7%. The intersection of the black solid lines indicates that the measured percentage of photons is greater than two times the maximum SD at a depth of 1.2 mm.

Figure 2.8A-E displays the difference between the measured DR spectra and the DR spectrum of pure cortical bone for various distances to the cortical bone layer

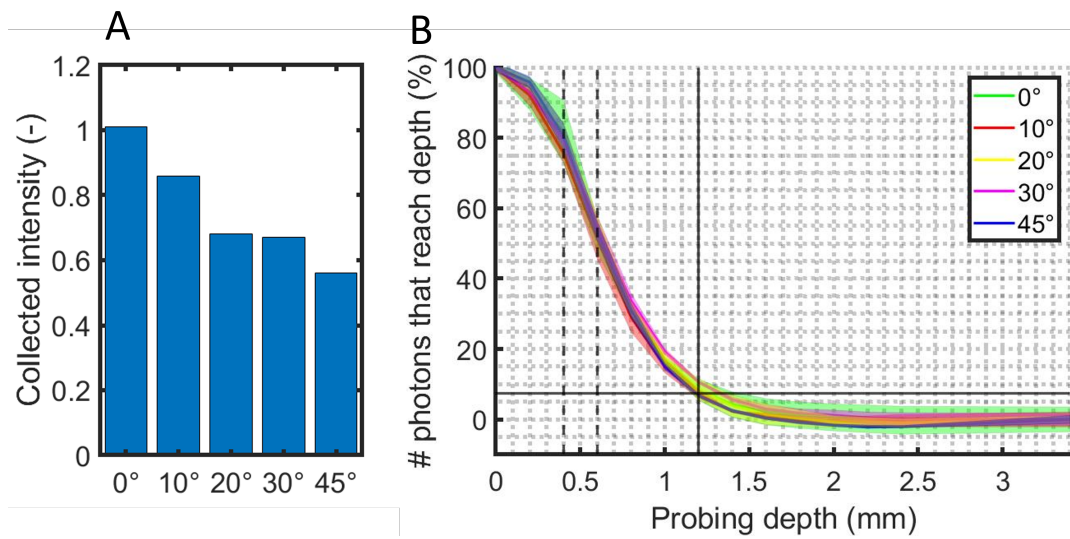


FIGURE 2.7: A) Intensity of collected light at wavelength of 1211 nm in pure cancellous bone for different fiber angulations B) Relation probing depth and amount of photons that reach a certain depth for different fiber angulations. This figure shows the mean amount of photons that reach a certain depth and the SD.

and various fiber angulations. The reflectance spectra at all distances and angulations show a dip around 1211 nm. Furthermore, the figure shows that for all angulations, the slope of the reflectance between 1100-1211 nm and 1211-1260 nm steadily increases as the distance from the cortical bone grows. Additionally, raising the angle of the emitting fiber gradually increases the difference between the reflectance spectra of pure cancellous and pure cortical bone.

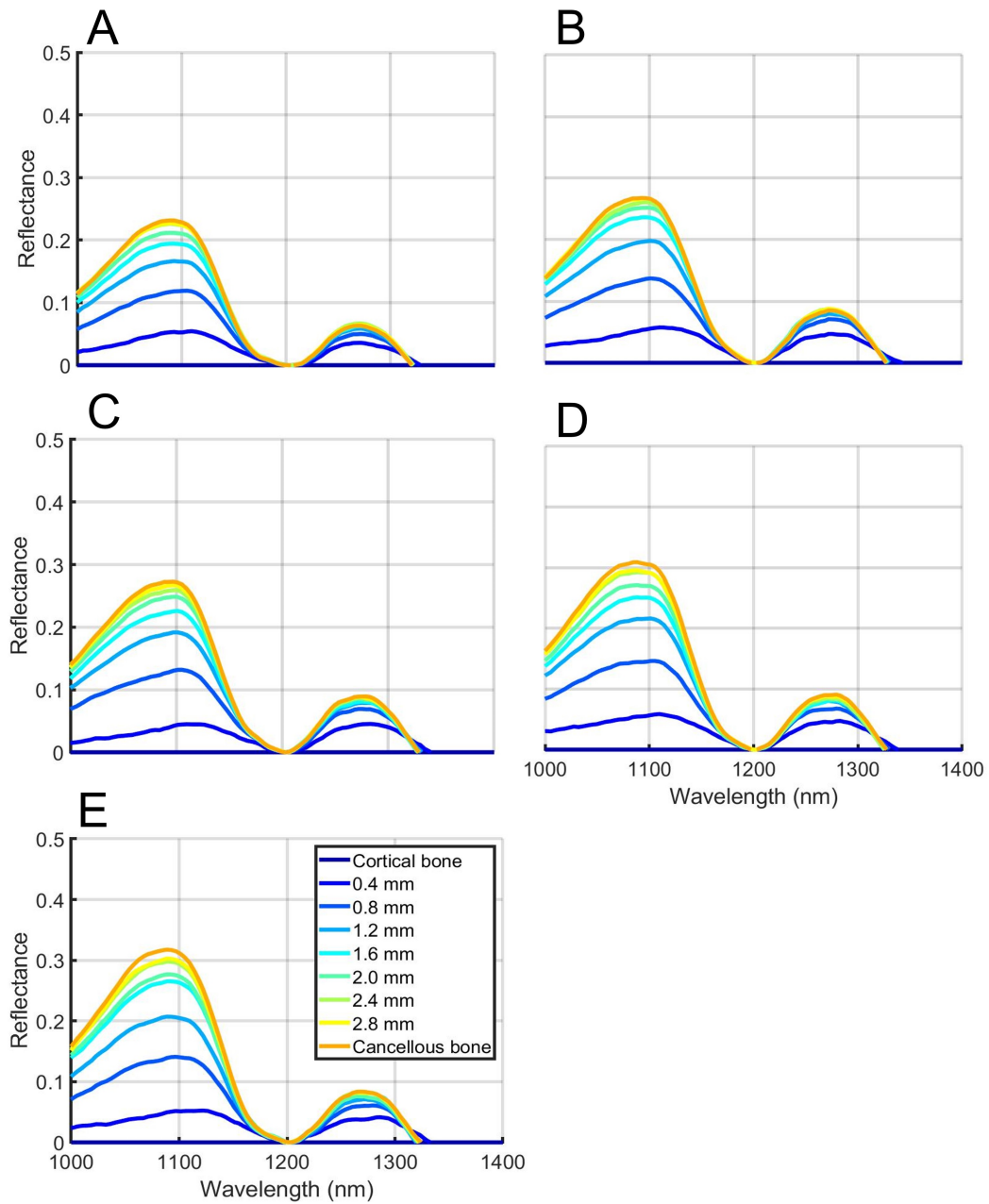


FIGURE 2.8: Difference between measured DR spectra at various distances to cortical bone and the pure cortical bone layer DR spectrum for varied fiber angulations (A-0°, B-10°, C-20°, D-30°, E-45°). All spectra are normalized at 1211 nm.

## 2.4 Discussion

### 2.4.1 Interpretation of the results

This study investigated the effect of angling the source in an optical probe away from the detector on detecting the proximity of cortical bone. The MC simulations show that the width of the photon banana slightly increases when increasing the angulation. However, the probing depth is independent of the angulation of the fibers. This can be explained by the fact that when the photons have traveled a short path, smaller than the transport mean free path length in tissue, the photon propagation is sensitive to the angle of emission [39]. However, in the deeper layers, total light diffusion occurs. This is because photons will lose their directionality after they have traveled a path that is longer than the transport mean free path length [40]. As a result, photons can be controlled in the more superficial layers. However, photons will diffuse randomly in all directions in the deeper layers, making it impossible to control the probing depth by angling the fibers.

Experiment 1 shows that the percentage of photons in a specific tissue layer is similar for all angulations. This is visible because the SDs of the detected proportion of photons overlap for all angulations. This implies that fiber angulation and LAD have no significant relationship, confirming the MC simulation findings. However, these findings are in contrast with the results of the studies of Thilwild et al. [23], Sing et al. [24], and Wang et al. [27], where it is found that the obliquity of fibers can control the depth of propagation. However, these studies were mainly focused on more superficial tissue layers (up to 0.5 mm) and inwards oriented fibers. As an outcome, it can be deduced that angling the fibers can change the depth of propagation in superficial layers in the tissue, but not in deep layers greater than 1.0 mm, as indicated in this study. This is supported by the fact that manipulating the direction of photons is only possible in the more superficial layers, as illustrated in the MC simulation. For all fiber angulations, the probe with an SDS of 1.2 mm has a LAD of 1.2 mm for light with a wavelength of 1211 nm. The probe has the highest optical sensitivity for the layers at a depth between 0.4 and 0.6 mm. These findings are in line with the LAD and optical sensitivity of a front-looking probe developed by Burström et al. [16], which has already proven its potential to detect the proximity of cortical bone with two parallel fibers. This suggests that a probe with fiber angles up to 45° should also be able to detect the proximity of cortical bone.

Additionally, the MC simulations and the results of Experiment 1 both show that increasing the angulation decreases the total intensity of collected photons. This supports the findings of previous studies by Thilwild et al. [23] and Wang et al. [27], where it is founded that outward-oriented fibers detect a lower amount of photons compared to parallel fibers. It can be explained by two factors: the directionality of photons, which causes fewer photons to propagate in the collector's direction, and the increase in path length due to the increase in width, which causes more light to be absorbed before it reaches the collector. According to the Lambert beer law for scattering medium [41], a 20 % increase in path length over an original path length of 1.8 mm due to a change in angulation to 45° reduces the intensity of collected photons by 25%. Therefore, of the 50% reduction in intensity observed in simulations and experiments, 25% is due to an increase in absorption and the remaining 25% should be attributed to a change in directionality. The decrease in the number of collected photons has as effect that the SNR decreases as the fiber angle increases [27].

Experiment 2 shows that a difference in DR spectrum between cortical bone and cancellous bone is visible for all angulations. The main difference is that the dip in the spectra around 1211 nm is deeper in the cancellous bone layer. This indicates that the difference in fat fraction between the tissue layers is detectable from the DR spectra measured with all fiber angulations. Furthermore, the results of this study show that the dip grows for all angulations as the distance to the cortical layer increases. This can be explained by the light entering the tissue up to a certain probing depth. When the distance to the cortical bone is smaller than the LAD of the probe, the light partially propagates through the cancellous layer and partially through the cortical layer. Increasing the distance to the cortical layer will increase the path length of the photons in the cancellous layer, which increases the amount of light absorption by the fat chromophores [42]. As a result, the amount of light absorbed at 1211 nm increases. A probe with a source angle up to 45° can identify the closeness of cortical bone based on the depth of the fat dip in the spectrum.

Furthermore, Experiment 2 shows that the difference in DR spectrum between pure cortical bone and pure cancellous bone increases as the fiber angulation increases. Therefore, the difference in DR spectrum between each increment of 0.4 mm increases as well. The signal difference is highest when the illumination fiber is at 45° relative to the collection fiber. The increase in the difference in DR spectrum between the cancellous bone and cortical bone for higher fiber angulations can be explained by the increase in path length of the photons through the tissue. As found in the results of the MC simulations, the width of the photon banana increases when the fiber angle increases. This has the effect that when the illumination fiber faces the tissue with an angle of 45°, the average path length within the cancellous bone layer increases. As an effect, the dip at 1211 nm will become deeper. The influence of approaching the cortical bone becomes more obvious in the spectrum for greater angulations, despite the lower SNR, because the difference between the cancellous and cortical bone spectra increases as the fiber angulation increases. These new findings could be utilized to improve the design of a fiber optic probe developed by Burström et al. [16] to prevent cortical breach or in the development of new fiber-optic probes to improve spinal fusion surgery.

### 2.4.2 Limitations

A significant drawback of the MC simulations in this study is that it is exclusively performed in the pure cancellous bone for only one wavelength to reduce simulation calculation time. As a result, the simulations do not show the effect of approaching the cortical bone. Therefore, it is difficult to say how the photon banana will alter as it enters the cortical bone at an angle. Earlier research by Swamy et al. [12] and Li et al. [19] demonstrates that MC simulations can be used to estimate the DR spectrum in cancellous bone for various distances from the cortical bone. Future research should focus on MC simulations to model the effect of angulation on the spectrum at different distances from the cortical bone layer. Because the experiments and MC simulations will be directly comparable, experimental findings such as the increase in the difference between the DR spectrum of cancellous and cortical bone as the angle increases will be easy to confirm.

Another relevant limitation of this study lies within the optical probe design. Because the optical fibers in the probe were not fixed, the actual location of the fiber terminating end could fluctuate slightly between measurements. This can affect the distance between the probe and the cortical bone. Therefore, the measured LAD can be slightly different from the probe's real LAD. However, the fluctuation in the

fibers is predicted to be minor because the SD between repeated measurements is always less than 5%. It should not have a substantial impact on the study's conclusion. Moreover, the step size of the experimental design has a more significant effect on the probe's LAD conclusion. Because of the 0.2 mm step size, the LAD has a 0.2 mm uncertainty. Although the LAD is between 1.2 and 1.4 mm, it is set to the lower to ensure that light always reaches the LAD [19]. The measurements should be repeated with a smaller step size to better estimate the actual LAD.

Another limitation of this study is the design of the optical bone phantom. The difference in fat percentages between the cancellous and cortical layer in the bone phantom (18%) are not exactly similar as human bone (20-30%) [31]. Furthermore, the bone phantom is made up of two homogeneous tissue layers, whereas actual tissue is made up of heterogeneous tissue layers consisting of a variety of chemical components [31]. Previous research by Swamy et al. [12] investigated that DR measurements in real vertebra are not directly comparable to simulation results on a two-layer model comprised of homogenous cancellous and cortical bone. According to Losch et al [31], the fat percentage in actual vertebrae is not uniform and gradually decreases as it approaches the cortical bone (the pre-cortical zone). As a result, the observed fat content drops gradually rather than abruptly in response to cortical bone closeness. Subsequently, when comparing measurements in real tissue to models or phantoms, the proximity of cortical bone is harder to identify. To see if it is also possible to detect the proximity of cortical bone when measuring in real cancellous bone, the optimal design that emerged from this study should be tested on actual tissue.

### 2.4.3 Conclusion

Conclusively, this research shows that fiber angulation up to  $45^\circ$  does not change the probing depth of an optical probe with an SDS of 1.2 mm. However, increasing the angulation of the emitting fiber up to  $45^\circ$  slightly increases the width of the photon banana. This means that the optical probe can detect the optical properties of a slightly wider area of the tissue. Furthermore, increasing the fiber angle decreases the SNR. However, the SNR is still large enough to identify the presence of cortical bone at an emitting angle of up to  $45^\circ$ . An emitting angle of  $45^\circ$  even results in a more significant difference in DR spectrum between cancellous and cortical bone due to a longer path length, making detecting cortical bone closeness easier.

In the scope of designing an optical probe that can be used in a steerable bone drill to detect the proximity of cortical bone, a probe with an SDS of 1.2 mm will measure the optical properties of tissue up to 1.2 mm depth. Furthermore, when the target tissue is parallel to the probe's longitudinal axis, the probe should emit light  $45^\circ$  off-axis and collect light  $90^\circ$  off-axis. This is the best optical design because it optimizes the measured tissue area and the difference in DR spectrum between the cancellous bone and cortical bone, making it easier to detect the proximity to cortical bone. This design will fulfill all the optical requirements, see Table 2.1.



## Chapter 3

# Flexible sideways-looking probe to detect proximity of cortical bone within vertebra: a conceptual design study

The goal of this chapter is to create a conceptual design of a sideways-looking probe that can be used in a steerable bone drill for spinal fusion surgery. All of the functional requirements, sub-functions, and specifications that the design should meet were defined in order to arrive at the best design. Several design strategies to implement the function within the design were investigated for all sub-functions. The methodical ACRREx design method was utilized to create a thorough overview of all strategies. ACRREx stands for Abstracting, Categorizing, Reflecting, Reformulating, and Extending [43]. The most promising strategies were integrated within a morphological scheme to create concepts [44]. Finally, each concept was rated to the design specifications. At the end of this chapter, the best conceptual design for a flexible sideways-looking probe to utilize in a steerable bone drill was found.

### 3.1 Design scope

#### 3.1.1 Functional requirements

The functional requirements describe the functions the design should fulfill. It is worth noting that this study is only focused on demonstrating the technical feasibility of employing a sideways-looking probe in a steerable bone drill to improve spinal fusion surgery. The design is not focused on a final product that can be used in clinical practice. Therefore, the requirements do not include requirements which should be based on user experiences such as usability, safety, and durability. These are design choices that can later be implemented to optimize the design. However, because this design is for research purposes, manufacturability is required. A prototype should be able to be manufactured within a specified time frame and with specific production capacities. The design of a sideways-looking probe for use in a steerable bone drill during spinal fusion surgery must meet three primary functional requirements. The probe should:

- measure diffuse reflectance spectrum of target tissue
- be insertable in curved hole in the vertebrae
- be manufacturable

### Measure diffuse reflectance spectrum of target tissue

The sideways-looking probe's first and most essential function is to measure the DR spectrum of tissue parallel to the drilling direction. Most sub-functions and specifications related to this function are extensively discussed in Chapter 2, see Table 2.1. These sub-functions were formulated to determine the ideal orientation of the light beams to measure the desired optical signal. However, when focusing on the best overall design of the probe itself, one additional sub-function is required to measure the DR spectrum of target tissue accurately.

- *Prevent light disturbances.* The probe should prevent light disturbances before the light comes in contact with the target tissue, the bone in the vertebrae. The probe must avoid light absorption and unwanted reflection and refraction, which results in a low SNR and incorrect measurements. Based on commonly used glue with excellent properties to fill optical probes, the maximum permitted absorption within the probe is 5% of the light intensity within the beam-width of the Gaussian beam exiting or entering the optical fiber [45]. In addition, the distance between the probe and the target tissue should not exceed 10% of the LAD. This will avoid light absorption in irrelevant tissue and ensure that the probe can penetrate at least 1 mm depth into the relevant tissue [12]. Based on the findings of the influence of angulation on the signal in Chapter 2, light refraction in undesired directions should be limited to a maximum of 10 degrees and there should be no internal reflection at the probe's interfaces.

### Be insertable in curved hole

The second primary function is that the probe should be insertable in a curved hole in the vertebrae. The probe should be included in a steerable bone drill that follows a curved path along the cortical shell in a vertebra. Due to the lack of knowledge on the drill's specific design, it is presumed in this study that a flexible probe that can be inserted into a curved hole in the spine is a generic design that can be employed in any steerable bone drill. Important in this assumption is that the curved hole should have a similar shape as the proposed drilling path. During spinal fusion surgery, the steerable bone drill will be used to drill a hole for a new anchoring system that will replace the pedicle screws. Most spinal fusion procedures, including pedicle screw placement, are conducted in the lumbar and thoracic regions of the spine [46]. To ensure that the probe will fit in drills that can be used by both sexes in these two zones, the size of the curved hole is based on the size of a female's smallest vertebra in the thoracic area [47, 48]. The following sub-functions are determined to ensure that the probe design can be appropriately inserted in the curved hole:

- *Fit in vertebra.* The probe should fit within the curved hole in the vertebra. The diameter of the probe should be no more than 3.5 mm, based on the size of the pedicles of the smallest vertebra in the thoracic region [47, 48].
- *Be flexible.* The probe should be flexible. Based on the dimensions of vertebrae, it should be possible to bend the probe with a minimal curvature radius of maximum 30 mm [47, 48].
- *Be robust.* The probe should be robust. The most critical part of the probe are the optical fibers [49]. No pulling forces should be applied directly to the fibers to minimize fiber breach, and bending forces should be limited to a maximum bending radius equal to the bending radius of the fibers.

## Be manufacturable

Lastly, the optical probe should be manufacturable. As the probe will be used for research purposes, it should be possible to produce the probe at Delft University of Technology. Furthermore, the probe should be cheap and fast to manufacture. The costs of the parts should not exceed 300 euros [50]. The time to produce the prototype should be within 1-2 weeks.

### 3.1.2 Specifications

A list of specifications related to the functional requirements and sub-functions is shown in Table 3.1. In general, there are different types of specifications, divided into must-have, performance, and delightful specifications [51]. Must-have specifications are those that the design must meet to be valid. Performance specifications are quantitative, with a number corresponding to satisfaction. Delightful specifications are wishes; it is a want to have them included in the design, but the design still functions without them. Because this design is solely focused on proving the technical feasibility, there are no delightful specifications included.

Functional requirements	Specifications	Nr.	Type
<b>Measure DR spectrum of target tissue</b>			
Illuminate target tissue	Target tissue: Parallel to drilling direction 1 mm depth	1	must-have
Collect light from target tissue	Light type: NIR light (1000-1400)	2	performance
	SNR: Able to detect different bone types	3	must-have
Prevent light disturbances	Absorption: Absorption in probe < 5% intensity	4	must-have
	Distance tissue and probe < 10% LAD	5	performance
	Reflection: No internal reflection	6	performance
	Refraction: Undesired light directional change < 10%	7	must-have
		8	performance
<b>Be insertable in curved hole in vertebra</b>			
Fit in vertebra	Diameter: 3.5 mm	9	performance
Be flexible	Curvature radius: 30 mm	10	performance
Be robust	Pulling forces: No pulling forces direct on fiber	11	must-have
	Bending forces: Maximum bending < bending radius fiber	12	must-have
<b>Be manufacturable</b>			
Is cheap to manufacture	Costs: Less than 300 euro	13	performance
Is fast to manufacture	Time: 1-2 weeks	14	performance
Is simple to manufacture	Production capacity: At Delft University	15	must-have

TABLE 3.1: List of functional requirements, sub-functions, specifications, and type of specification.

The final design should meet all of the specifications to the best of its ability. Table 3.2 can be used to score different concepts towards the specifications. The must-have specifications should always be included to have a functioning design. However, for the performance specifications, the level of fulfillment can vary based on a quantitative number. The fulfillment of a specification can be critical(-), basic (0), or optimal(+).

## 3.2 Design strategies

### 3.2.1 Measure diffuse reflectance spectrum of target tissue

There are various design challenges to appropriately measure the DR spectrum of the target tissue, which are defined in the previous paragraph as sub-functions that the design should fulfill. The best strategies to fulfill some of these sub-functions are already investigated in Chapter 2. As a result, only an overview of all conceivable design options has been generated for the remaining challenges.

Nr.	critical (-)	basic (0)	optimal (+)
[1] Tissue parallel to drilling direction	X	V	-
[2] Measurement depth in tissue	< 1 mm	1-2 mm	> 2mm
[3] NIR light	X	V	-
[4] Able to detect different bone types	X	V	-
[5] Light absorption in probe	> 5 % $I_0$	[1-5 %] $I_0$	< 1% $I_0$
[6] Distance probe tissue	>10% LAD	[1-10 %] LAD	<1% LAD
[7] No internal light reflection	X	V	-
[8] Undesired light refraction	>10°	10-1°	<1°
[9] Diameter	>3.5 mm	3.5-2.5 mm	<2.5 mm
[10] Curvature radius	>30 mm	30-25 mm	< 25 mm
[11] No pulling forces on fiber	X	V	-
[12] Maximum bending < bending radius fiber	X	V	-
[13] Costs	> 300 euro	300-100 euro	<100 euro
[14] Time	>2 weeks	1-2 weeks	< 1 week
[15] Production TU Delft	X	V	-

TABLE 3.2: Specification with different scores which describe degree of fulfilment, (-) is critical, (0) is basic, and (+) is optimal. V means that a must-have requirements is included and X means that a must-have requirement is not included.

### Illuminate target tissue/Collect light from target tissue

The optical experiments and simulations in Chapter 2 were mainly focused on investigating the ideal orientation of the optical fibers within the probe. This concluded that the best strategy is to emit light at 45° and collect light at 90° to the probe's longitudinal axis with a distance of 1.2 mm between the two fibers.

### Prevent light disturbances

A remaining challenge to correctly measure the DR spectrum of the target tissue is preventing light disturbances before the light comes in contact with the tissue. An overview of all possible design strategies to fulfill this function is shown in Figure 3.1. There are two methods to prevent light from being absorbed before it reaches the tissue. The first way is placing the fiber terminating end in direct contact with the tissue. However, when indirect contact between the fiber terminating end and the tissue is required due to design constraints, light absorption can be avoided by locating a totally transparent material between the fiber terminating end and the tissue. Internal reflection and unwanted refraction can be avoided by aligning the indices within the probe and between the probe and the tissue or modifying the probe's geometry such that light always enters surfaces between two materials at a 90° angle.

These solutions are all viable options for including into the design to prevent light disturbances before the light reaches the tissue.

### 3.2.2 Be insertable in curved hole

Aside from optical design considerations, the probe should fit into a curved hole in the vertebrae. The limitations of using the probe within a curved hole in the spine were not taken into account in the optical design strategy examined in Chapter 2. As a result, to create an optimal design, the optical design choices must be merged

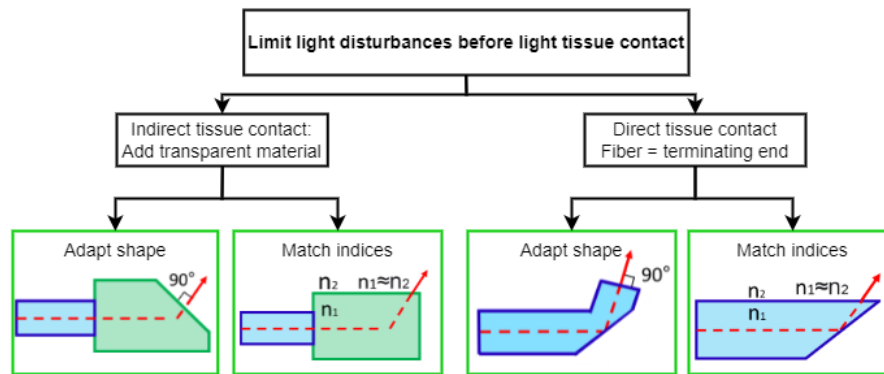


FIGURE 3.1: Acrcex tree of the function: prevent light disturbances. Blue beams are the optical fibers, the red line the light beam, and the green box the additional transparent material between the fiber and the tissue.

into a design that can be inserted into a curved hole in the vertebrae. To investigate all design possibilities, strategies for all sub-functions were created.

### Fit in vertebra

This function describes the first challenge for which several solution strategies must be developed to make the design insertable in a curved hole. An overview of all possible design strategies to fulfill this function is shown in Figure 3.2. For the proposed optical design, the light entering or exiting the fibers should be steered at an angle to the drilling direction. The light can be steered at either the distal or proximal end of the fiber. However, when steering light at the proximal end of the fiber, the complete fiber must rotate. This is not feasible within the limits of a maximum probe diameter of 3.5 mm. Therefore, the light should be steered in the desired direction at the distal end of the probe. A patent review of light steering in fiber-optic medical devices at the distal end was generated in the first part of this research project [14]. This review gives a comprehensive overview of all possible strategies to steer light. The distal end of the probe should have two fibers with a reflective surface that can be inside the optical fiber, at the fiber end surface, or outside the optical fiber to generate a sideways-looking probe. Furthermore, the surfaces can be separated in the longitudinal or radial direction.

The generation of a reflective surface at the fiber end or outside the optical fiber are the most promising strategies. The fibers can be separated in both radial and longitudinal directions. Because optical fibers cannot bend with the small radius required, using the reflective surface within the fiber is not possible.

### Be flexible

Another challenge is that the probe must be flexible enough to fit into a curved hole of various sizes. An overview of all possible design strategies to fulfill this function is shown in Figure 3.3. The different design possibilities of a flexible probe are that it can be either a continuous body or a segmented body. A segmented body can contain flexible segments, rigid segments, or a combination of flexible and rigid segments. A segmented body with rigid and flexible portions is the most promising design. A fully flexible body will not perform well since the light-guiding will not be stable, making the optical probe unpredictable and inaccurate. A design made

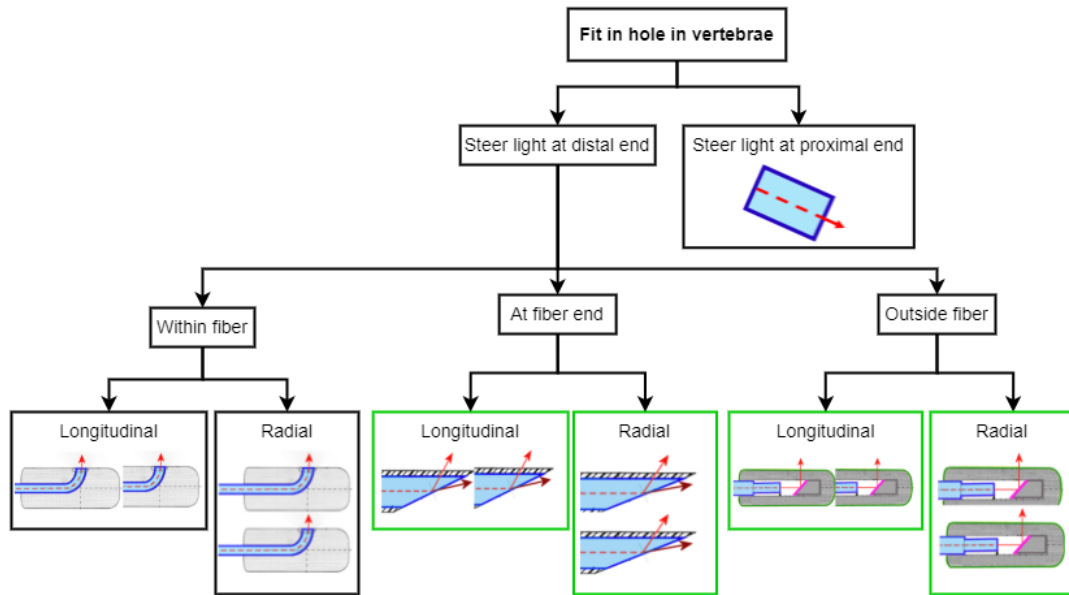


FIGURE 3.2: Acrcex tree of the function: probe should fit in hole in vertebra. Blue beams are the optical fibers, and the red lines the light beams.

entirely of rigid pieces will bend the fiber abruptly rather than gradually. As a result, due to the limited bending radius of the fibers, the probe can not be as flexible as desired.

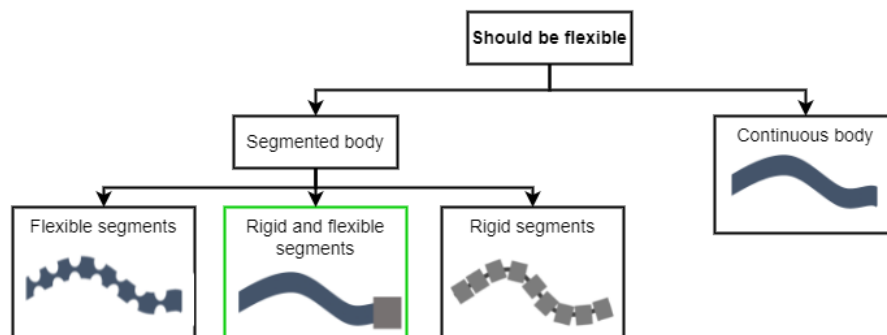


FIGURE 3.3: Acrcex tree of the function: probe should be flexible. The rigid parts are depicted in light grey, while the flexible parts are indicated in dark grey.

### Be robust

The third challenge is that the probe must be robust. An overview of all possible design strategies to fulfill this function is shown in Figure 3.4. The most critical aspect is that the optical fibers should not damage when using the probe. There are two strategies to prevent fiber damage: ensure that the fibers are strong enough to withstand all forces, or absorb the forces externally with a buffer layer. Because the fibers are designed to allow for maximum light transmission, using another material to increase the fiber's strength will have a negative impact on light transmission. Therefore, the best strategy is to use a buffer layer. This buffer layer can be open,

exposing the fibers to the environment or enclosed, surrounding the fibers. Furthermore, the fibers in the buffer layer can be loose or tightly coupled.

Using a surrounding buffer layer with the optical fibers loose is the most promising strategy. The fibers will be protected from tension, compression, and impact forces. An open buffer will not protect the fiber from impact forces, and a tight buffer will not protect the fiber from tension and compression forces [52].

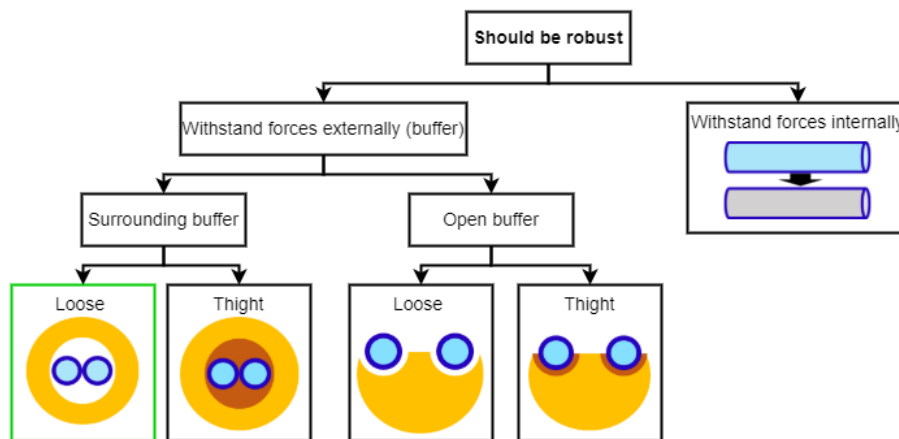


FIGURE 3.4: Acrcex tree of the function: probe should be robust. The buffer layer is indicated in yellow and the fibers in blue.

### 3.2.3 Be manufacturable

Another functional requirements is that the probe should be fast, cheap, and simple to manufacture. The focus of this design project is on 3D printing as a production process. This is chosen because the design freedom, speed, and low costs allow for the creation and testing of multiple concepts in several iterations [53]. In a research setting, this is desirable in order to study the best potential concept and prototype. 3D printing also has the advantage of being within the university's production capabilities, allowing manufacturing to be done on campus.

## 3.3 Concept design

### 3.3.1 Final design

The most promising strategies for all sub-functions were included in a morphological scheme, shown in Figure 3.5. A combination of all different potential strategies gives 16 different concepts. All concepts are scored towards the specifications, using Table 3.2. The different combinations with the corresponding score on the specifications are shown in Appendix B. The final design choices for all challenges are shown in yellow in the morphological scheme. Important optical and mechanical features are included in the final design.

#### Optical design

The optical part of the final design consists of two optical fibers separated in the longitudinal direction. The fibers within the probe are step-index multi-mode fiber optic cables from Thorlabs, with a core diameter of 0.2 mm, a NA of 0.22, and a

Functional requirements	Strategy 1	Strategy 2	Strategy 3	Strategy 4
<b>Measure DR spectrum:</b> Emit/Collect light				
Prevent light disturbances				
<b>Be insertable in curved hole:</b> Fit in hole in vertebra				
Is flexible				
Is robust				
<b>Manufacturable:</b>				

FIGURE 3.5: Morphological scheme of all functional requirements with most promising solutions. Yellow marked solutions show the final design.

low OH concentration [36]. These fibers ensure that the optical behavior is similar to the behavior investigated in Chapter 2. Both fibers are optically connected to a mirror. The light leaves or enters the probe at a terminating window designed on top of the probe. The space between the optical fibers and the mirror and between the mirror and the terminating window is filled with UV curable transparent glue. The UV curable transparent glue that is chosen is Norland Optical Adhesive 88 [54]. This adhesive is chosen because it has sufficient viscosity to fit into the small holes of the terminating windows and is transparent to NIR light. The glue has a refractive index of 1.56.

To predict the light behavior within the probe and to design the geometry of and distances between the optical components, an optical simulation in Zemax Optic-Studio was employed [55]. The simulation's purpose was to indicate how light beams propagate through the probe and interact with the optical elements. Because mainly reflection and refraction were expected, the simulations were run in Zemax's sequential mode. The illumination fiber and collecting fiber were simulated separately. Both simulations contained a fiber with a diameter of 0.2 mm and a NA of 0.22, a fully reflective mirror, and a terminating window. Furthermore, all empty space between the optical elements within the probe was filled with glass with a refractive index of 1.56. During spinal fusion surgery, the probe is considered to be in contact with the cancellous bone tissue or blood. As a result, the refractive index of the surrounding tissue is simulated in the range between 1.3-1.55 [56]. The light leaving or entering the optical fiber is designed as a Gaussian beam, meaning that the beam diameter is the light with 86% of the light intensity [57].

The Zemax simulations resulted in several design choices. The angle of the mirror connected to the emitting fiber is  $25^\circ$ , changing the direction of light with  $50^\circ$  which results, based on the difference in refractive index between the probe and the tissue, in the emitted light beam entering the tissue at an angle between  $42^\circ$ - $50^\circ$ . The angle of the mirror connected to the collecting fiber is  $45^\circ$ , changing the direction of light by  $90^\circ$  which results in light entering the probe at an angle of  $90^\circ$ . The mirrors and terminating windows diameters have been chosen to ensure that all light within an intensity of 86% is directed in the desired direction. Furthermore, the distances between the optical elements are selected so that light beam divergence is minimized and the light beams of the two distinct fibers do not overlap within the probe. The probe is blackened around the terminating windows to guarantee that only light within the beam-width enters or leaves the probe. The result of both simulations is shown in Figure 3.6. All diameters and distances of the optical elements are shown in Table 3.3. Resulting from the best optical design the SDS should be 1.2 mm. However, because of divergence, the simulation shows that a SDS of 1.2 mm is not possible without interference of the light beams of the two different fibers. Therefore was decided to increase the SDS of the final design to 2.1 mm.

SDS	2.1 mm
Diameter mirror collecting	0.6 mm
Diameter mirror emitting	1.4 mm
Diameter Terminating window collecting	0.7 mm
Diameter Terminating window emitting	1.5 mm
Distance mirror/mirror vertical ( $a$ )	0.8 mm
Distance mirror/mirror horizontal ( $b$ )	0.8 mm
Distance fiber and mirror collecting( $c$ )	0.5 mm
Distance fiber and mirror emitting( $d$ )	0.7 mm
Distance mirror and terminating window collecting ( $e$ )	0.8 mm
Distance mirror and terminating window emitting( $f$ )	1.6 mm

TABLE 3.3: Minimum sizes of optical elements in optical probe and distances between optical elements, see Figure 3.6.

### Mechanical design

The mechanical part of the conceptual design consists of a flexible buffer coating surrounding the optical fibers fixed to a rigid tip incorporating the optical design.

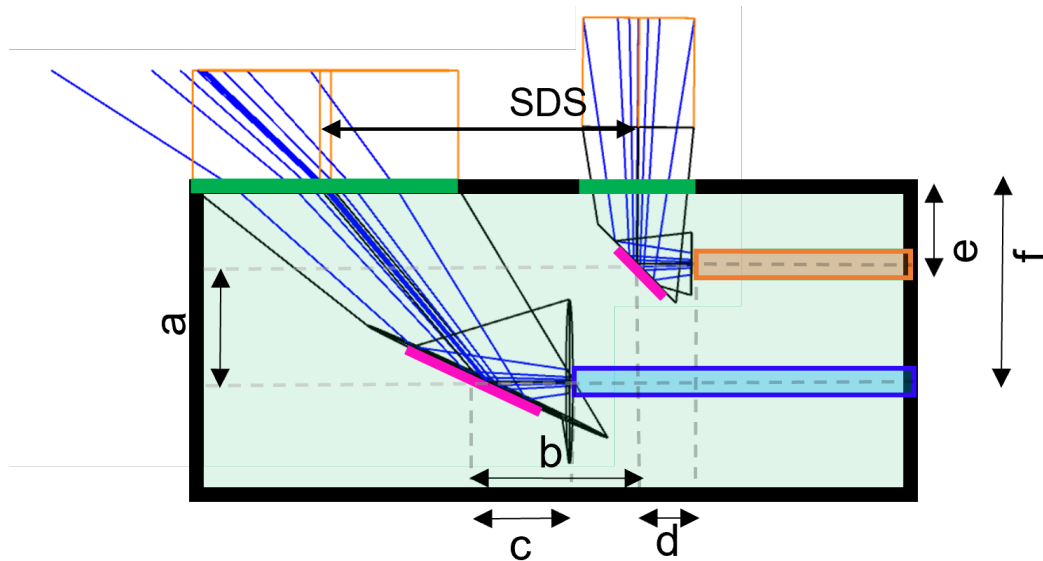


FIGURE 3.6: Side-view of optical probe including light behaviour. The blue beam is the emitting fiber and orange beam the collecting fiber. The blue lines are the light beams, the pink lines are the mirrors, and the green lines the terminating windows.

The used flexible coating is from Thorlabs, has a diameter of 2.3 mm, and is made of stainless steel [58]. This coating has the property of being flexible, although it can only bend to a minimum radius of 24 mm. The flexible coating is connected to the rigid tip by a cylindrical press-fit connection fixed by transparent glue [54]. The optical fibers are loose in the buffer coating, and only the coating is directly fixed to the rigid tip.

The rigid tip is composed of Formlabs Tough 1500 3D printing material [35]. The dimensions of the rigid tip are limited to ensure that the probe can be inserted in a curved hole. The rigid tip has a diameter of 2.9 mm and a length of 6.66 mm. These dimensions are a trade-off between maximizing the space for the optical elements, limiting the radial distance between the probe and the tissue, and minimizing the diameter and curvature radius of the hole. With this design, it should be possible to insert the probe in a curved hole with a diameter of 3.4 mm and a curvature radius of 24 mm, see Formula in Appendix C.

### 3.3.2 Theoretical performance

Based on the design geometry and material decisions, this conceptual design incorporates all the design specifications. This section discusses the level of fulfillment of all of the specifications, and Table 3.4 provides an overview.

The probe's optical design ensures that NIR light is emitted and collected in the same direction as was explored in Chapter 2 as the ideal design. However, the measured DR spectra from the tissue parallel to the probe can deviate slightly because the SDS and the spot size of the light beam entering the tissue are slightly larger than in Chapter 2. Based on the research of Hennessy et al. [18] on the effect of probe geometry on the optical properties, it is expected that the LAD is slightly greater than 1.2 mm and the SNR lower than investigated in Chapter 2. Because the SDS and the spot size are still in the size range of those explored in Chapter 2, it is expected that the probe should still be able to distinguish between cortical and cancellous bone

from the DR spectra. A prototype will be manufactured and validated to verify this hypothesis, detailed in Chapter 4.

The space between the optical fibers and terminating windows within the probe is filled with transparent glue. This adhesive absorbs less than 5% of the light in the NIR region, according to the transmission spectrum investigated by Norland [54]. This means that less than 5% of the light intensity within the beam width is absorbed inside the probe. The refractive index of the glue is 1.56 [54], and the refractive index of the surrounding tissue is in the range between 1.3-1.55 [56]. As a result, there will be no internal reflection, and the refraction of light beams at the probe-tissue interface will be maximum 5°.

Furthermore, the diameter of the probe is 2.9 mm, and the diameter of the curved hole in which it can be inserted is 3.4 mm. This means that the distance between the target tissue and probe can be maximum 0.5 mm, or approximately 40% of the probe's LAD. However, this is based on the assumption that the curved hole's wall has a high Young's modulus and hence is rigid. Because the cancellous bone is a spongy substance, it has a low Young's modulus [59], which means it is elastic. This causes the tissue to form around the probe, allowing the probe to be inserted into a curved hole with a diameter of 2.9 mm without leaving a gap between the probe and the tissue (0% of the probe's LAD). Future research should investigate if this assumption is correct when testing the probe in tissue.

The mechanical design of the probe results in a probe diameter of 2.9 mm and a minimum bending radius of 24 mm. The fibers minimum long-term bending radius is 24 mm, and the minimum short-term bending radius is 14 mm [36]. The tubing's limited bending radius assures that the fibers do not bend any further than the minimum fiber bending radius [58]. Furthermore, because the fibers are loose in the tubing that is rigidly attached to a rigid tip, all tension and compression forces will be applied to the tubing rather than the fibers.

The probe consists of seven components: two optical fibers, two mirrors, fiber tubing, transparent glue, and a rigid tip. Thorlabs produces the optical fibers, and fiber tubing [36, 58], and Norland produces the transparent glue [54]. It costs a total of 156.60 euros to purchase. A Formlabs 3D printer can be used to create the rigid tip with the features for the optical elements [34]. Furthermore, the mirrors can be made from any block of stainless steel with a wire EDM machine. Assuming that a 3D printer with several printing materials and a wire EDM machine is available in a research setting, these steps will not incur many additional expenditures. As a result, the probe may be manufactured in less than a week and for less than 300 euros.

The theoretical performance demonstrates that the conceptual design incorporates all specifications, thereby meeting all functional requirements. This suggests that the probe design presented in this chapter could be utilized to measure the parallel closeness of cortical bone when measuring along the cortical wall of a vertebra. A prototype was created and tested to validate the design's performance and debate enhancement options, as explained in Chapter 4.

Despite the positive expected performance, the design already has a significant limitation: the conceptual design is not a finalized product that can be utilized during spinal fusion surgery. However, it can only be used to demonstrate the potential of using a sideways-looking probe in a steerable bone drill to improve spinal fusion surgery. Several functional requirements focused on usability and safety should be added to the design to make a final product. An example of a critical specification related to safety is the use of bio-compatible materials; a list of possible materials for

the probe is listed in the research of Utzinger [45]. Usability requirements have to be developed in conjunction with clinical experts.

Nr.	critical (-)	basic (0)	optimal (+)
[1] Tissue parallel to drilling direction	X	V	-
[2] Measurement depth in tissue	< 1 mm	1-2 mm	> 2mm
[3] NIR light	X	V	-
[4] Able to detect different bone types	X	V	-
[5] Light absorption in probe	> 5 % I <sub>0</sub>	[1-5 %]I <sub>0</sub>	< 1% I <sub>0</sub>
[6] Distance probe tissue	>10% LAD	[1-10 %] LAD	<1% LAD
[7] No internal light reflection	X	V	-
[8] Undesired light refraction	>10°	10-1°	<1°
[9] Diameter	>3.5 mm	3.5-2.5 mm	<2.5 mm
[10] Curvature radius	>30 mm	30-25 mm	< 25 mm
[11] No pulling forces on fiber	X	V	-
[12] Maximum bending < bending radius fiber	X	V	-
[13] Costs	> 300 euro	300-100 euro	<100 euro
[14] Time	>2 weeks	1-2 weeks	< 1 week
[15] Production TU Delft	X	V	-

TABLE 3.4: Specification score of final design which describes level of fulfilment.

## Chapter 4

# Performance analysis of flexible sideways-looking probe: a phantom and ex-vivo study

### 4.1 Introduction

#### 4.1.1 Background

The conceptual design of a flexible sideways-looking probe developed in Chapter 3 is expected to be a functioning product. However, to adequately conclude the functioning of the design, a prototype should be built, tested, and validated. The primary purpose of the flexible probe is to detect the proximity of cortical bone when measuring the DR spectrum along the cortical wall of the vertebrae. The test setup should mimic the conditions of the probe within the vertebrae during spinal fusion surgery. There are two major components to these conditions. The prototype's optical properties should be tested on an object having similar optical properties to the vertebrae. Moreover, the prototype's mechanical properties should be tested on an object with a geometry similar to the desired drilling path of the steerable bone drill in the vertebrae. The drilling path should go through the vertebral pedicles and follow the cortical wall.

#### 4.1.2 Goal and structure

The aim of this chapter is to design, test, and validate a prototype of a flexible sideways-looking probe that could detect the proximity of cortical along the wall of the vertebrae. The conceptual design was first transformed into a prototype that should meet the main functional requirements. Secondly, the optical properties of the probe were tested by measuring the DR spectrum of a two-layer bone mimicking phantom. This test aimed to investigate if the probe can detect the proximity of cortical bone parallel to the longitudinal axis of the probe in an ideal phantom setting. Additionally, the probe was tested on ex-vivo porcine vertebrae. The purpose of this test was to see if the probe could still distinguish between the cortical and cancellous bone in real tissue with optical properties close to human tissue [60]. Lastly, the flexibility of the prototype was tested. This was done by simply inserting the probe in a curved hole with a geometry similar to the desired drilling path. A conclusion on the performance of the flexible sideways-looking probe design should be possible based on the findings of these experiments.

## 4.2 Method

### 4.2.1 Prototyping

#### Part production

The conceptual design developed in Chapter 3 was transformed into a prototype that can be tested toward the requirements. Critical of this prototype is that it matches all optical and mechanical specifications of the conceptual design. The prototype consists of 8 individual components: two optical fibers, stainless steel tubing, transparent glue, a fiber connector, a rigid tip, and two mirrors. The commercially available optical fibers [36], stainless steel fiber tubing [58], and transparent glue [54] were purchased from the respective suppliers. The fiber connector, rigid probe tip, and mirrors were designed and manufactured at Delft University.

The fiber connector's purpose is to allow two fibers to be placed into a single fiber tube. The fiber connector was designed in SolidWorks and preprocessed in Ultimaker Cura [32, 61]; technical drawings of the connector are shown in Appendix A. An Ultimaker S3 printer [62] was used to produce the fiber connector in PLA [63] with a layer thickness of 0.4 mm.

The rigid tip was designed in such a way that it can include all essential optical elements, as indicated in the optical design in Figure 3.6. The rigid tip was made of two parts. The first part was created to make connecting the fibers and fiber tubing to the rigid tip in the proper location as simple as possible. The second part was designed so that the mirrors could be easily placed and the light would travel in the proper direction to the terminating windows. Two holes of the correct size, see Table 3.3, were constructed to include the terminating windows in the design. The planes of the terminating windows were made straight so that a smooth glass surface could be produced on top of them during the production process. Finally, the two parts were made so that they fit together precisely and can be glued together to constrain rotation. The two parts of the rigid tip are shown in Figure 4.1, technical drawings of the two parts are shown in Appendix A.

The rigid tip was designed in Solidworks [32] and pre-processed in PreForm [33]. The probe was printed with a Formlabs 3B printer [34] in the material Tough 1500 V1 [35]. This material was chosen since it was discovered after numerous printing cycles that it would produce precise results for the small details within the rigid tip. The parts were printed with a 0.050 mm layer thickness. The small holes for connecting the fibers and the mirrors were closed during printing. Therefore, these holes were drilled at the correct location after printing.

The two mirrors were designed to direct the light in the desired direction. The mirror that is optically connected to the emitting fiber was designed under an angle of 25° to the fiber axis, and the mirror that is optically connected to the collecting fiber was designed under an angle of 45° to the fiber axis. To guarantee that all light is directed in the proper direction, the mirrors were slightly larger than the dimensions shown in Table 3.3. The mirrors are shown in pink in Figure 4.1. The mirrors were made out of a stainless steel block. First, a wire EDM machine was used to shape the stainless steel block to the correct dimensions. Secondly, the angled surface was polished to a mirror finish. Appendix A shows the exact dimensions of the mirrors.

#### Assembly

First, the optical fibers, fiber connector, and fiber tubing were combined into a 2.3 mm thick optical needle. The fibers coating was stripped away for 10 centimeters,

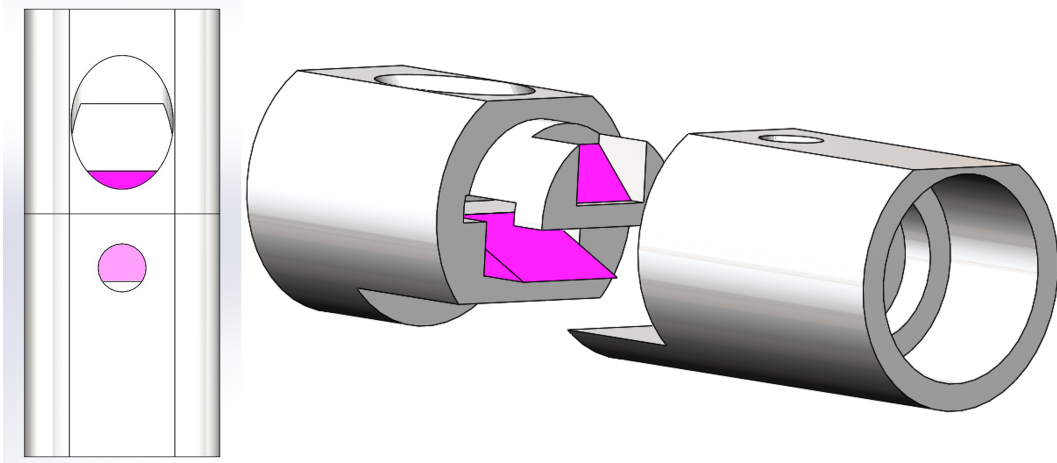


FIGURE 4.1: Rigid tip design consisting of the two rigid parts (grey) and two mirrors (pink).

leaving only the optical fiber core, cladding, and a thin protective layer. The stripped fibers were put into the fiber tubing. The remaining optical fiber coating and the fiber tubing were glued into the fiber connector. The result of this assembly step is shown in Figure 4.2A.

Second, the first part of the rigid tip was joined to the optical needle. The fibers were stripped of their thin protective coating and put into the holes in the rigid tip. In addition, the fiber tubing was pushed into the cylindrical hole. Then, UV curable adhesive was poured between the fiber tube and the rigid tip. The entire needle was placed under a UV lamp from Formlabs for 30 minutes to cure the adhesive [64].

Afterward, the mirrors were glued into the second part of the rigid tip, see Figure 4.2B. The part, including the mirrors, was coupled to the optical needle. Except for the terminating windows, the tip was painted black with black nail polish from Hema [65], see Figure 4.2C. Finally, the holes for the terminating windows were filled with UV curable transparent adhesive to secure the two parts together, prevent the needle from contamination, and match the refractive indices of the probe and tissue [54]. The adhesive was polished out with a small mirror and then exposed to a UV lamp for an additional 60 minutes to guarantee that the surface of the terminating windows was smooth [64]. The final prototype is shown inside a vertebra for scale in Figure 4.2D.

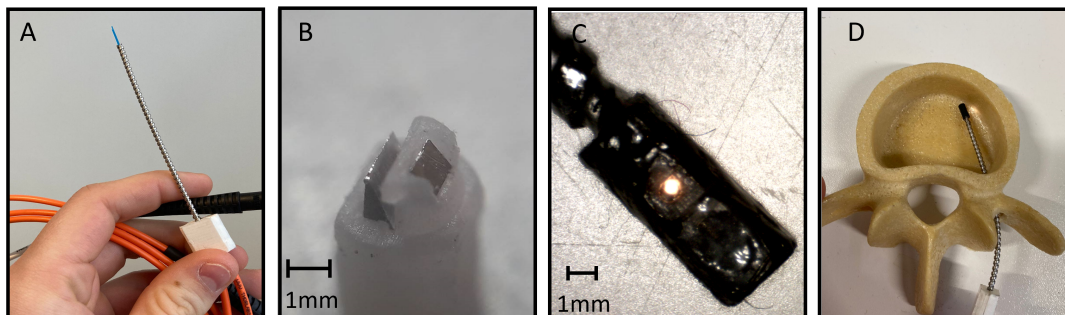


FIGURE 4.2: Assembly process of flexible optical probe. A) Optical needle. B) Microscopic picture of rigid part including small mirrors. C) Microscopic picture of final rigid tip design with light beam leaving the collection fiber. D) Final prototype.

## 4.2.2 Phantom experiments

### Phantom preparation

The phantom used during the experiments was a two-layer bone mimicking phantom. The bottom layer of the phantom had optical properties comparable to cortical bone and the upper layer to cancellous bone. The cortical bone and cancellous bone layer were made similar as described in Chapter 2. In contrast to the studies in Chapter 2, the two layers of the phantom were split horizontally rather than vertically. To make this, first the cortical bone layer was placed in a small square tray and cut in half to form a straight surface in the middle of the tray. Subsequently, the empty half of the tray was filled with coconut milk.

### Measurements

The experimental set-up consisted of the optical probe, a 3D printed holder, a micro stage, a spectrometer, and the bone phantom. The set-up is shown in Figure 4.3. Before the measurements were started, the spectrometer and the probe were calibrated as explained in Chapter 2. The spectroscope emitted and collected light with wavelengths 900-1700 nm during the measurements. The integration time of the spectrometer was 1000 ms.

As a starting point of the measurements, the probe was positioned in the cancellous bone layer with the cortical bone layer parallel to it and in contact with it. Important was that the terminating windows of the probe were in direct contact with the cortical bone layer. In this configuration, 5 reflection measurements were taken. Consecutively, the distance between the probe and the cortical bone layer was adjusted in steps of 0.5 mm from 0 to 3 mm, and 5 reflection measurements were taken at each distance. Subsequently, 5 measurements were taken in the pure cancellous bone layer without the proximity of the cortical bone layer. Finally, all steps were done three times in order to triple the amount of measurements.

### Data-analysis

The reflectance spectrum was calculated from the raw measurement data by using Formula 2.4. Furthermore, the data was filtered with a Savitzky-Golay smoothing filter of the third order with a frame length of 21. This is done to remove the noise from the reflectance spectrum.

The purpose of the phantom tests was to see if the probe could identify the proximity of cortical bone. The difference in the DR spectra measured in the cancellous bone layer with varying distances to the cortical bone layer can be used to investigate this. All DR spectra were normalized to the intensity observed at the wavelength of 1211 nm to compare the differences appropriately. Furthermore, all reflectance spectra from the same distance to cortical bone were averaged and represented as mean reflectance spectra with SD. The capacity to detect the proximity of cortical bone was determined by comparing all mean spectra and SDs.

## 4.2.3 Ex-vivo experiments

### Tissue preparation

Porcine vertebrae were used in the ex-vivo experiments. The pig spine was split in half along the spinal canal in the sagittal plane, and only one-half of the vertebrae were used in the experiment. The half vertebrae were restored in the freezer and

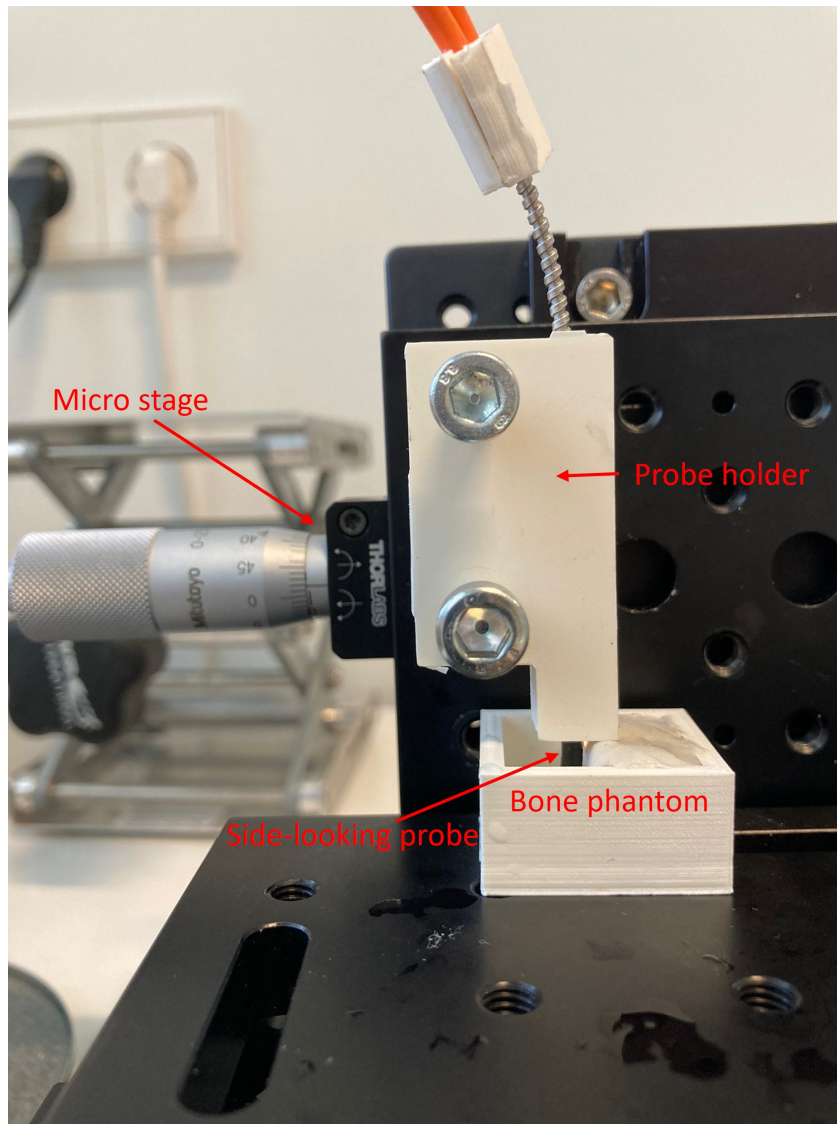


FIGURE 4.3: Test set-up of phantom experiments including micro stage, 3D printed holder, the side-looking probe, and bone phantom with only cortical bone layer.

taken out 3 hours before the start of the experiments. All distinct vertebrae were solely detached from each other just before the measurements. Finally, two vertebra were chosen for the experiment; these were vertebrae in which the boundary between cancellous and cortical bone was clearly visible.

### Measurements

The experimental set-up consisted of the optical probe, a spectrometer, a water bath, and the tissue. Before the measurements were started, the spectrometer and the probe were calibrated similarly to the phantom experiments. The spectroscope emitted and collected light with wavelengths 900-1700 nm during the measurements. The integration time of the spectrometer was 1000 ms.

The vertebrae were placed in a water bath during the experiments. When using the probe during spinal fusion surgery, blood is expected to be around the probe and the tissue. Because the functionality of the probe depends on the difference in

refractive index between the probe and the environment, the tests are performed in a water bath, as blood has a refractive index comparable to water [56]. DR measurements were taken by locating the terminating windows of the probe against cortical and cancellous tissue respectively, see Figure 4.4. First, 5 measurements were taken at 3 independent locations at the cancellous bone in the first vertebra. In addition, 5 measurements were taken at 3 independent locations at the cortical bone in the vertebra. Finally, the measurements steps were repeated in a second vertebra to double to amount of measurements.

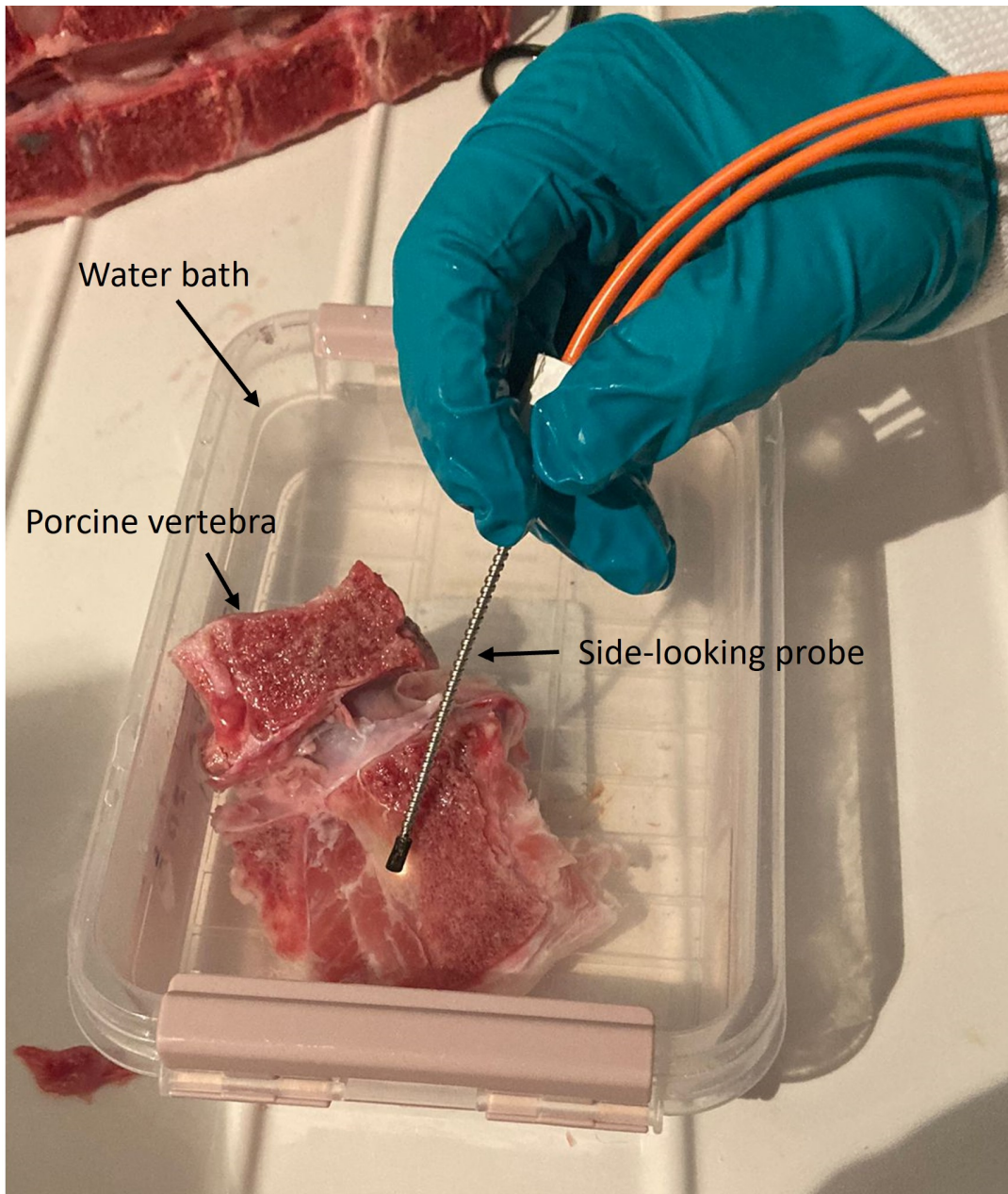


FIGURE 4.4: Measurement of DR spectrum of cortical bone in porcine vertebra with sideways-looking probe in water bath.

## Data-analysis

The reflectance spectrum was calculated from the raw measurement data by using Formula 2.4. Furthermore, the data was again filtered with a Savitzky-Golay smoothing filter of the third order with a frame length of 21. This is done to remove the noise from the reflectance spectrum.

The goal of the tissue experiment was to see if the probe could distinguish between the cortical and cancellous bone in actual tissue rather than in an ideal phantom setting. The difference in DR spectra between the two tissue types can be used to investigate this. All reflectance spectra were normalized to the intensity observed at the wavelength of 1211 nm to compare the different data appropriately. Furthermore, all reflectance spectra from the same tissue type were averaged and represented as a mean reflectance spectrum with SD. The probe's capacity to distinguish between cancellous and cortical bone tissue was determined by comparing the mean spectra and SD of the two tissue types.

### 4.2.4 Flexibility test

For the flexibility test, a geometric phantom was made. The dimensions of this phantom correspond to the mechanical requirements of the probe, which were based on the dimensions of the thoracic region's smallest vertebra [47, 48]. The phantom has a half-circular shape with a curvature radius of 24 mm and a curved hole in the edge with a diameter of 3.4 mm. The phantom was made in SolidWorks [32] and preprocessed in Ultimaker Cura [61]. The 2D drawing of the phantom is shown in Appendix A. Using the Ultimaker S3 printer [62], the phantom was 3D printed in PLA [63] with a layer thickness of 0.4 mm. To test if the probe is insertable in a curved hole in the vertebrae, the probe was inserted in the geometric phantom. To demonstrate that this was possible, pictures were taken, and the probe was examined for damage.

## 4.3 Results

### 4.3.1 Phantom experiments

The results of the phantom experiments are shown in Figure 4.5. This graph shows the normalized reflectance spectra between 1000-1400 nm measured from bone phantoms with different distances to cortical bone. This figure shows that there is a dip in the reflectance spectrum around 1211 nm for all measured distances. However, as shown clearly by the rise in slope in the spectrum between 1150-1211 nm, and 1211-1250 nm, this dip becomes steadily deeper as the distance to the cortical bone increases. In this region, the reflectance spectra of cortical bone at 0, 0.5, 1.0, and 1.5 mm distances show a significant difference from cancellous bone. On the other hand, the DR spectra of 2.0 mm and pure cancellous bone strongly overlap.

Furthermore, the reflectance in the region between 1000-1130 steadily increases from 1.0 mm up to 2.0 mm distance to cortical bone. However, the reflectance spectrum of pure cortical bone and 0.5 mm to cortical bone has different shapes. The observed reflectance and SD are higher compared with the other spectra.

### 4.3.2 Ex-vivo experiments

The results of the ex-vivo experiments are shown in Figure 4.6. This graph depicts the normalized reflectance spectra of porcine vertebra cancellous and cortical bone

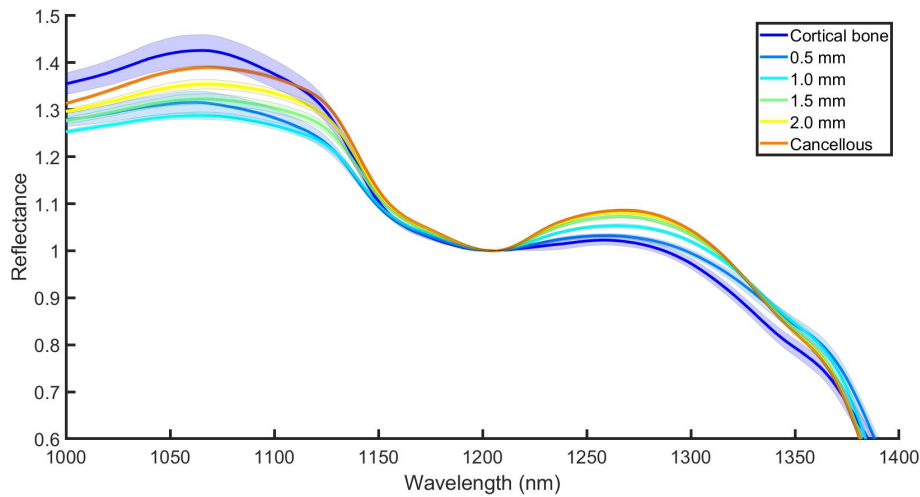


FIGURE 4.5: Normalized reflectance spectra measured from a two layer bone-mimicking phantom with different distances to cortical bone. The solid line represents the mean and the shaded region the SD.

measured between 1000 and 1400 nm. The reflectance spectra of both tissues show a dip around 1211 nm. However, the steeper slope in the spectra between 1130-1211 and 1211-1250 nm indicates that the cancellous bone spectrum has a deeper dip.

Additionally, the intensity in the spectrum of cancellous bone is also larger between 1000 and 1130 nm, but the SDs partially overlap in this region. Furthermore, the shape of the two spectra differs between 1000 and 1130 nm, leading the cancellous bone spectrum to peak at 1120 nm and the cortical bone spectrum to peak at 1050 nm.

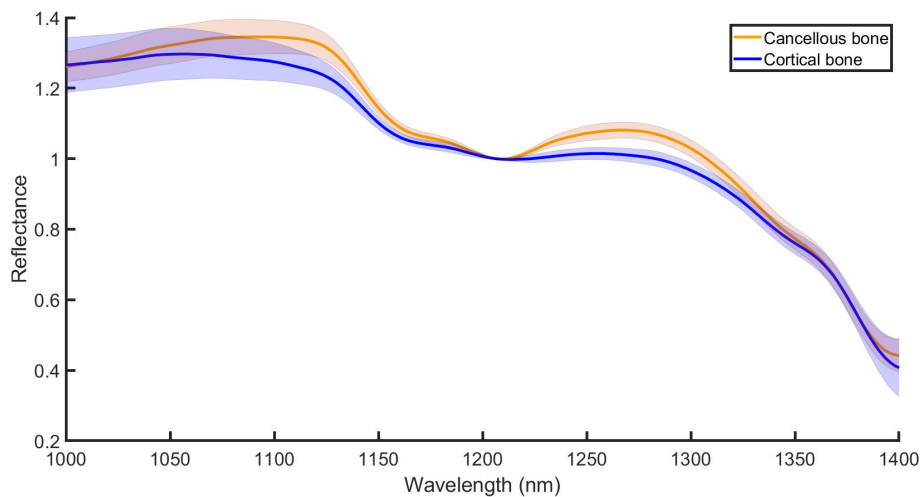


FIGURE 4.6: Normalized reflectance spectra measured from cancellous and cortical bone in a porcine vertebra. The solid line represents the mean and the shaded region the SD.

### 4.3.3 Flexibility tests

The result of the flexibility test is shown in Figure 4.7. This figure shows a picture of the probe inserted in a curved hole with a diameter of 3.4 mm and a curvature radius of 24 mm.

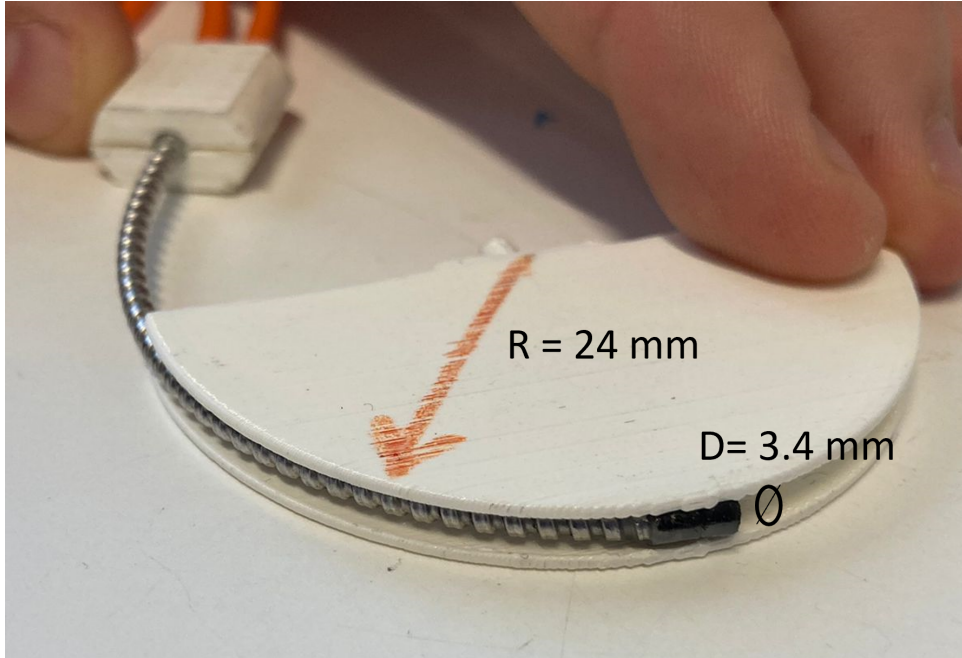


FIGURE 4.7: Picture of the optical probe inserted in a geometric phantom including a curved hole with a diameter of 3.4 mm and a curvature radius of 24 mm.

## 4.4 Discussion

### 4.4.1 Interpretation of the results

The goal of this study was to manufacture, test, and validate a prototype of the flexible sideways-looking probe designed in Chapter 3. This study shows that it is possible to manufacture a prototype that includes all optical and mechanical characteristics.

The phantom experiment demonstrates that the probe detects a different DR spectrum for cancellous and cortical bone positioned parallel to the probe. The main difference is that the dip in the spectra around 1211 nm is deeper in the cancellous bone layer. Furthermore, the results of this study show that the dip grows as the parallel distance to the cortical layer increases. As mentioned in detail in Chapter 2, this can be explained by the differences in fat fraction between the phantom layers in combination with the probing depth of the optical probe. The rise in the dip with increasing distance from the cortical bone is most noticeable between 1150 and 1300 nm. The DR spectra of the phantom with parallel distances to the cortical bone of 0 mm to 1.5 mm can be distinguished from those of pure cancellous bone based on the significant differences in this part of the spectrum. Conclusively, when tested in a phantom setting, the probe can determine the closeness of cortical bone while measuring within cancellous bone when the parallel distance to cortical bone is 1.5 mm or smaller. As a result, in addition to the previously developed front-looking

probe for frontal breach identification by Burström et al. [16], the probe created in this thesis improves spinal fusion surgery by providing an intraoperative method for parallel breach detection.

The tissue experiments show that the probe also detects a significant difference between the DR spectrum of cancellous and cortical bone in real tissue. The key difference is that the dip in the spectra at 1211 nm is deeper in the cancellous bone compared to cortical bone, which is similar to the phantom experiments. From this can be concluded that the probe developed in this study can distinguish between cancellous and cortical tissue based on the differences in fat fraction [13]. When the tissue data are paired with the phantom results, it suggests that spectra measured within a 1.5 mm distance to cortical tissue will fall somewhere between the cancellous and cortical tissue spectra. This indicates that the flexible sideways-looking probe can also be used to detect the parallel proximity of cortical bone in real tissue.

Even though the differences between the DR spectra obtained in tissue and a bone phantom are similar, the phantom and tissue studies show a notable difference. In the range of 1150-1300 nm, both results reveal a significant difference between the two measured spectra; however, the SD of the measured reflectance spectra on actual tissue is higher. The heterogeneity of tissue can explain this. The DR spectrum of cortical and cancellous bone varies between subjects and within a single subject [31]. Furthermore, as Losch et al. [31] discovered, the fat level in actual tissue steadily decreases as it approaches the cortical bone, with a lot of variance across subjects. As a result, the universal difference between the cancellous and cortical bone in real tissue is smaller. As investigated from the phantom experiments, it is possible to determine the proximity of cortical bone up to 1.5 mm distance. However, as detecting cortical bone proximity will be more complex in real tissue, the distance at which it can still be identified may reduce. Future research should concentrate on defining the universal difference between cancellous and cortical bone and enhancing the interpretation of the measurements to overcome this.

According to the phantom and tissue experiments, the DR spectrum of pure cortical bone has a slightly different shape and larger SD than the cancellous bone spectrum between 1000 and 1130 nm. The difference is most noticeable in the phantom studies. This effect can be tissue-specific, resulting from optical tissue characteristics like absorption and scattering, or spectral distortions generated by probe or experiment properties. A common cause of DR spectrum distortion is specular reflection, as shown in DRS studies in other areas such as soil [66] and chemical [67] compound research. The quantity of specular reflection depends on the surface material and geometry of the phantom or tissue. Nonetheless, because only experimental data is available, it is difficult to confirm what is causing the spectral differences in this study. MC simulations with the optical characteristics of the layers of the bone phantom and the tissue should be done and compared to the experimental data to investigate the source of the difference. The MC simulation on pure cancellous and cortical bone of Swamy et al. [12], see Figure 2.1, show that a spectral difference between 1000 and 1130 nm is visible in simulated spectra. Future MC simulations should focus on the change in the DR spectrum as it approaches the cortical bone to further understand this. If the MC simulations show similar differences between 1000 and 1130 nm as the experiments, it's reasonable to assume that the optical tissue properties are responsible. Future research should look at whether it makes distinguishing between cancellous and cortical bone more difficult or whether it can be used as a tool to determine cortical bone proximity.

Lastly, the flexibility test shows that it is possible to insert the probe in a curved hole with similar dimensions as the required drilling path during spinal fusion surgery.

From this and the optical experiments can be concluded that the flexible probe design developed in this study has the potential to be a proper functioning probe that can detect the proximity of cortical bone when measuring along the cortical wall of a vertebra. This probe opens the opportunity to improve spinal fusion surgery by increasing the cortical bone contact without perforating it.

#### 4.4.2 Limitations

The prototype's important limitation is the low SNR, which requires filtering to obtain a smooth DR spectrum from the measurements. The difference in DR spectrum between the cancellous bone and cortical bone in actual tissue is small [13]. Because of the necessity for filtering, some tissue-specific characteristics may be filtered out, and the difference becomes even smaller. To improve the accuracy of the probe, the SNR should be improved by increasing the intensity of light that reaches the collecting fiber. This can be done by improving the design of the optical probe developed in Chapter 3. A major improvement is diminishing the divergence of the emitting light beam so that the light reaches the tissue with smaller spot size. Because the emitting fiber's spot size is large, more light is lost, and a smaller percentage of emitted light reaches the collector [68, 69]. A simple way to decrease the divergence is by using optical fibers with a lower diameter or NA. Moreover, reducing the diameter of the probe or the distance between the optical elements also reduces the divergence of the light beams. As in Fulghum's sideways-looking probe design [70], the diameter of the probe can be lowered by using one mirror that emits light in a different direction than it collects. Additionally, adding a converging lens to the design, as in the sideways-looking probe of Jono et al. [71], or adding an additional fiber between the mirror and terminating window, as in the sideways-looking lung biopsy device of Reich et al. [72], are two ways to decrease the divergence of the light beam within the probe. Limiting the light beam's divergence has the additional advantage of allowing the SDS to decrease, which improves the SNR even further.

Furthermore, manufacturing the optical probe with a different technique than SLA 3D printing will also improve the probe's performance. Because the pieces were printed on a Formlabs printer, the minimum wall thickness and hence the area for the optical elements within the probe were limited. The light beam does not enter the mirrors in the exact same direction as intended due to the limited space combined with the 3D printer's inaccuracy influenced by material, process settings, and printer type [73]. Subsequently, some light is scattered within the probe, preventing it from reaching the tissue and collecting fiber. Changing the material and enhancing the precision will increase the SNR and hence the probe's performance. Furthermore, using a different material for the probe allows for a smaller diameter due to the thinner allowable wall thickness, enabling the probe to be used in smaller vertebrae as well [74]. Different types of bio-compatible metals, such as stainless steel, titanium, or aluminum, are suggested as suitable materials [45]. When a probe is made of metal, it can be made using a variety of extremely precise micro-machining techniques, such as wire EDM cutting [75].

The experimental setup of the ex-vivo experiment is the last limitation of this study. Due to the small number of measurements and substantial variability in optical properties of the tissue [31], the findings may be biased by the specific characteristics of the used pig or vertebra. According to the results of this study, the flexible sideways-looking probe can distinguish between the cortical and cancellous bone in this specific pig. However, it is difficult to conclude that this is true for all pigs of various weights and ages, let alone all humans. More ex-vivo measurements on more

distinct vertebrae should be conducted in future research. This allows the identification and elimination of vertebra-specific properties and a better understanding of the uniform differences between cancellous and cortical bone.

#### **4.4.3 Conclusion**

This chapter demonstrates that it is possible to manufacture a prototype of a flexible sideways-looking probe that is able to detect the proximity of cortical bone when measuring along the cortical wall of the vertebrae. The study results show that the prototype can detect the closeness of cortical bone located parallel to the probe at a depth up to 1.5 mm in an ideal phantom setting. Furthermore, the probe can also detect the differences in fat content between pure cancellous and cortical bone in porcine vertebrae. Moreover, the probe can be inserted in a curved hole with similar dimensions as the required drilling path during spinal fusion surgery. Conclusively, the probe developed in this study opens the opportunity to improve spinal fusion surgery by increasing the cortical bone contact without perforating it.

Future research should improve the SNR of the probe by reducing the divergence of the light beams and improving the accuracy of the optical element positioning within the probe. Furthermore, future research should focus on establishing the uniform differences between cancellous and cortical bone to improve the spectra interpretation.

## Chapter 5

# Overall conclusion

### 5.1 Conclusion

This thesis aims to design, prototype, and test a sideways-looking DRS probe that can detect the proximity of cortical bone when measuring along the cortical wall of a vertebra. The four research phases of this thesis demonstrate a structured approach to achieving the best possible design.

A patent review about already-existing fiber-integrated biomedical devices that can steer light indicates that the research topic of this thesis is relevant. The development of innovative sideways-looking probe designs will help healthcare by expanding the use of optical sensors in various new medical applications, including spinal fusion surgery.

New scientific findings have resulted from discovering the best fiber angulation for detecting the DR spectrum of tissue parallel to the longitudinal axis of the optical probe. The results demonstrate that the ideal light signal is achieved when the probe emits light  $45^\circ$  off-axis and collects light  $90^\circ$  off-axis. Because the emitting fiber is at a  $45^\circ$  angle to the collector rather than parallel, the probe can detect the optical properties of a slightly wider tissue area, and there is a more significant difference in the DR spectrum between cancellous and cortical bone.

The best approach for making the probe insertable into a vertebra combined with the ideal optical design results in a flexible sideways-looking probe design that meets all technical requirements. This concept comprises a flexible needle with two optical fibers attached to a rigid tip with a diameter of 2.9 mm. The rigid tip contains two mirrors directing light  $45^\circ$  toward tissue and collecting light  $90^\circ$  from tissue with an SDS of 2.1 mm.

A prototype was made that demonstrates that the designed probe can detect the parallel closeness of cortical bone at a depth up to 1.5 mm in an ideal phantom setting. Moreover, the manufactured prototype can also discriminate between pure cancellous and cortical bone in porcine vertebrae. Additionally, the probe can be placed into the pedicles and bent along a vertebra's cortical wall. Based on the positive results of all experiments, the flexible probe designed in this thesis can be used to identify the proximity of cortical bone while measuring along the cortical wall of a vertebra.

### 5.2 Future recommendations

Overall, the findings of this thesis show that the flexible sideways-looking probe created in this research has the potential to improve spinal fusion surgery by enabling an increase in cortical bone contact without perforating it. However, to be a usable product, it must overcome several challenges to improve the probe's accuracy and

increase the SNR. The optical elements must be optimized by reducing light beam divergence and increasing the accuracy of optical element positioning by using a different material such as metal. Before it can be used in clinical trials, the design must be improved for usability and safety. The exact requirements for usability and safety must be developed in collaboration with clinical experts.

Moreover, the sideways-looking probe should be combined with a front-looking probe to detect cortical bone closeness in all directions and provide 3D feedback to the surgeon during spinal fusion surgery. Because the sideways-looking probe emits light at a  $45^\circ$  angle to the drilling direction, it may easily be transformed into a probe that can measure tissue parallel to and in front of it by simply adding one extra collecting fiber facing the front. Based on the findings of this thesis, future research should design, prototype, and test a side- and front-looking probe.

Finally, before DRS measurements can be used to assist spinal fusion surgery, future research should focus on making the discrepancies between the cortical and cancellous bone in human tissue more interpretable. Obtaining DR spectra from pure cortical and cancellous bone should define all tissue-specific properties. A deeper understanding of the characteristic differences enables accurate identification of the tissue type being assessed.

# Bibliography

- [1] Rajae S, Bae S, Kanim L, Delamarter R. Spinal fusion in the United States: analysis of trends from 1998 to 2008. *Spine*. 2012 jan;37(1):67-76.
- [2] Marieb E, Hoehn K. *Human Anatomy Physiology*. Pearson Education Limited; 2015.
- [3] Izzo R, Guarnieri G, Guglielmi G, Muto M. Biomechanics of the spine. Part II: Spinal instability. *European Journal of Radiology*. 2013 jan;82(1):127-38.
- [4] Hartl R, Theodore N, Dickman CA, Sonntag VKH. Technique of thoracic pedicle screw fixation for trauma. *Operative Techniques in Neurosurgery*. 2004 mar;7(1):22-30.
- [5] Gaines J. The use of pedicle-screw internal fixation for the operative treatment of spinal disorders. *Journal of Bone and Joint Surgery - Series A*. 2000;82(10):1458-76.
- [6] Nouh MR. Spinal fusion-hardware construct: Basic concepts and imaging review. *World Journal of Radiology*. 2012;4(5):193.
- [7] Eswaran S, Gupta A, Adams M, Keaveny T. Cortical and trabecular load sharing in the human vertebral body. *Journal of bone and mineral research : the official journal of the American Society for Bone and Mineral Research*. 2006 feb;21(2):307-14.
- [8] Brasiliense LBC, Theodore N, Lazaro BCR, Sayed ZA, Deniz FE, Sonntag VKH, et al. Quantitative analysis of misplaced pedicle screws in the thoracic spine: how much pullout strength is lost?: Presented at the 2009 Joint Spine Section Meeting. *Journal of Neurosurgery: Spine*. 2010 may;12(5):503-8.
- [9] de Kater E. NWO – SPINE STABILIZATION;. Available from: <https://www.bitegroup.nl/category/research-projects/steerable-bone-drill/>.
- [10] Bydlon TM, Nachabé R, Ramanujam N, Sterenborg HJCM, Hendriks BHW. Chromophore based analyses of steady-state diffuse reflectance spectroscopy: current status and perspectives for clinical adoption. *Journal of Biophotonics*. 2015 jan;8(1-2):9-24.
- [11] Swamy A. Breach detection using diffuse reflectance spectroscopy during spinal screw placement; 2021. Available from: <https://doi.org/10.4233/uuid:8c5055e3-477e-438c-b722-f55d2c3e41fc>.
- [12] Swamy A, Burström G, Spliethoff J, Babic D, Reich C, Groen J, et al. Diffuse reflectance spectroscopy, a potential optical sensing technology for the detection of cortical breaches during spinal screw placement. *Journal of biomedical optics*. 2019 jan;24(1):1.

- [13] Swamy A, Spliethoff JW, Burström G, Babic D, Reich C, Groen J, et al. Diffuse reflectance spectroscopy for breach detection during pedicle screw placement: a first in vivo investigation in a porcine model. *BioMedical Engineering OnLine* 2020 19:1. 2020 jun;19(1):1-12.
- [14] Losch MS, Kardux F, Dankelman J, Benno, Hendriks BHW. Steering light in fiber-optic medical devices: a patent review. *Expert Review of Medical Devices*. 2022 mar:1-13.
- [15] Althobaiti M, Al-Naib I. Recent Developments in Instrumentation of Functional Near-Infrared Spectroscopy Systems. *Applied Sciences* 2020, Vol 10, Page 6522. 2020 sep;10(18):6522.
- [16] Burström G, Burström G, Swamy A, Swamy A, Spliethoff JW, Reich C, et al. Diffuse reflectance spectroscopy accurately identifies the pre-cortical zone to avoid impending pedicle screw breach in spinal fixation surgery. *Biomedical Optics Express*, Vol 10, Issue 11, pp 5905-5920. 2019 nov;10(11):5905-20.
- [17] Kholodtsova MN, Grachev PV, Savelieva TA, Kalyagina NA, Blondel W, Loschenov VB. Scattered and fluorescent photon track reconstruction in a biological tissue. *International Journal of Photoenergy*. 2014;2014.
- [18] Hennessy R, Goth W, Sharma M, Markey MK, Tunnell JW. Effect of probe geometry and optical properties on the sampling depth for diffuse reflectance spectroscopy. *Journal of biomedical optics*. 2014 oct;19(10):107002.
- [19] Li W, Liu Y, Qian Z. Determination of detection depth of optical probe in pedicle screw measurement device. *BioMedical Engineering Online*. 2014 nov;13(1).
- [20] Chatterjee S, Phillips JP, Kyriacou PA. Differential pathlength factor estimation for brain-like tissue from a single-layer Monte Carlo model. *Annual International Conference of the IEEE Engineering in Medicine and Biology Society IEEE Engineering in Medicine and Biology Society Annual International Conference*. 2015 nov;2015:3279-82.
- [21] Wang L, Ayaz H, Izzetoglu M. Investigation of the source-detector separation in near infrared spectroscopy for healthy and clinical applications. *Journal of biophotonics*. 2019 nov;12(11).
- [22] Ming A, Wang J, Bender JE, Pfefer J, Utzinger U, Drezek RA. Depth-sensitive reflectance measurements using obliquely oriented fiber probes. *Journal of Biomedical Optics*. 2005 jul;10(4):044017.
- [23] Thilwind RE, T'Hooft GW, Uzunbajakava N. Improved depth resolution in near-infrared diffuse reflectance spectroscopy using obliquely oriented fibers. *Journal of Biomedical Optics*. 2009 mar;14(2):024026.
- [24] Singh P, Pandey P, Shukla S, Naik N, Pradhan A. Modelling, Design and Validation of Spatially Resolved Reflectance Based Fiber Optic Probe for Epithelial Precancer Diagnostics. *Applied Sciences* 2020, Vol 10, Page 8836. 2020 dec;10(24):8836.
- [25] Prahl SA. A Monte Carlo model of light propagation in tissue. vol. 10305. *SPIE*; 1989. p. 105-14. *Proceedings Volume 10305, Dosimetry of Laser Radiation in Medicine and Biology*; 1030509, 1988, Berlin, Germany.

- [26] Marti D, Aasbjerg RNN, Andersen PEE, Hansen AKK. MCmatlab: an open-source, user-friendly, MATLAB-integrated three-dimensional Monte Carlo light transport solver with heat diffusion and tissue damage. *Journal of Biomedical Optics*. 2018 dec;23(12):121622.
- [27] Wang L, Jacques SL, Zheng L. MCML—Monte Carlo modeling of light transport in multi-layered tissues. *Computer Methods and Programs in Biomedicine*. 1995 jul;47(2):131-46.
- [28] HPX. Gaffer tape matt black;. Available from: <https://hpx.eu/product/gaffer-tape-matt-black/>.
- [29] Lepore M, Delfino I. Intralipid-Based Phantoms for the Development of New Optical Diagnostic Techniques. *The Open Biotechnology Journal*. 2019 dec;13(1):163-72.
- [30] Go-Tan. Coconut milk;. Available from: <https://www.go-tan.com/en/products/cocos/go-tan-kokosmelk-250-mlt-pak/>.
- [31] Losch MS, Swamy A, Elmi-Terander A, Edström E, Hendriks BHW, Dankelman J. Proton density fat fraction of the spinal column: an MRI cadaver study. *Biomedical engineering online*. 2021 dec;20(1).
- [32] SolidWorks. SolidWorks 3.19.0;.
- [33] PreForm. PreForm 3.19.0;.
- [34] Formlabs. Form 3B;. Available from: <https://dental.formlabs.com/products/form-3b/>.
- [35] Formlabs. SMA-SMA Fiber Patch Cable;. Available from: <https://formlabs.com/store/tough-1500-resin/>.
- [36] Thorlabs. SMA-SMA Fiber Patch Cable;. Available from: <https://www.thorlabs.com/thorproduct.cfm?partnumber=M25L02>.
- [37] Labsphere. Spectralon® Diffuse Reflectance Standards;. Available from: <https://labsphere.com/product/spectralon-diffuse-reflectance-standards/>.
- [38] Qian Z, Victor SS, Gu Y, Giller CA, Liu H, Benaron DA, et al. “Look-Ahead Distance” of a fiber probe used to assist neurosurgery: Phantom and Monte Carlo study. *Optics Express*, Vol 11, Issue 16, pp 1844-1855. 2003 aug;11(16):1844-55.
- [39] Depeursinge C, Bevilacqua F. Monte Carlo study of diffuse reflectance at source–detector separations close to one transport mean free path. *JOSA A*, Vol 16, Issue 12, pp 2935-2945. 1999 dec;16(12):2935-45.
- [40] Jacques SL, Pogue BW. Tutorial on diffuse light transport. *Journal of Biomedical Optics*. 2008 jul;13(4):041302.
- [41] Hernández SE, Rodríguez VD, Pérez J, Martín FA, Castellano MA, Gonzalez-Mora JL. Diffuse reflectance spectroscopy characterization of hemoglobin and intralipid solutions: in vitro measurements with continuous variation of absorption and scattering. *Journal of biomedical optics*. 2009;14(3):034026.
- [42] Swinehart DF, The E, Law BL. The Beer-Lambert Law. *Journal of Chemical Education*. 1962;39(7):333-5.

- [43] Breedveld P, Herder J, Tomiyama T. Teaching creativity in mechanical design. In: s n, editor. Diversity and Unity. Proceedings of IASDR2011. s.n.; 2011. p. 1-10. Diversity and Unity. Proceedings of IASDR2011, the 4th World Conference on Design Research ; Conference date: 31-10-2011 Through 04-11-2011.
- [44] van Boeijen A, Daalhuizen J, Zijlstra J, van der Schoor R. Delft Design Guide: Design strategies and methods. BIS Publishers; 2013.
- [45] Utzinger U, Richards-Kortum RR. Fiber optic probes for biomedical optical spectroscopy. *Journal of Biomedical Optics*. 2003 jan;8(1):121-47.
- [46] Puvanesarajah V, Liauw JA, Lo SF, Lina IA, Witham TF. Techniques and accuracy of thoracolumbar pedicle screw placement. *World Journal of Orthopedics*. 2014;5(2):112-23.
- [47] Singh R, Srivastva SK, Prasath CSV, Rohilla RK, Siwach R, Magu NK. Morphometric measurements of cadaveric thoracic spine in Indian population and its clinical applications. *Asian spine journal*. 2011 mar;5(1):20-34.
- [48] Muteti E, Teaching M, Hospital R, ElBadawi M. A CT-based study of the thoracic spine pedicle and pedicle-rib unit morphometry in a Kenyan population. *East African Orthopaedic Journal*. 2019 apr;13(1):2-7.
- [49] Biswas DR. Optical fiber coatings for biomedical applications. *Optical Engineering*. 1992 jul;31(7):1400-3.
- [50] The PediGuard for placing pedicle screws in spinal surgery Medtech innovation briefing. 2015.
- [51] Berger C, Blauth RE, Boger D. KANO'S METHODS FOR UNDERSTANDING CUSTOMER-DEFINED QUALITY; 1993. .
- [52] Méndez A, Morse TF. In: Specialty Optical Fibers Handbook, Chapter 4: Optical Fiber Coatings. Elsevier INC; 2007. .
- [53] Attaran M. The rise of 3-D printing: The advantages of additive manufacturing over traditional manufacturing. *Business Horizons*. 2017 sep;60(5):677-88.
- [54] Norland Products. Norland Optical Adhesive 81;. Available from: <https://www.norlandprod.com/adhesives/NOA%2081.html>.
- [55] Zemax. Zemax OpticStudio 22.1;.
- [56] Berke IM, Miola JP, David MA, Smith MK, Price C. Seeing through musculoskeletal tissues: Improving in situ imaging of bone and the lacunar canalicular system through optical clearing. *PLoS ONE*. 2016 mar;11(3).
- [57] Marshall GF. In: Gaussian Laser Beam Diameters. Boca Raton; 1985. .
- [58] Thorlabs. FT023SS - Ø2.3 mm Stainless Steel Tubing;. Available from: <https://www.thorlabs.com/thorproduct.cfm?partnumber=FT023SS>.
- [59] Nicholson PHF, Cheng XG, Lowet G, Boonen S, Davie MWJ, Dequeker J, et al. Structural and material mechanical properties of human vertebral cancellous bone. *Medical engineering & physics*. 1997 oct;19(8):729-37.

- [60] Bozkus H, Crawford NR, Chamberlain RH, Valenzuela TD, Espinoza A, Yüksel Z, et al. Comparative anatomy of the porcine and human thoracic spines with reference to thoracoscopic surgical techniques. *Surgical endoscopy*. 2005 dec;19(12):1652-65.
- [61] Ultimaker. Ultimaker Cura 4.13.0;.
- [62] Ultimaker. Ultimaker S3;. Available from: <https://ultimaker.com/nl/3d-printers/ultimaker-s3>.
- [63] Ultimaker. Ultimaker PLA;. Available from: <https://ultimaker.com/nl/materials/pla>.
- [64] Formlabs. Formlabs Form Cure;. Available from: <https://formlabs.com/store/form-cure/>.
- [65] Hema. longlasting nagellak;. Available from: [https://www.hema.nl/mooi-gezond/make-up/nagellak/long-lasting-nagellak/longlasting-nagellak-11241022.html?utm\\_source=Google%20Platform&utm\\_medium=Organic&utm\\_campaign=FreeShopping&gclid=Cj0KCQjwmPSSBhCNARIsAH3cYgYDBB171ytCcLPYFN4umP0oDQwfimhZIrMOK38uUa\\_qM0JW800hy90aAut0EALw\\_wcB&gclsrc=aw.ds](https://www.hema.nl/mooi-gezond/make-up/nagellak/long-lasting-nagellak/longlasting-nagellak-11241022.html?utm_source=Google%20Platform&utm_medium=Organic&utm_campaign=FreeShopping&gclid=Cj0KCQjwmPSSBhCNARIsAH3cYgYDBB171ytCcLPYFN4umP0oDQwfimhZIrMOK38uUa_qM0JW800hy90aAut0EALw_wcB&gclsrc=aw.ds).
- [66] Reeves JB, Francis BA, Hamilton SK. Specular reflection and diffuse reflectance spectroscopy of soils. *Applied Spectroscopy*. 2005 jan;59(1):39-46.
- [67] Kaihara M, Sato Y. Extraction of diffuse reflection spectrum on reflectance spectroscopy for solid or powder surfaces. *Spectrochimica Acta Part A: Molecular and Biomolecular Spectroscopy*. 2000 apr;56(5):897-900.
- [68] Arimoto H, Egawa M, Yamada Y. Depth profile of diffuse reflectance near-infrared spectroscopy for measurement of water content in skin. *Skin Research and Technology*. 2005 feb;11(1):27-35.
- [69] Zhu C, Liu Q, Ramanujam N. Effect of fiber optic probe geometry on depth-resolved fluorescence measurements from epithelial tissues: a Monte Carlo simulation. *Journal of Biomedical Optics*. 2003 apr;8(2):237-47.
- [70] Fulghum S. Optical probe for raman scattering from arterial tissue; United States Patent 20070038123, 2007.
- [71] Jono J, Takimura T, Tao S. Probe; United States Patent 20130209034, 2013.
- [72] Reich c, Hendriks bhw, Bierhoff W, Bydlon TM, Parthasarathy V, Stoffelen S. Side-looking lung biopsy device; World patent 2016030533, 2016.
- [73] Cuellar JS, Smit G, Zadpoor AA, Breedveld P. Ten guidelines for the design of non-assembly mechanisms: The case of 3D-printed prosthetic hands. *Proceedings of the Institution of Mechanical Engineers Part H, Journal of engineering in medicine*. 2018 sep;232(9):962-71.
- [74] Prameela MD, Prabhu LV, Murlimanju BV, Pai MM, Rai RL, Kumar CG. Anatomical dimensions of the typical cervical vertebrae and their clinical implications. *Eur J Anat*. 2020;24(1):9-15.
- [75] Masuzawa T, Tönshoff HK. Three-Dimensional Micromachining by Machine Tools. *CIRP Annals*. 1997 jan;46(2):621-8.



## Appendix A

# 2D Drawings

### All 2D drawings of designed parts:

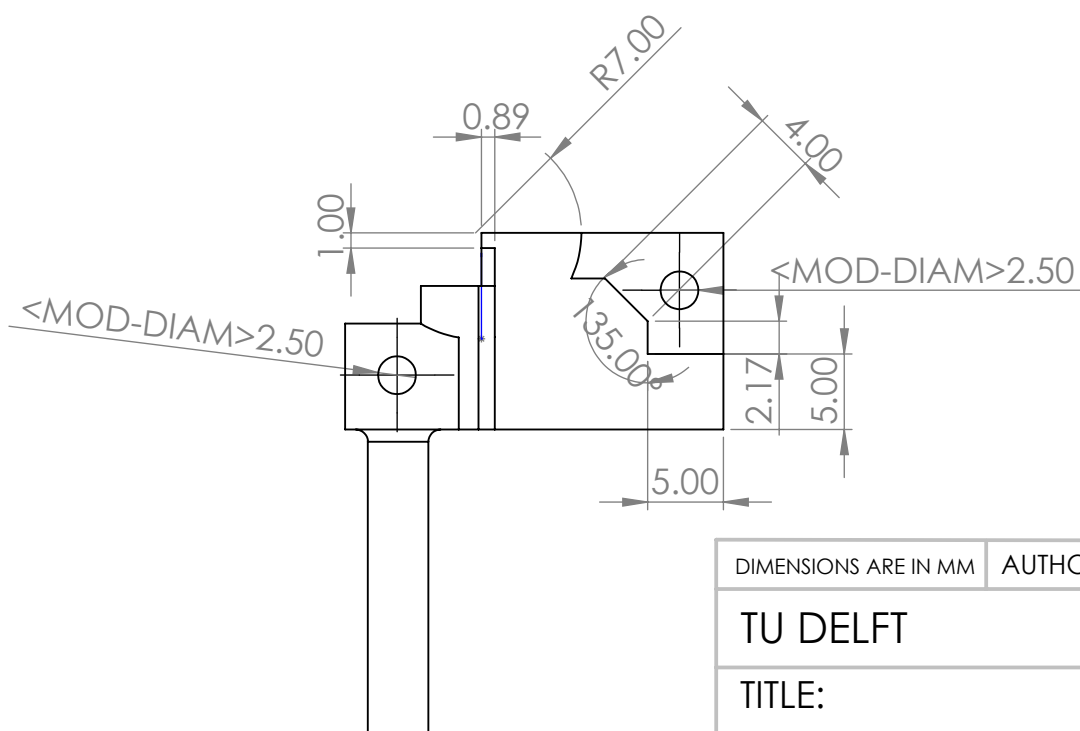
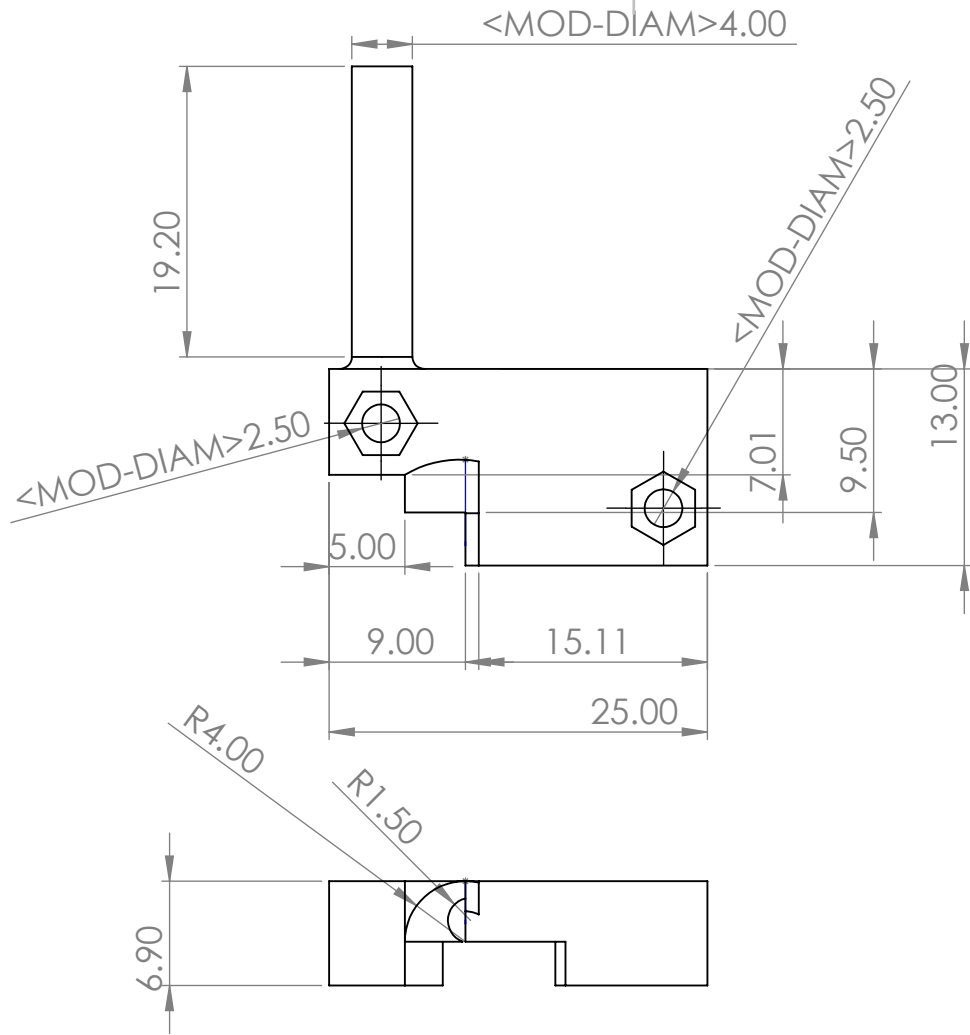
A1-A3 Parts of angulation probe

A4 fibers connector

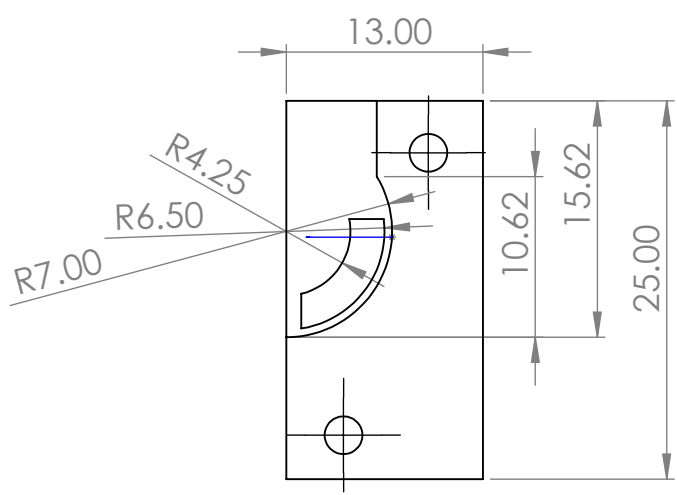
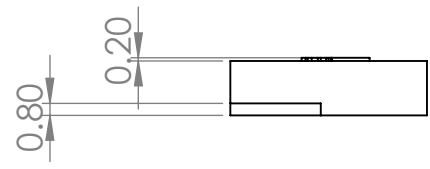
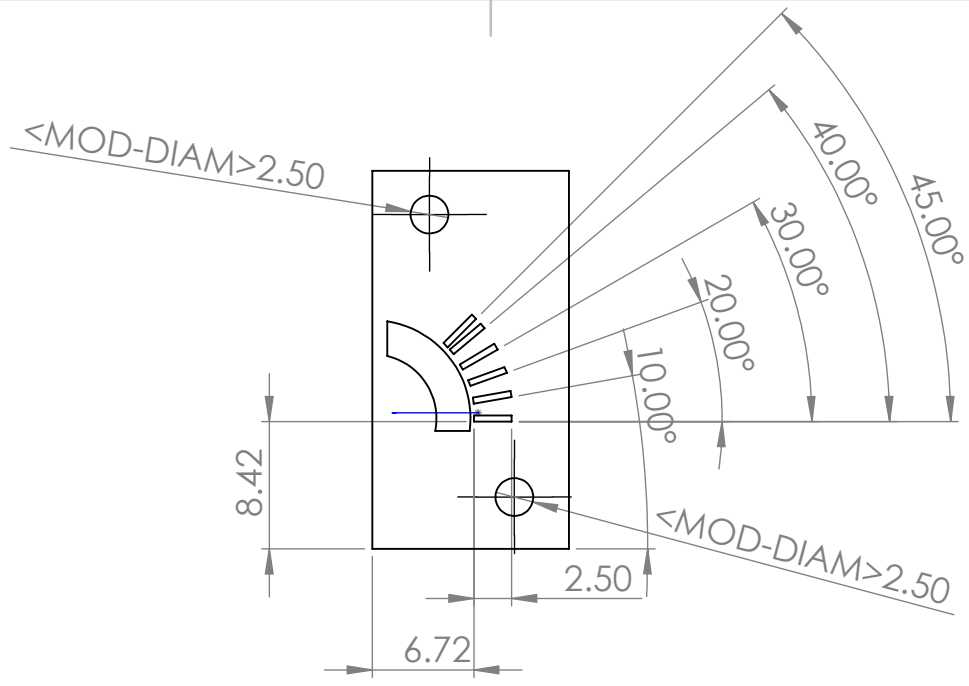
A5 Mall for flexibility tests

A6-A7 Mirrors of prototype

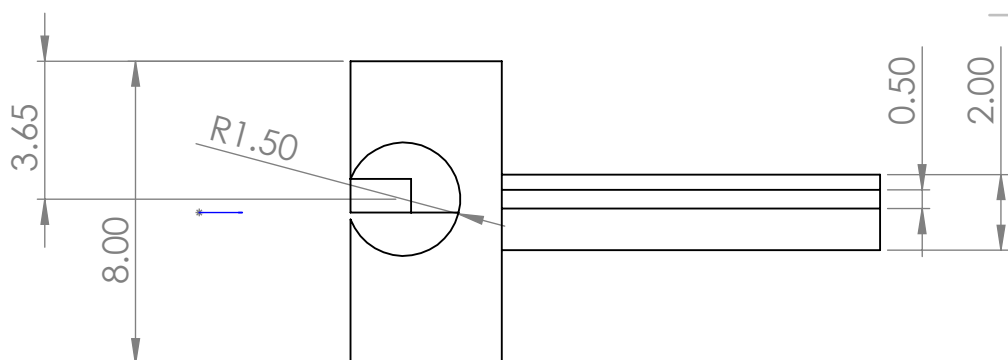
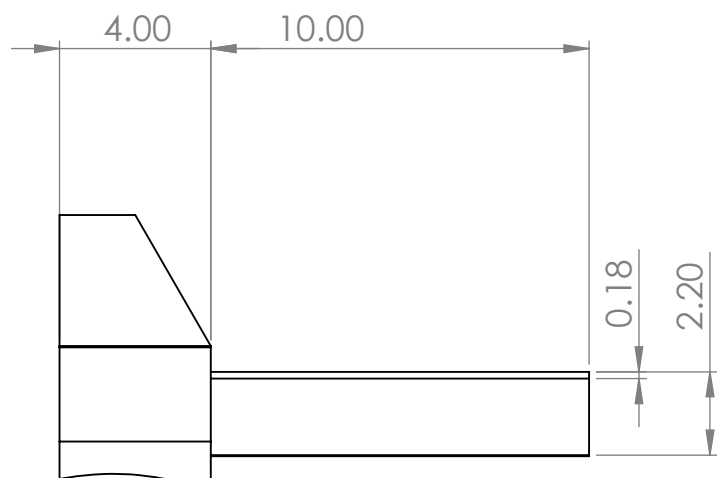
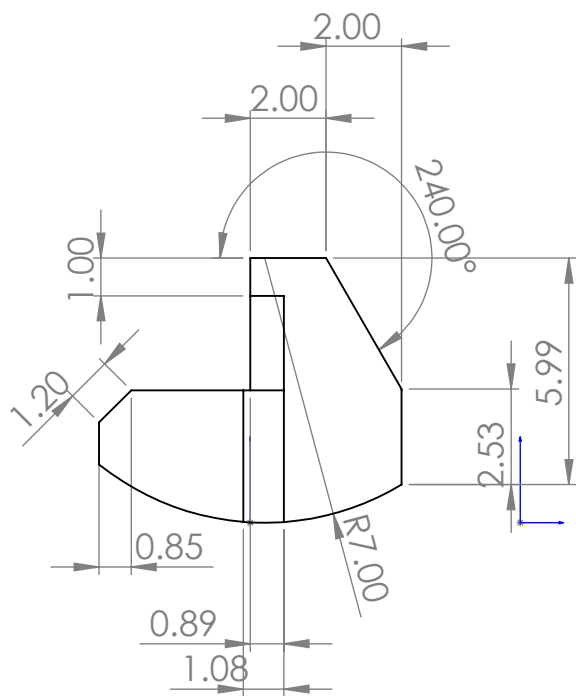
A8-A9 Parts of rigid tip of prototype



DIMENSIONS ARE IN MM		AUTHOR: FAMKE KARDUX	
TU DELFT			
TITLE:			
Angulation probe			
DWG NO.			A4
Angulation_1			
SCALE:2:1		SHEET 1 OF 1	



DIMENSIONS ARE IN MM		AUTHOR: FAMKE KARDUX	
TU DELFT			
TITLE:			
Angulation probe			
DWG NO.		A4	
Angulation_2			
SCALE:2:1		SHEET 1 OF 1	



DIMENSIONS ARE IN MM | AUTHOR: FAMKE KARDUX

TU DELFT

TITLE:

Angulation probe

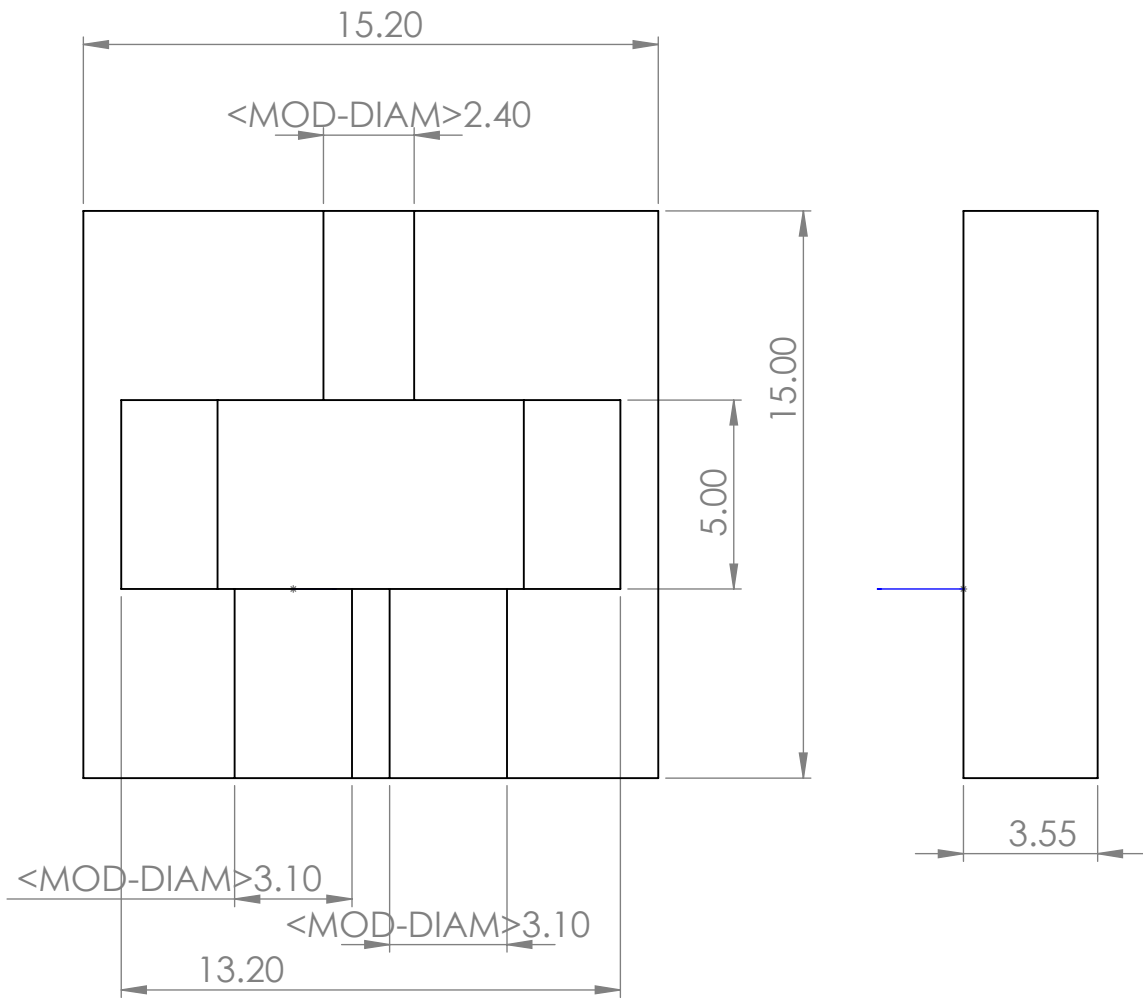
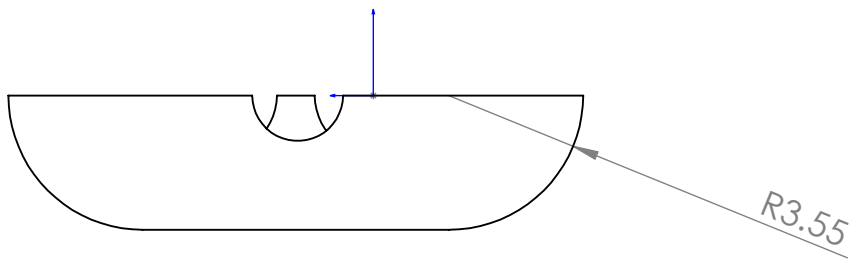
DWG NO.

Angulation\_3

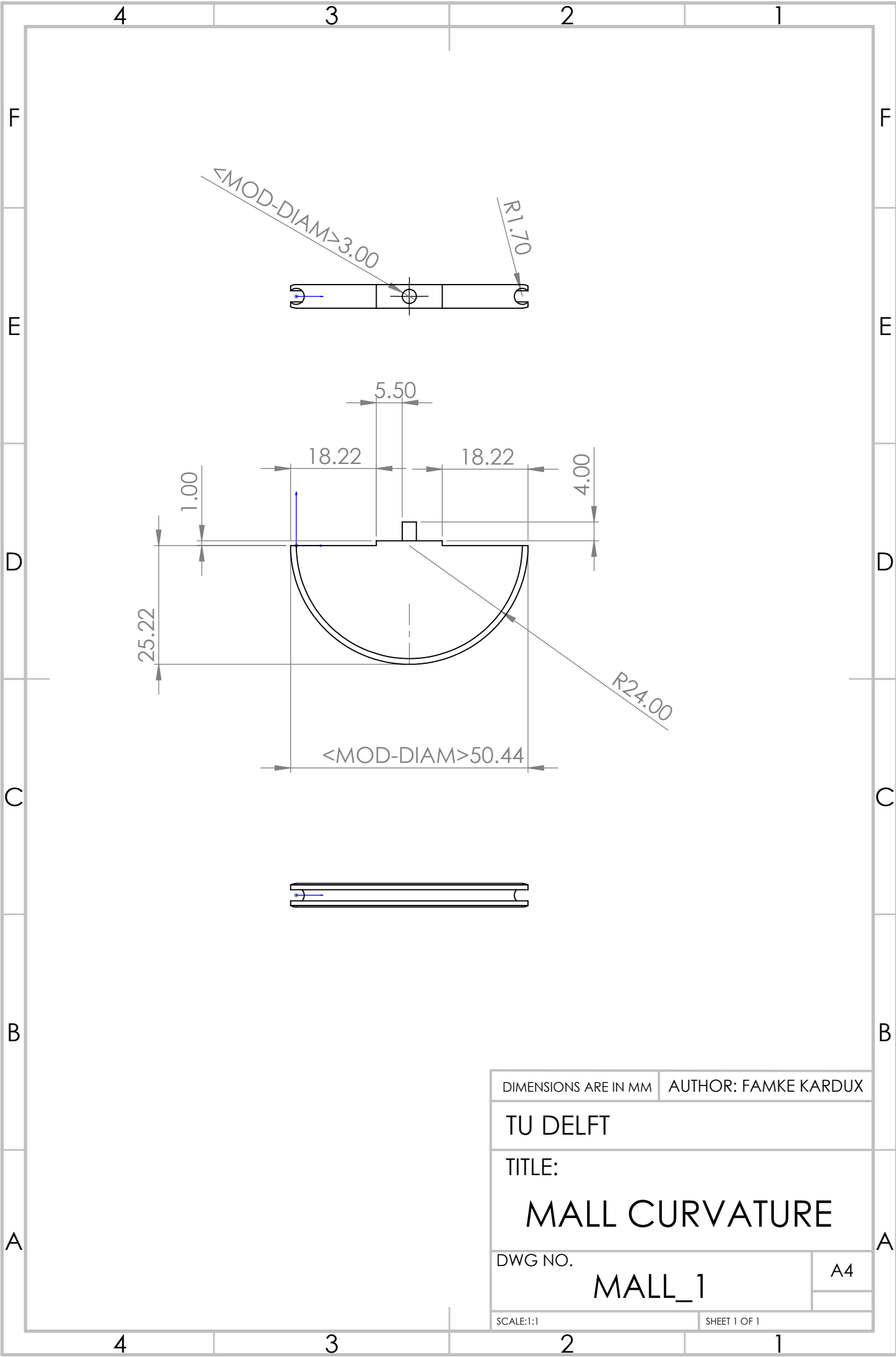
A4

SCALE:5:1

SHEET 1 OF 1



DIMENSIONS ARE IN MM		AUTHOR: FAMKE KARDUX	
TU DELFT			
TITLE:			
FIBER CONNECTOR			
DWG NO.		A4	
CONNECTOR_1			
SCALE:5:1		SHEET 1 OF 1	

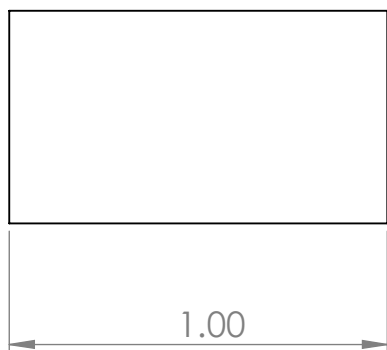
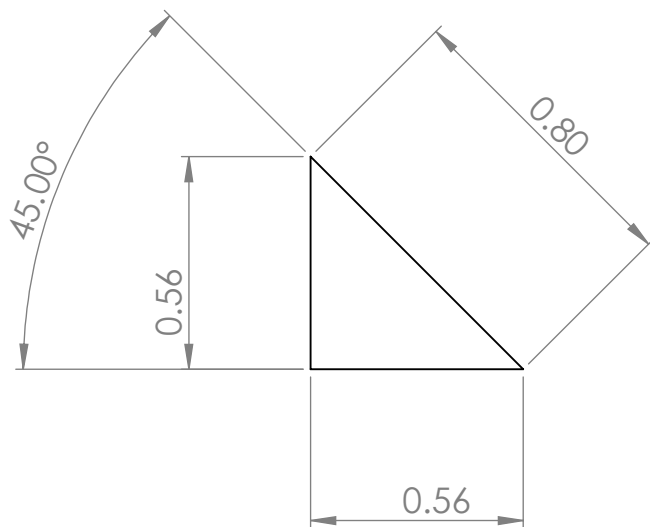
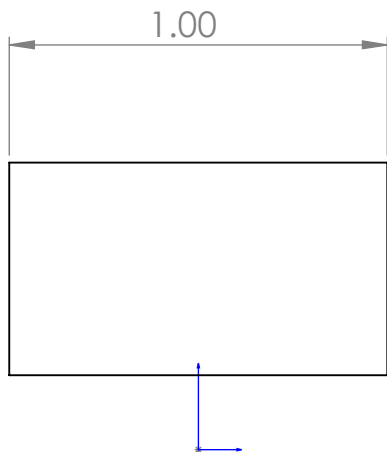


DIMENSIONS ARE IN MM		AUTHOR: FAMKE KARDUX	
TU DELFT			
TITLE:			
<b>MALL CURVATURE</b>			
DWG NO.		A4	
<b>MALL_1</b>			
SCALE:1:1		SHEET 1 OF 1	

4 3 2 1

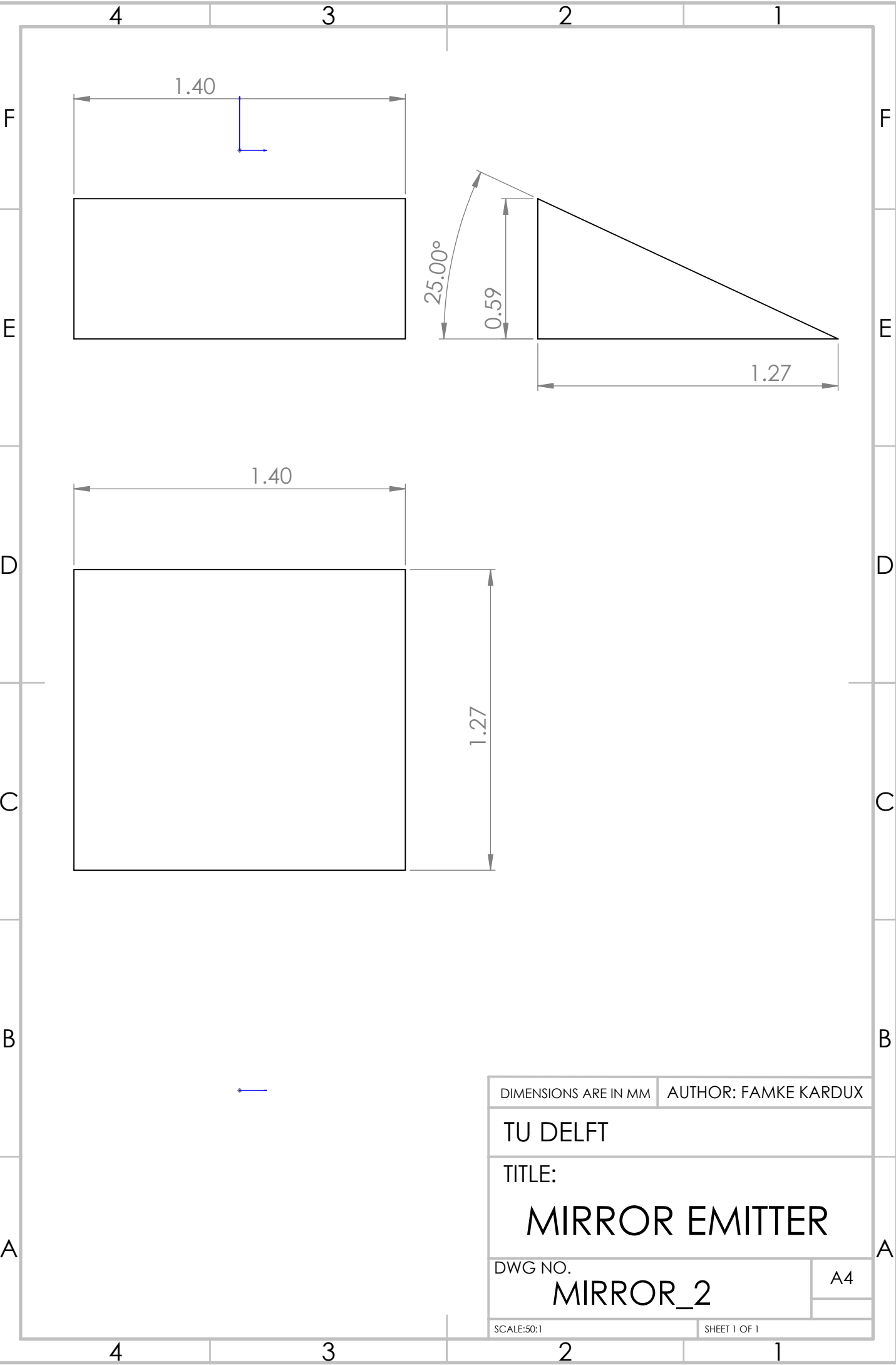
F  
E  
D  
C  
B  
A

F  
E  
D  
C  
B  
A

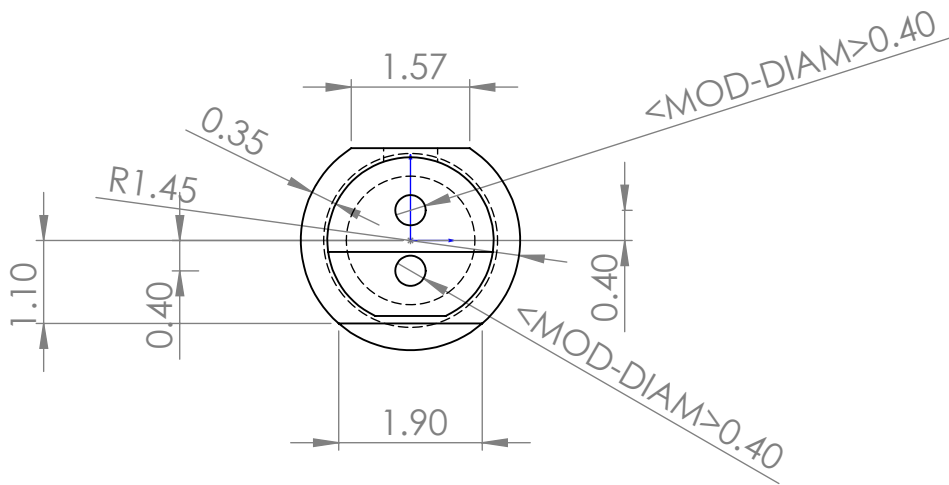
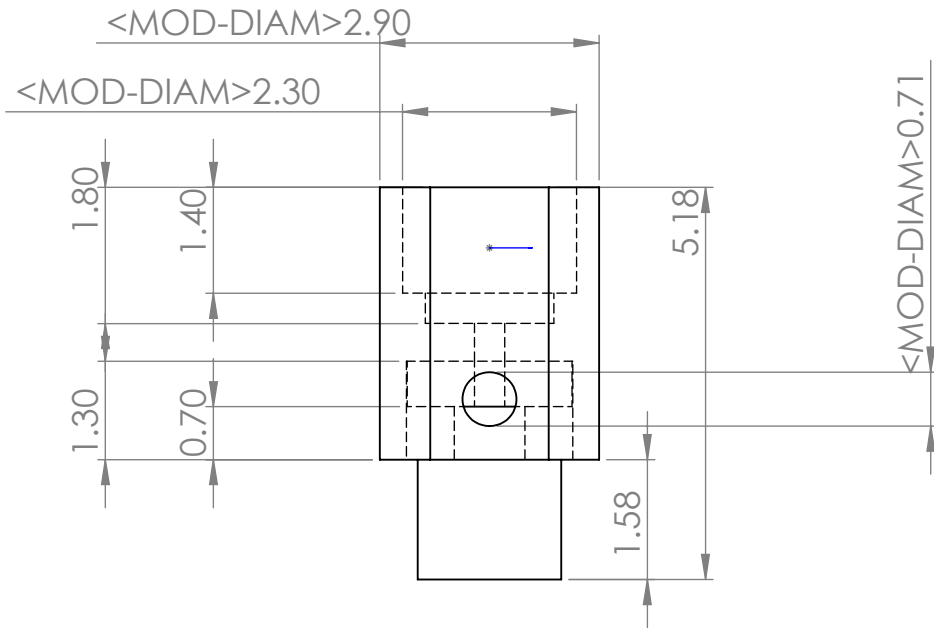


DIMENSIONS ARE IN MM		AUTHOR: FAMKE KARDUX	
TU DELFT			
TITLE: MIRROR COLLECTOR			
DWG NO. MIRROR_1			A4
SCALE:50:1		SHEET 1 OF 1	

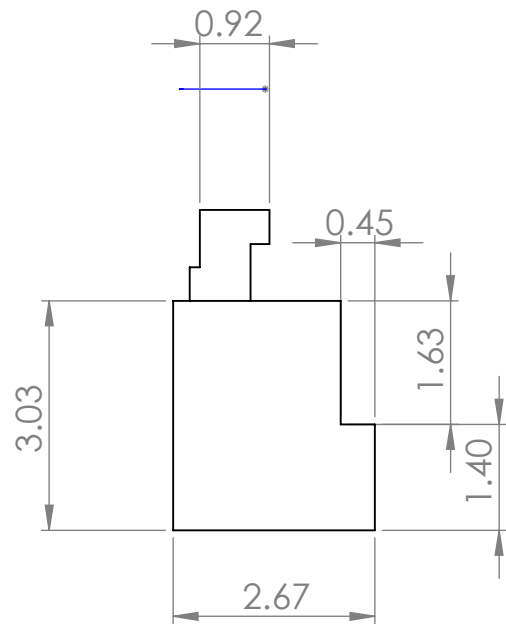
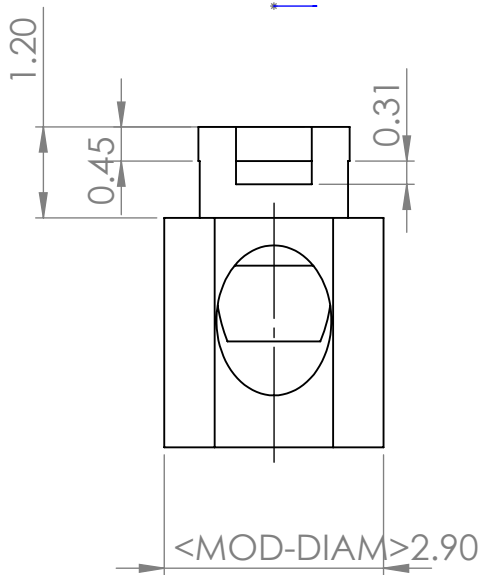
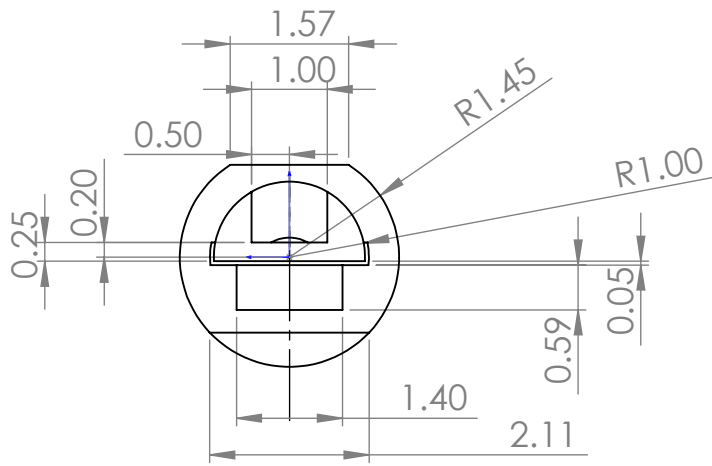
4 3 2 1



DIMENSIONS ARE IN MM		AUTHOR: FAMKE KARDUX	
TU DELFT			
TITLE:			
<b>MIRROR EMITTER</b>			
DWG NO.			A4
<b>MIRROR_2</b>			
SCALE:50:1		SHEET 1 OF 1	



DIMENSIONS ARE IN MM		AUTHOR: FAMKE KARDUX	
TU DELFT			
TITLE:			
<b>RIGID TIP PROBE</b>			
DWG NO.			A4
<b>RIGIDTIP_PROBE1</b>			
SCALE:10:1		SHEET 1 OF 1	



DIMENSIONS ARE IN MM | AUTHOR: FAMKE KARDUX

TU DELFT

TITLE:

**RIGID TIP PROBE**

DWG NO.

**RIGIDTIP\_PROBE2**

A4

SCALE:10:1

SHEET 1 OF 1

## Appendix B

# Design concepts

All possible concepts consisting of different combinations of strategies are shown in Figure B.1. The combinations of strategies which are not feasible are shown in Figure B.2. These combinations are not possible because direct fiber tissue contact is impossible when employing a mirror to shift the direction of light. The score of all concepts towards the specifications is shown in Figure B.3. A short explanation to the corresponding scores is listed below:

- 1-4 all concepts should score basic on these specifications. This is because all designs does include the optical design investigated in Chapter 2.
- 5 The light absorption in the probe is optimal for the probes with direct fiber tissue contact and basic for designs that include an additional transparent material between fiber and tissue.
- 6 The distance between the probe and the tissue is good for designs where the indices of the probe and tissue match and critical for the designs with a special shaped terminating end to prevent light reflection and refraction.
- 7 There is no internal reflection in the design with matched indices. However, there will be specular reflection in the design with a large mismatch in index between probe and tissue.
- 8 Due to inaccuracy in the manufacturing of the slanted fibers and the expected damage on the straight surfaces, undesired refraction will take place in all designs except F and H.
- 9 All designs with fibers separated in the radial direction cannot be so small that they fit into a hole with a diameter of less than 3.5 mm. As a result, they receive a critical rating on this criterion.
- 10-12 The same strategies for flexibility and robustness are used in all concepts. As a result, all designs get comparable scores on these specifications. The radius of curvature is ideal, and force prevention is basic.
- 13-15 The costs of the probe is for all concepts basic. However, the design that includes small features within the fiber glass can not be accurately created at Delft university. When production should be done externally, the production time is always longer than 1-2 weeks.

	Concepts
A	
B	
C	
D	
E	
F	
G	
H	
I	
J	
K	
L	

FIGURE B.1: All possible concepts based on combinations of different strategies for the sub functions

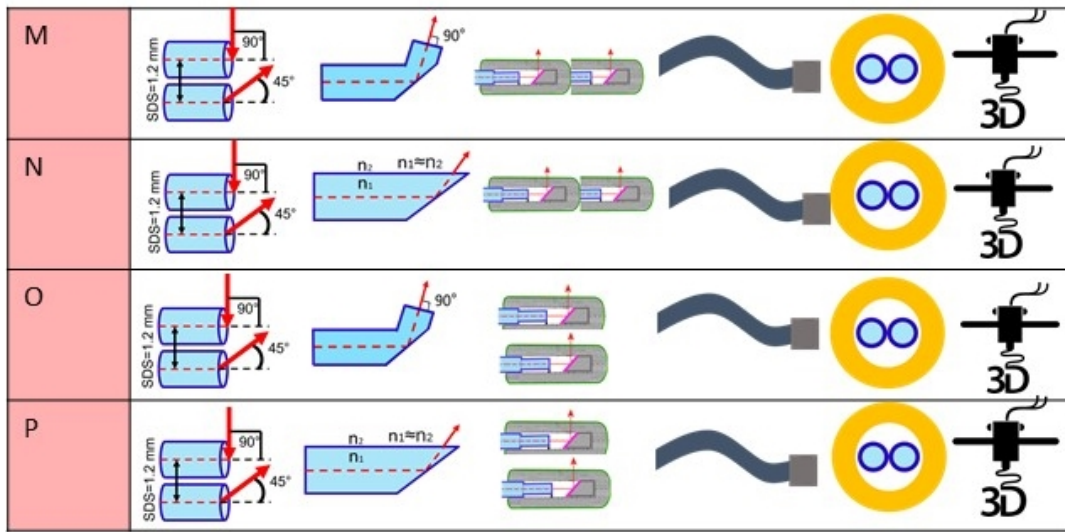


FIGURE B.2: Combinations of different strategies for the sub functions which are not feasible to realize

	1	2	3	4	5	6	7	8	9	10	11	12	13	14	15
A	Yellow	Yellow	Yellow	Yellow	Yellow	Red	Red	Red	Yellow	Green	Yellow	Yellow	Yellow	Red	Red
B	Yellow	Yellow	Yellow	Yellow	Yellow	Green	Yellow	Red	Yellow	Green	Yellow	Yellow	Yellow	Red	Red
C	Yellow	Yellow	Yellow	Yellow	Yellow	Red	Red	Red	Red	Green	Yellow	Yellow	Yellow	Red	Red
D	Yellow	Yellow	Yellow	Yellow	Yellow	Green	Yellow	Red	Red	Green	Yellow	Yellow	Yellow	Red	Red
E	Yellow	Yellow	Yellow	Yellow	Yellow	Red	Red	Red	Yellow	Green	Yellow	Yellow	Yellow	Green	Yellow
<b>F</b>	Yellow	Yellow	Yellow	Yellow	Yellow	Green	Yellow	Yellow	Yellow	Green	Yellow	Yellow	Yellow	Green	Yellow
G	Yellow	Yellow	Yellow	Yellow	Yellow	Red	Red	Red	Red	Green	Yellow	Yellow	Yellow	Green	Yellow
H	Yellow	Yellow	Yellow	Yellow	Yellow	Green	Yellow	Yellow	Red	Green	Yellow	Yellow	Yellow	Green	Yellow
I	Yellow	Yellow	Yellow	Yellow	Green	Red	Red	Red	Yellow	Green	Yellow	Yellow	Yellow	Red	Red
J	Yellow	Yellow	Yellow	Yellow	Green	Green	Yellow	Red	Yellow	Green	Yellow	Yellow	Yellow	Red	Red
K	Yellow	Yellow	Yellow	Yellow	Green	Red	Red	Red	Red	Green	Yellow	Yellow	Yellow	Red	Red
L	Yellow	Yellow	Yellow	Yellow	Green	Green	Yellow	Red	Red	Green	Yellow	Yellow	Yellow	Red	Red

FIGURE B.3: Score of all concepts (rows) towards the specifications (columns). The color red indicates a critical level of fulfillment, orange indicates a basic level of fulfillment, and green indicates an excellent level of fulfillment.



## Appendix C

# Geometry formula

Figure C.1 shows the derivation and formula of calculating the maximal dimensions of a rigid part which can be inserted in a curved hole.

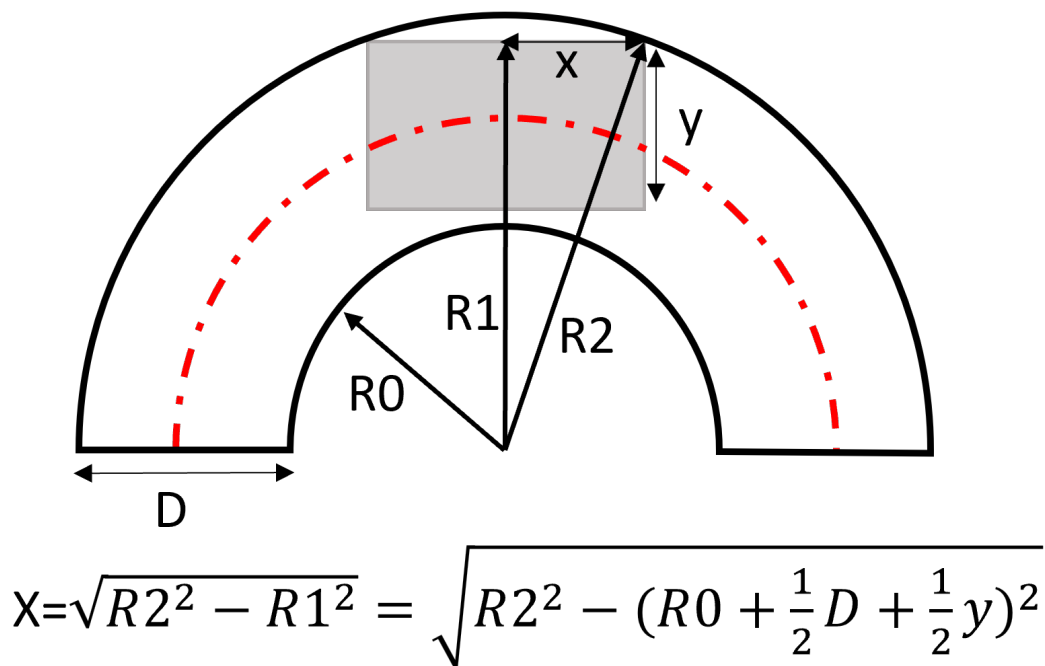


FIGURE C.1: Geometric analysis of the maximum dimensions of a rigid part within a curved hole